Retinal input

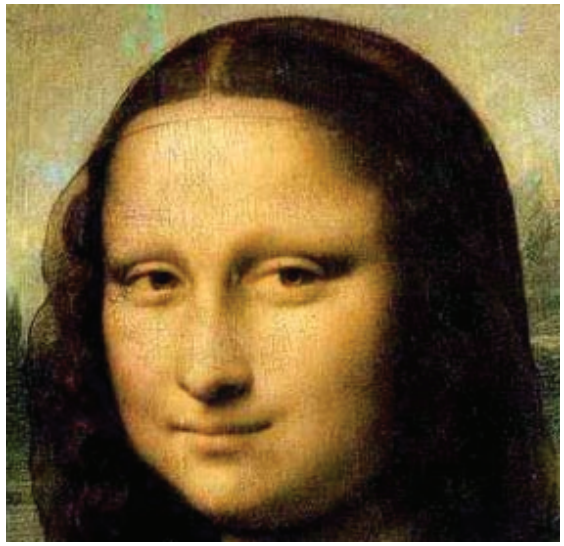

Retinal output

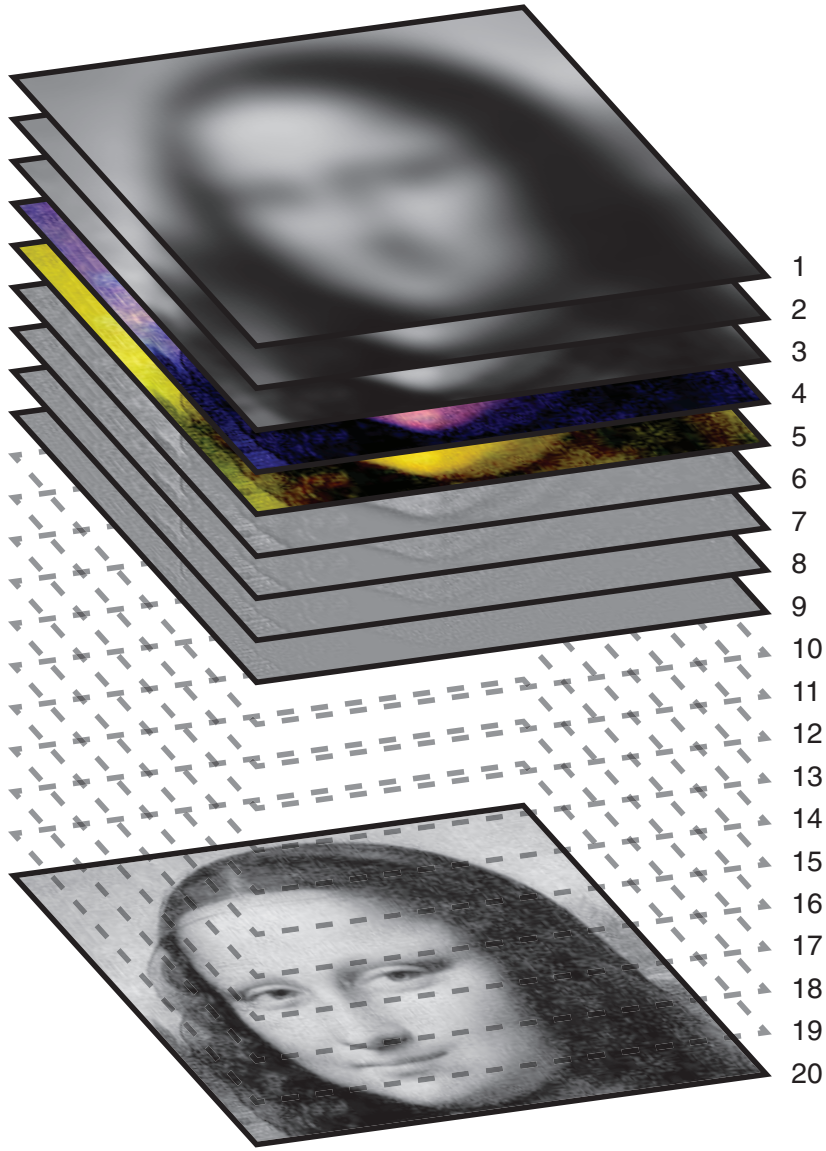

The retina creates 20 neural representations of the “movie” that enters the eye.

Roska and Meister, 2014

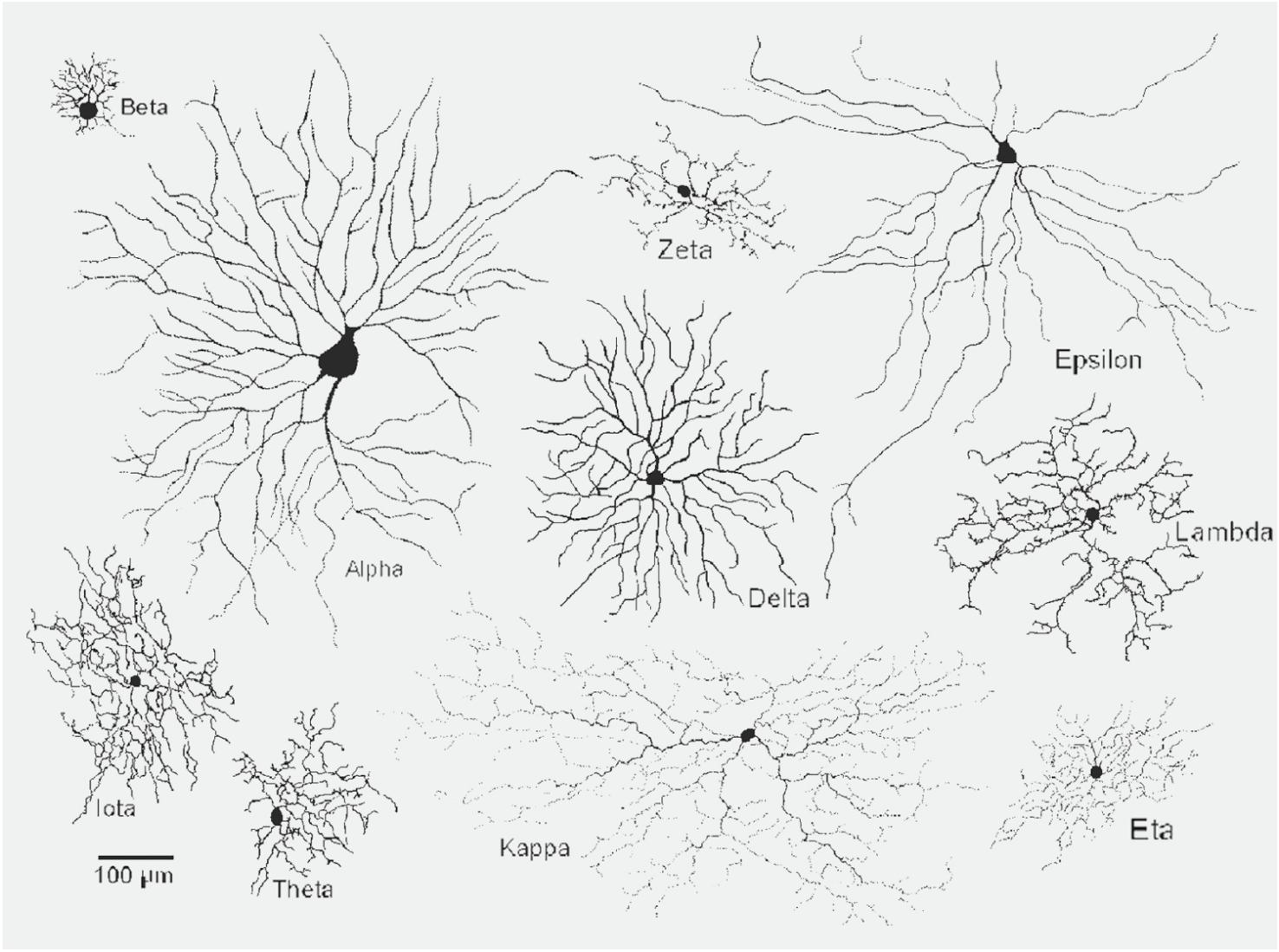

Fig. 5. The types of ganglion cells identified thus far in the retina of the cat. Ongoing work in the rabbit and monkey confirms this diversity, and many of the cells observed are probably homologs of those seen in the cat. Courtesy of D. Berson[77–80].

Masland, 2001

J. Physiol. (1966), **187**, *pp.* 517–552
With 17 *text-figures*
Printed in Great Britain

THE CONTRAST SENSITIVITY OF RETINAL GANGLION CELLS OF THE CAT

BY CHRISTINA ENROTH-CUGELL AND J. G. ROBSON*

From the Biomedical Engineering Center, Technological Institute, Northwestern University, Evanston, Illinois, U.S.A.† and the Department of Physiology, Northwestern University Medical School, Chicago, U.S.A.

(*Received* 19 *April* 1966)

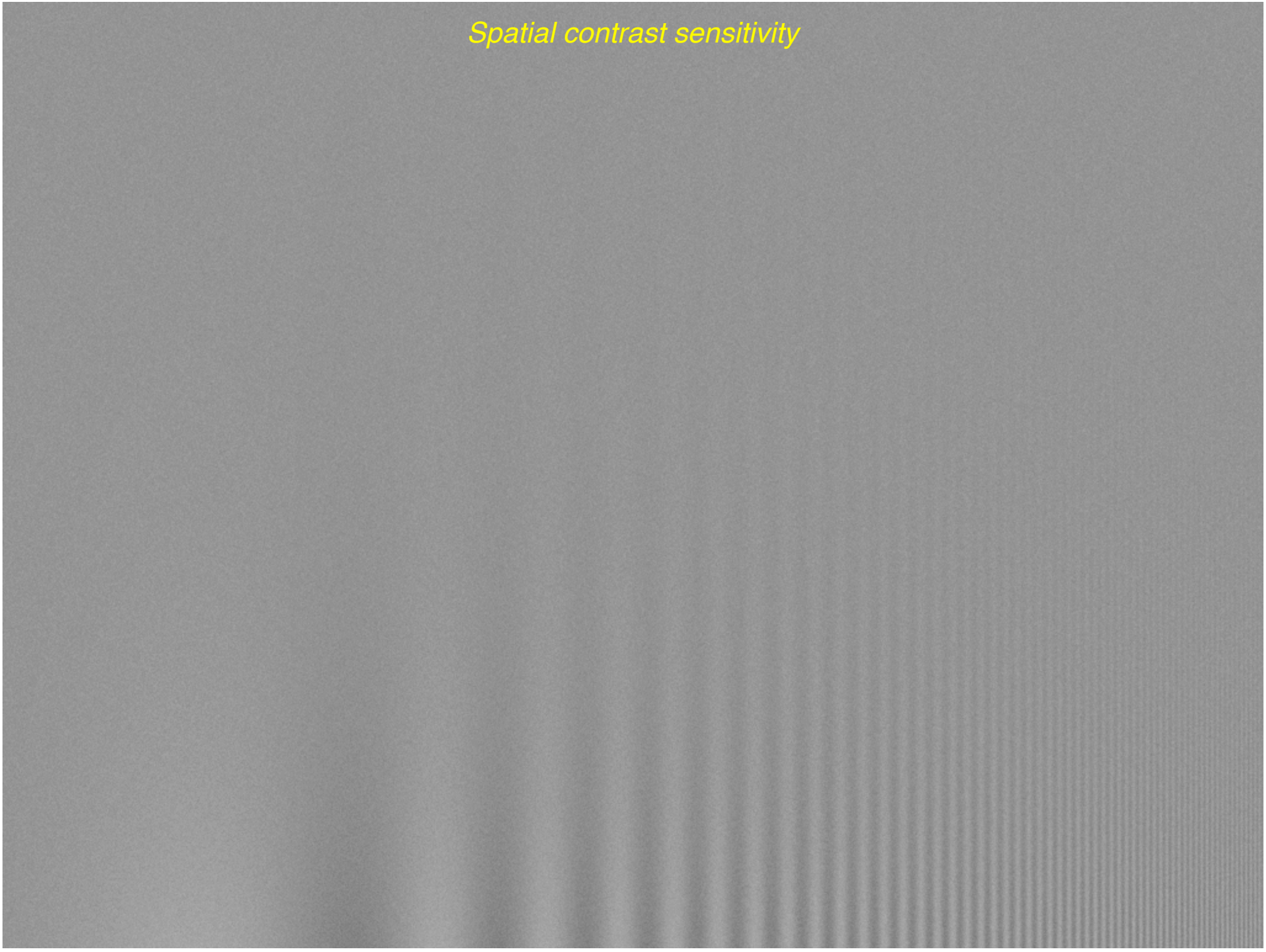
Spatial contrast sensitivity

Ganglion cell receptive field modeled as difference of Gaussians

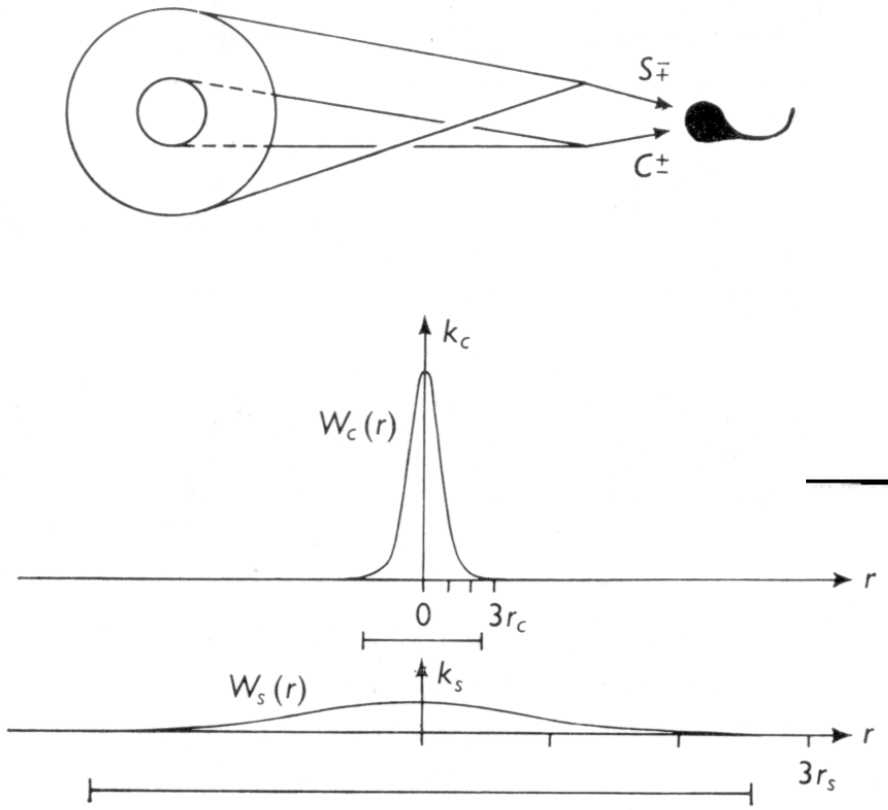

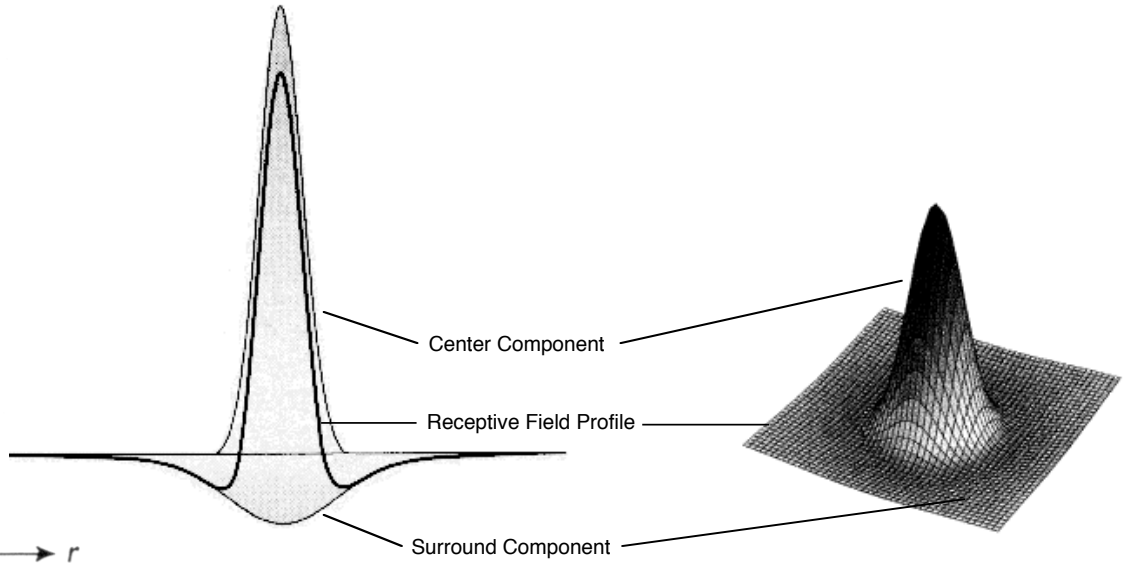

Rodieck (1965); Enroth-Cugell & Robson (1966)

Cat Retinal Ganglion Cell Additivity Test

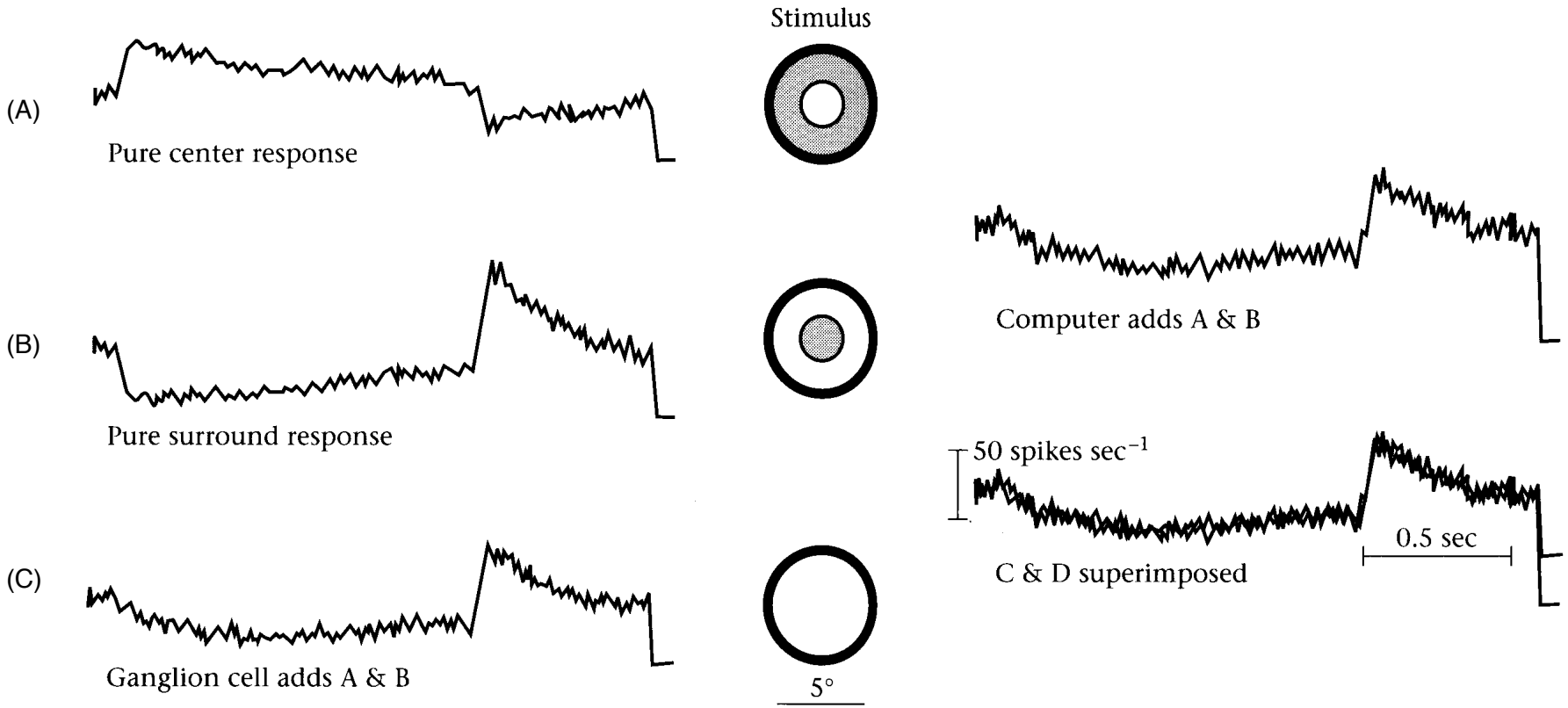

Enroth-Cugell & Pinto (1970)

Ganglion cell receptive field modeled as difference of Gaussians

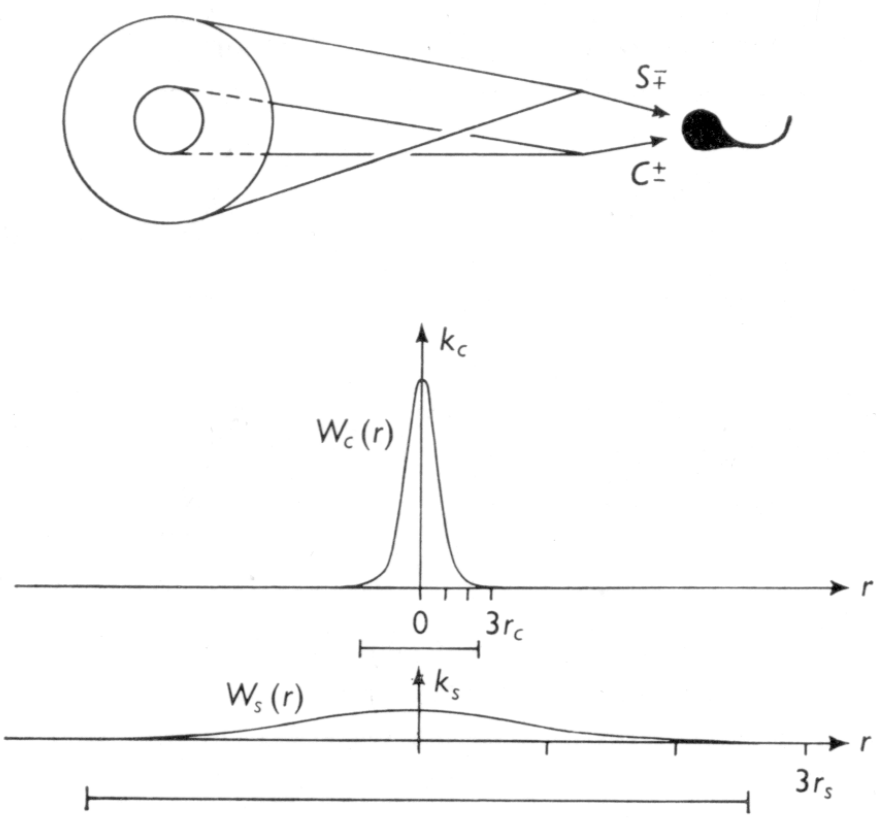

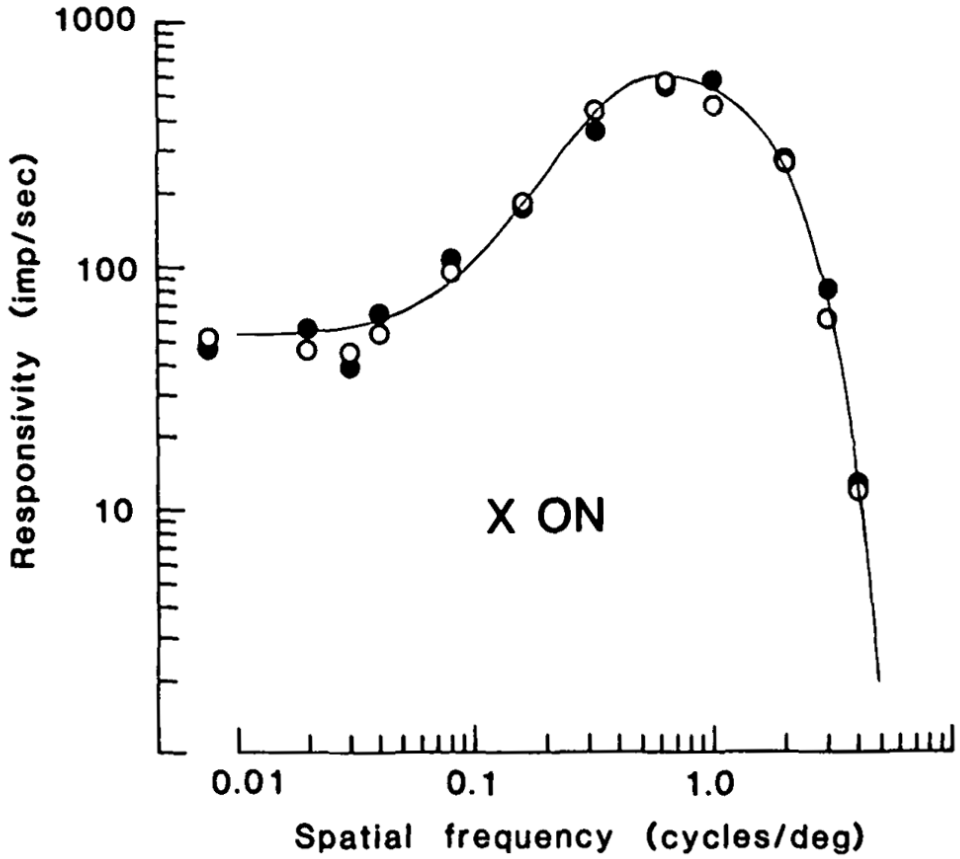

Enroth-Cugell & Robson (1966)

Frequency-domain representation of the difference of Gaussians

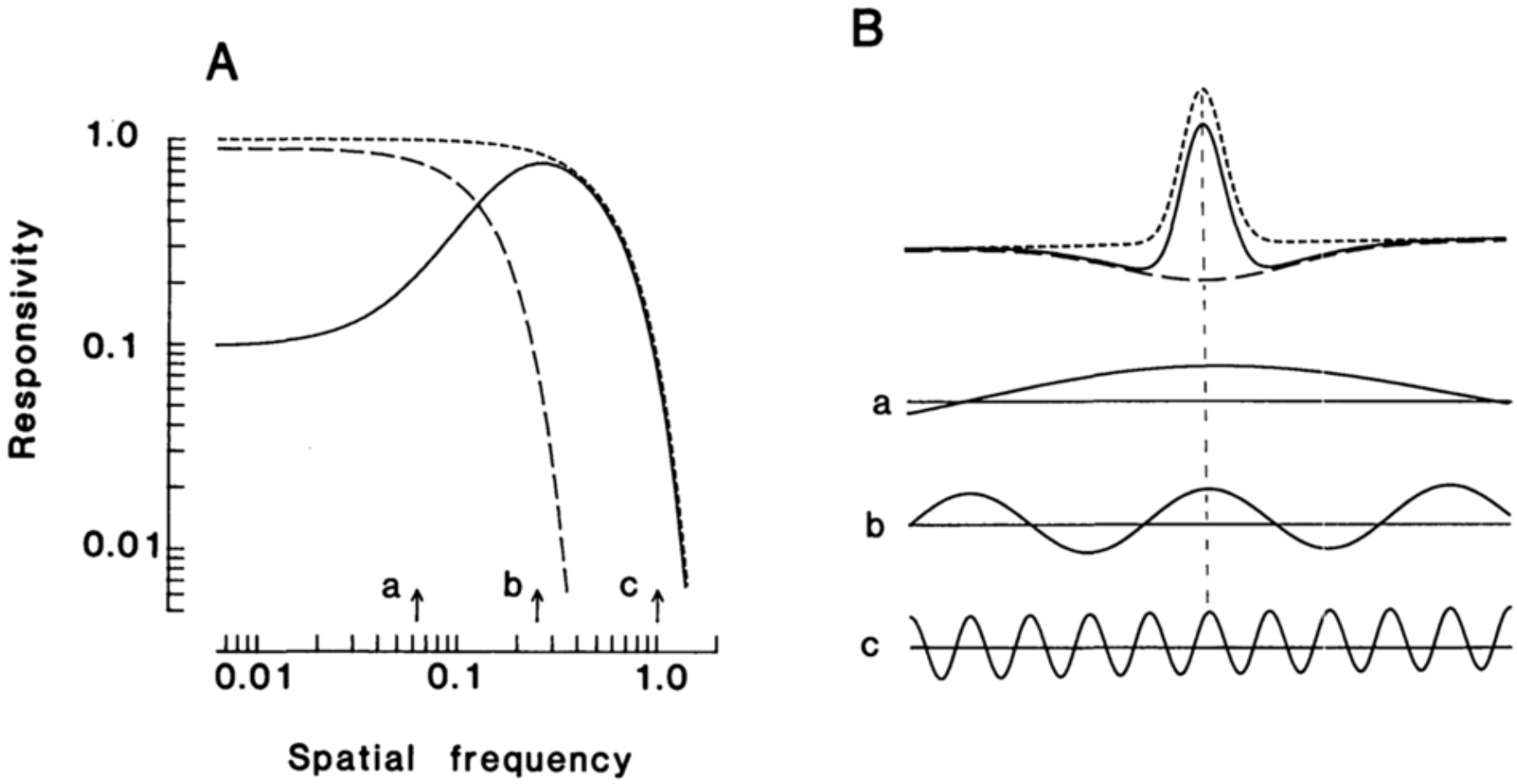

Enroth-Cugell & Robson (1984)

Linearity of summation in X cells

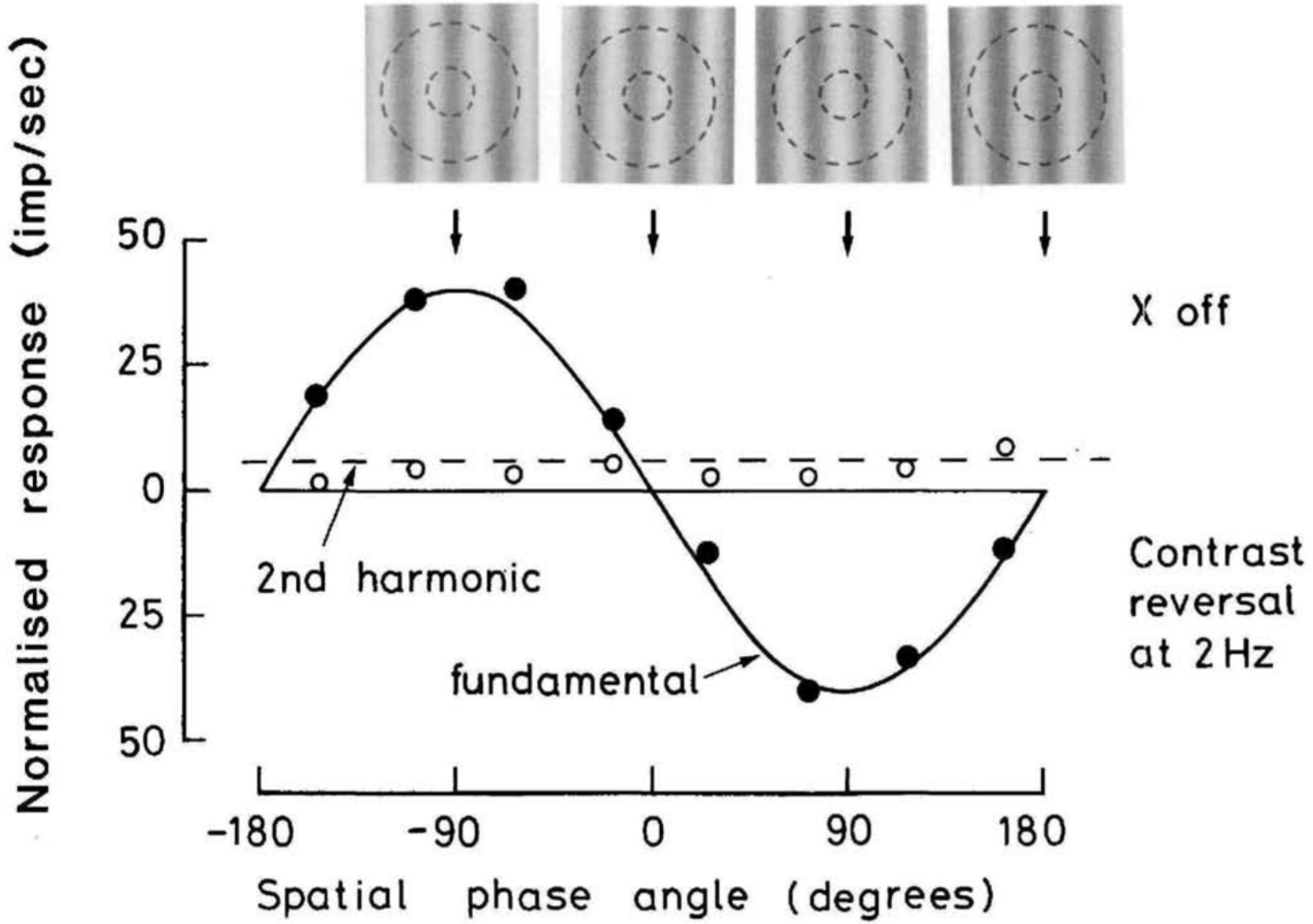

Enroth-Cugell & Robson (1984)

Linearity of summation in X cells, but not Y cells

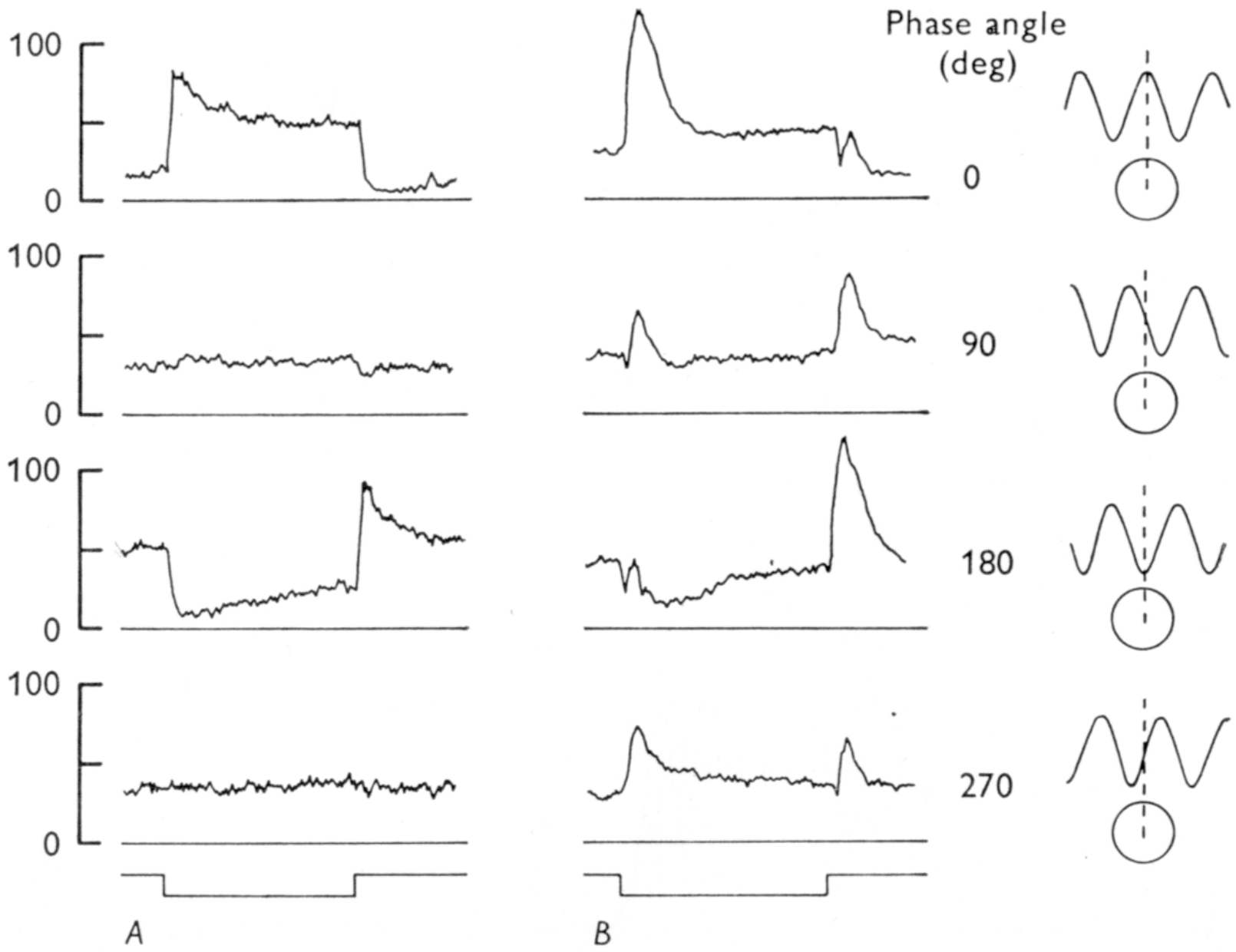

Enroth-Cugell & Robson (1966)

Linearity of summation in X cells, but not Y cells

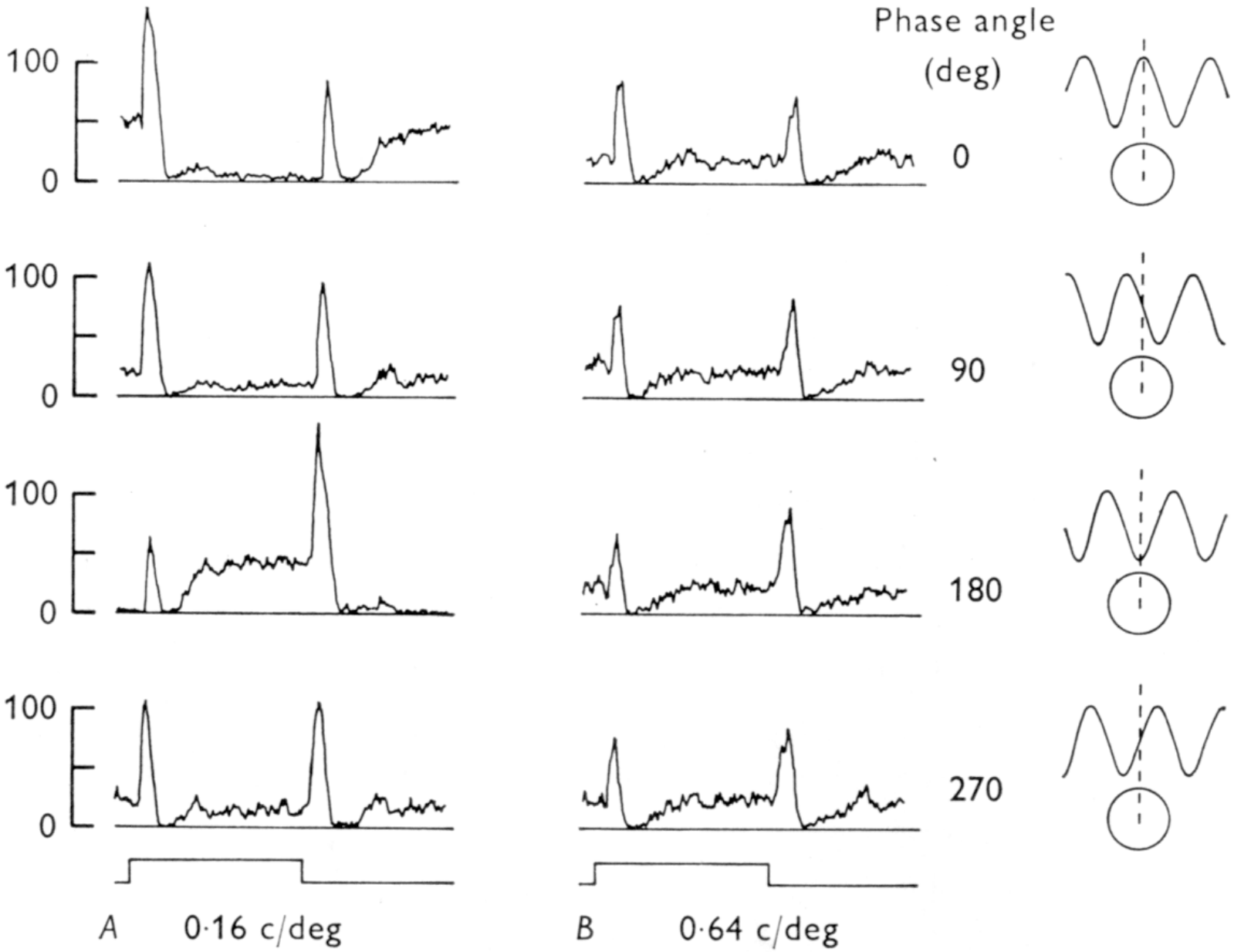

Enroth-Cugell & Robson (1966)

Nonlinear mechanisms of the Y cell receptive field

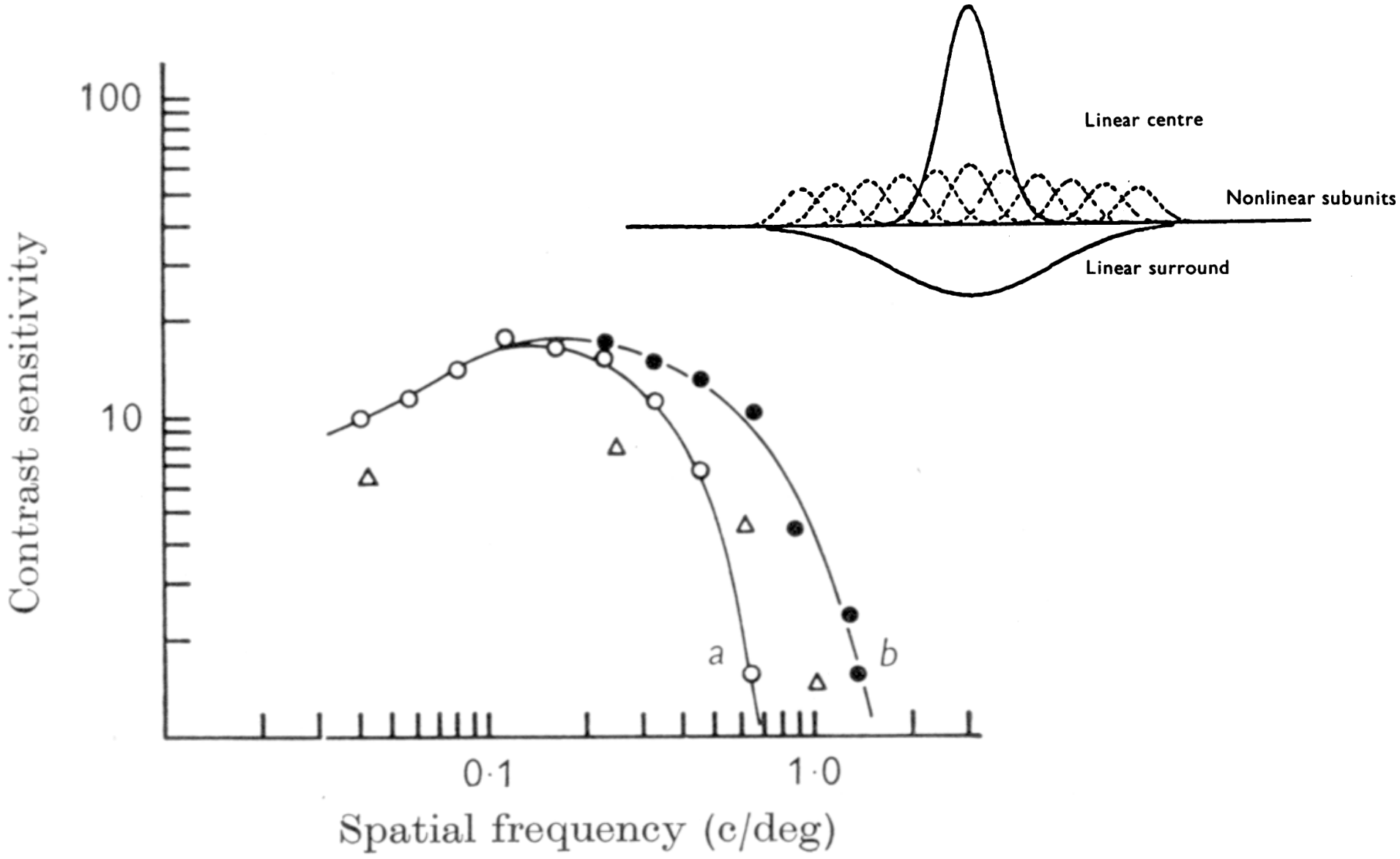

Enroth-Cugell & Robson (1966); Hochstein & Shapley (1976)

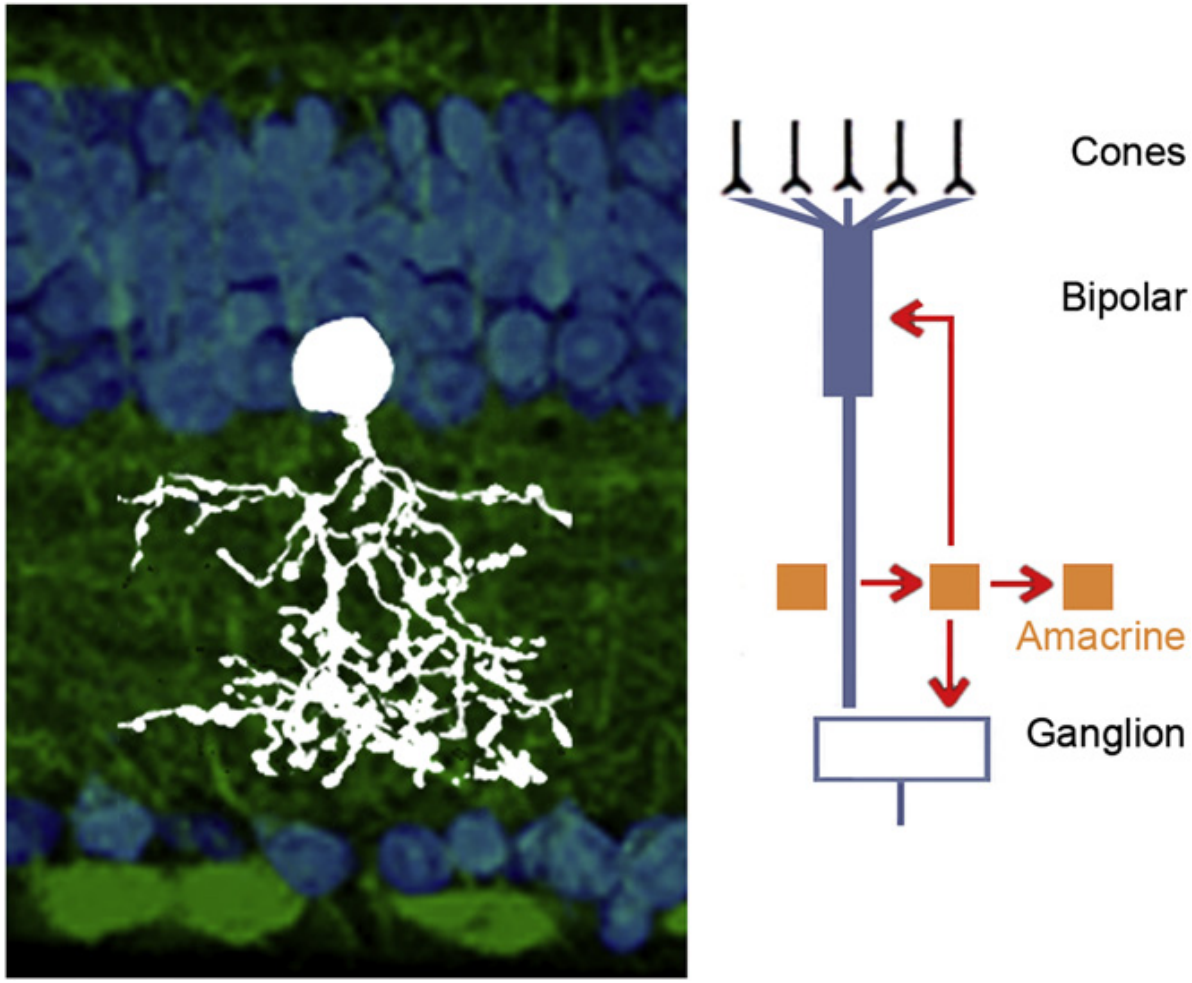

Figure 5. The Structure and Generalized Connectivity of Narrow Field Amacrine Cells

(A) Type 7 glycinergic amacrine cell of the mouse retina. Note that this cell communicates "vertically," interconnecting the ON and the OFF layers of the IPL. Cell image is adapted from Menger et al. (1998).

(B) Block diagram of amacrine cell pathways. Amacrine cells receive input from bipolar cells and other amacrine cells. They make outputs back upon bipolar cells, to ganglion cells, or to other amacrine cells. Thus amacrine cells participate in feedback inhibition, feed-forward inhibition, and lateral inhibition. A single amacrine cell can have all of these arrangements or a subset of them.

Masland, 2012

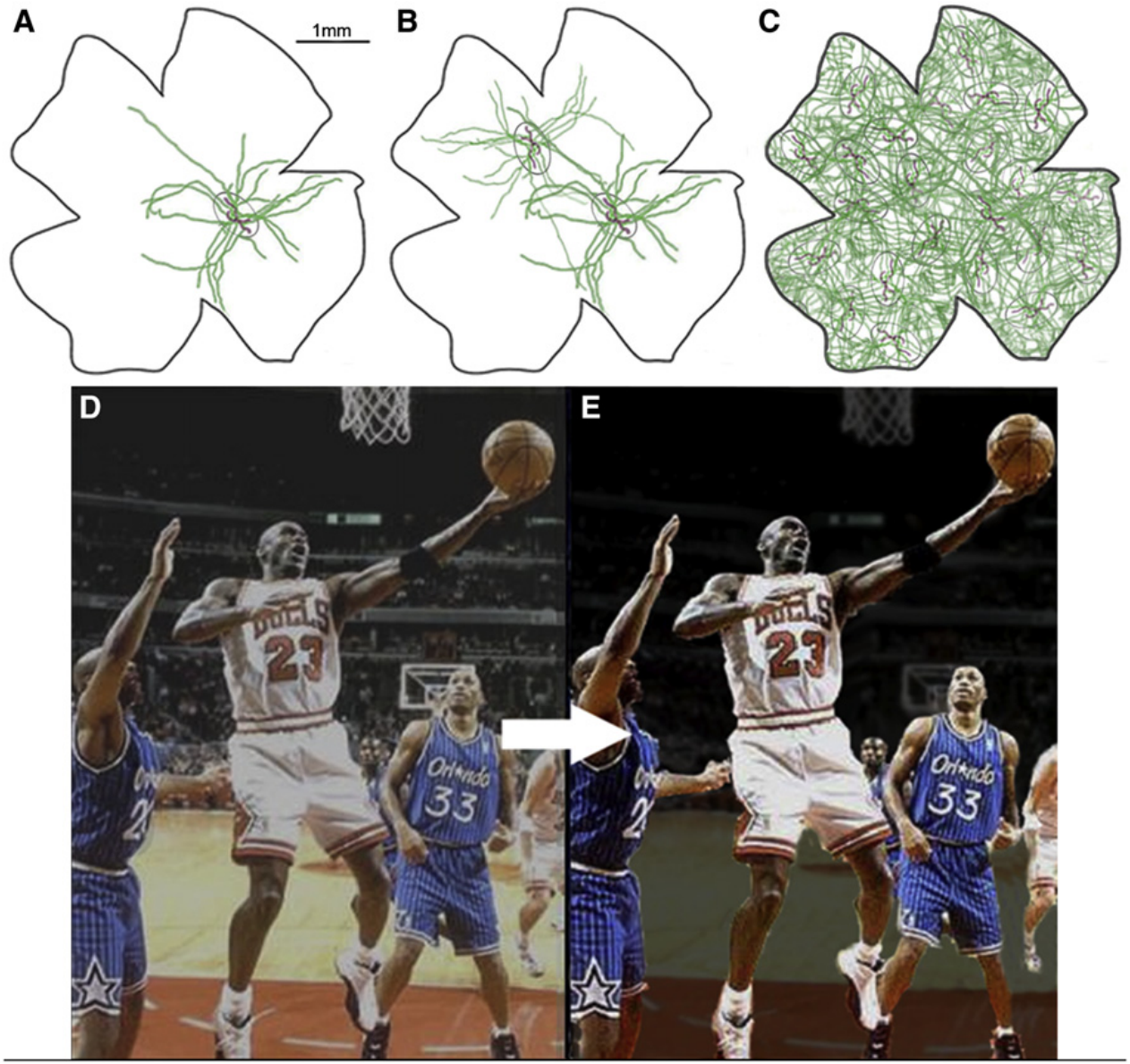

Figure 6. Wide-Field Amacrine Cells Can Span Most of the Surface of the Retina

(A) Whole-mount view of a wide-field amacrine cell termed WA5-1 in the survey of Lin and Masland (2006). This cell's axonal arbor (green) would affect visual stimuli falling in approximately half of the animal's field of view. But the cell receives input from only a limited region of their dendritic fields (red), and presumably the population of cells of this type seamlessly affect images throughout the field, without the gaps that appear when a single cell or only a few of them are taken in isolation, as shown in (B). It does not take a large number of these cells to achieve the nearly complete axonal (green) coverage of the retina shown in (C). If we assume that the dendritic fields (ellipses) nearly tile the retina, the network of axonal processes is dense enough to affect the visual input with an adequate spatial resolution. In fact, the illustration shown here does not achieve tiling of the dendritic fields. If we assume a dendritic coverage of at least unity—higher than is shown here—the axonal coverage would blanket the retina at a very high density indeed. This is the arrangement to be predicted from other known types of retinal cells; whether or not it pertains to this cell will await a population stain.

(D and E) These cells appear to mediate a variety of contextual effects, in which visual events surrounding a particular stimulus condition the response of a ganglion cell to that stimulus. An example is "object motion detection," in which objects that move relative to the general visual field are preferentially reported to the brain (Ölveczky et al., 2003). The effect of this computation is artificially simulated in the lower panels. A native image is shown in (D). The image transmitted to the brain after object motion enhancement is shown in (E): the retinal ganglion cells respond most strongly to objects that are moving relative to the stationary surroundings. (D) and (E) reprinted from (Masland, 2003).

Masland, 2012

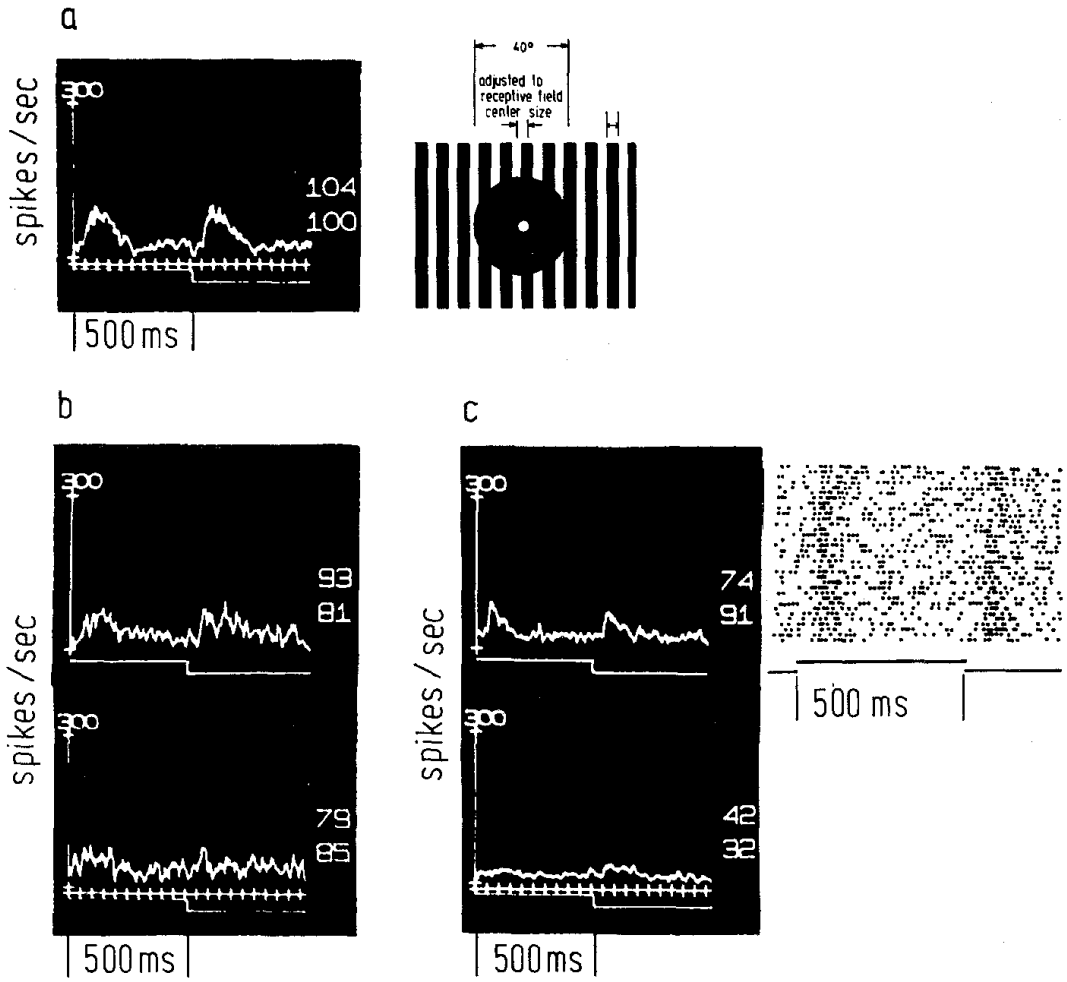

Fig. 1. Shift-effect in retinal neurons of rhesus monkey. (a) Shift responses of an on-center retinal ganglion cell and stimulus configuration. The grating is shifted to and fro in about 20° distance from the receptive field center. Blank area diameter 40 degrees; grating bar width and shift amplitude 2 degrees (arrows); stationary spot diameter 1.8 degrees: total pattern covering 100×100 deg. of the visual field. (b) Shift response of an off-center retinal ganglion cell after the introduction of a dark stationary center spot. Top: during the first 10 seconds, bottom: during the 50th—60th sec. (c) Shift response of the same neuron as in b. Top: A grating covered the total 100 deg. field including the receptive field (Bar width and shift amplitude 0.6 deg.). A slow drift of about 0.1 deg./sec was superposed on the grating shifts in order to exclude a stimulus configuration fortuitously symmetrical to the receptive field center. The dot display shows the similarity of all single responses. Bottom: Same grating restricted to the receptive field center. Other stimulus parameters unchanged. The ordinate in the post-stimulus time histograms is spike frequency, the numbers at right are peak frequencies in the two halves of the histogram (in spikes/second). A grating shift occurs each 500 ms (step trace below all frames). Ten to 60 stimulus presentations were averaged depending on the clarity of the response

Krüger, Fischer & Barth (1975)

On- and off-cells are each other's inverses

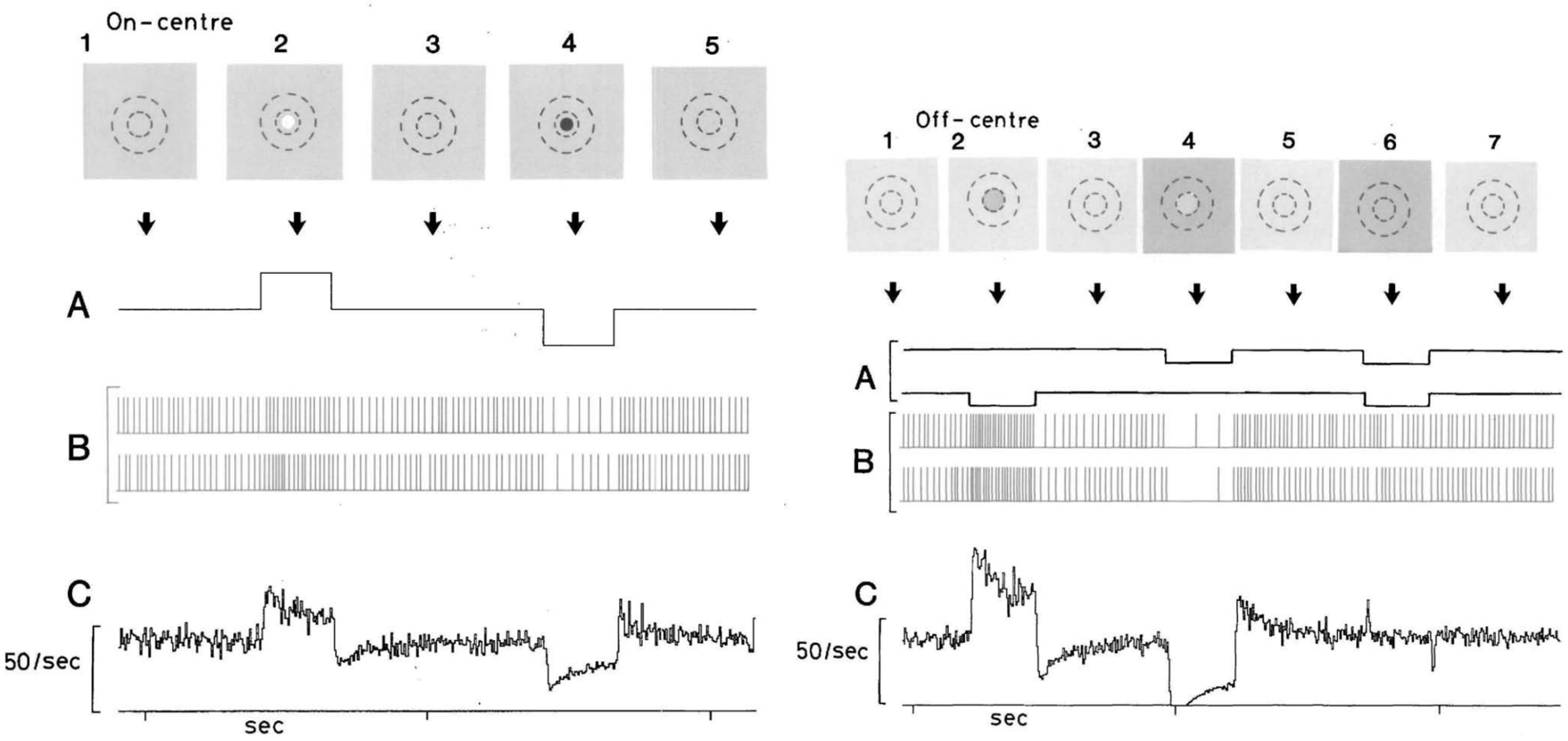

Enroth-Cugell & Robson (1984)

On-off asymmetry

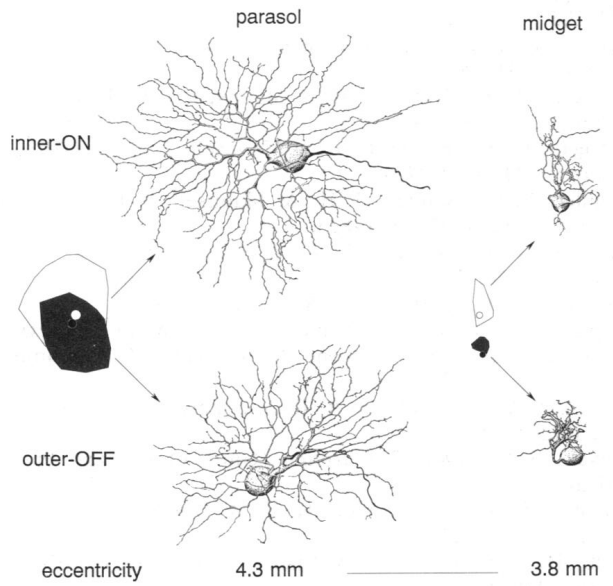

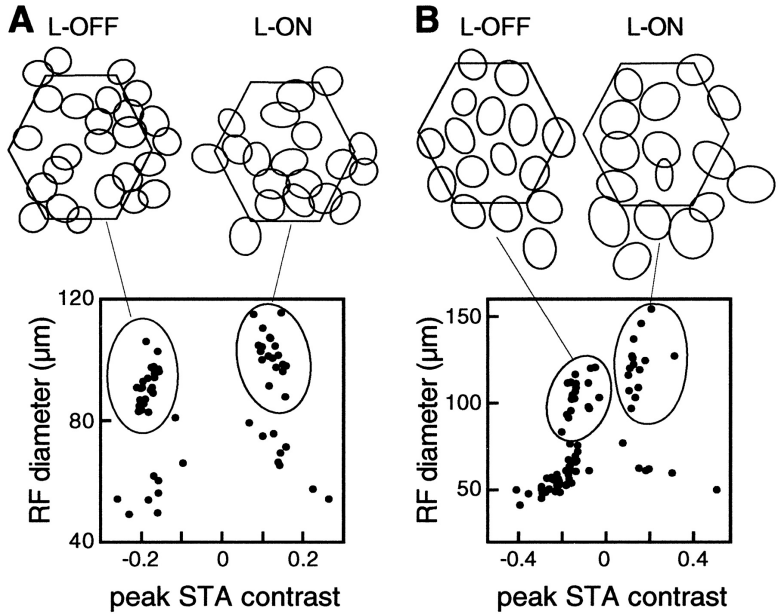

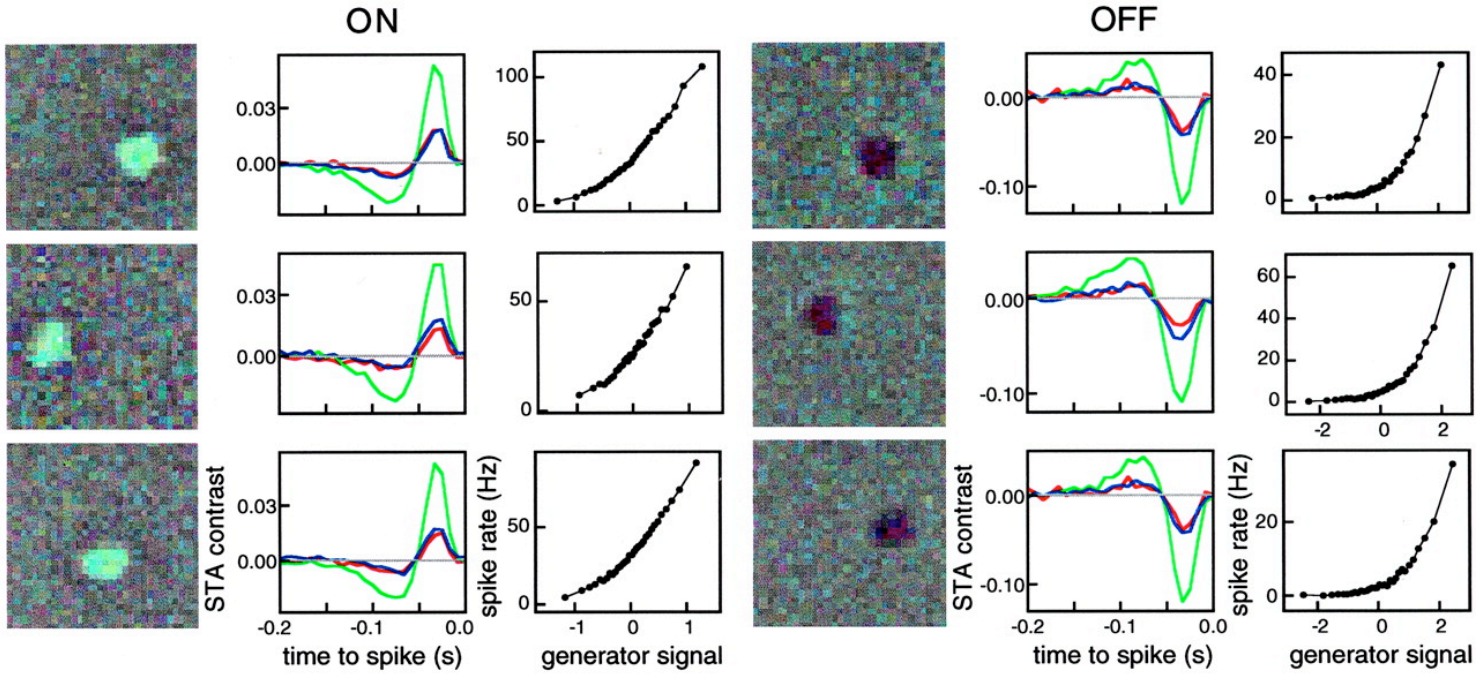

Dacey & Peterson, 1992;
Chichilnisky & Kalmar, 2002

Retinal input

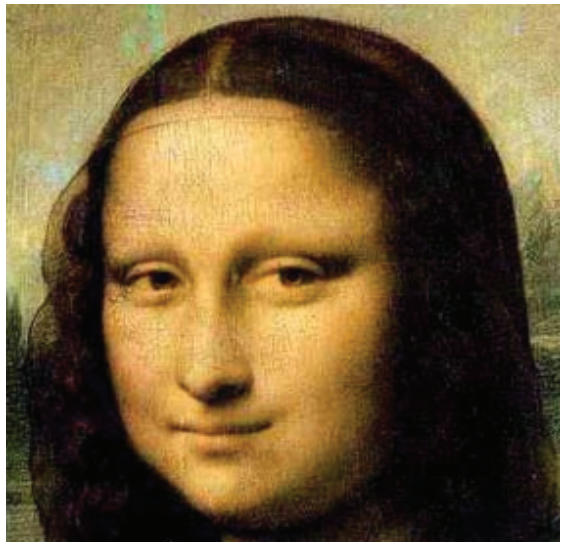

Retinal output

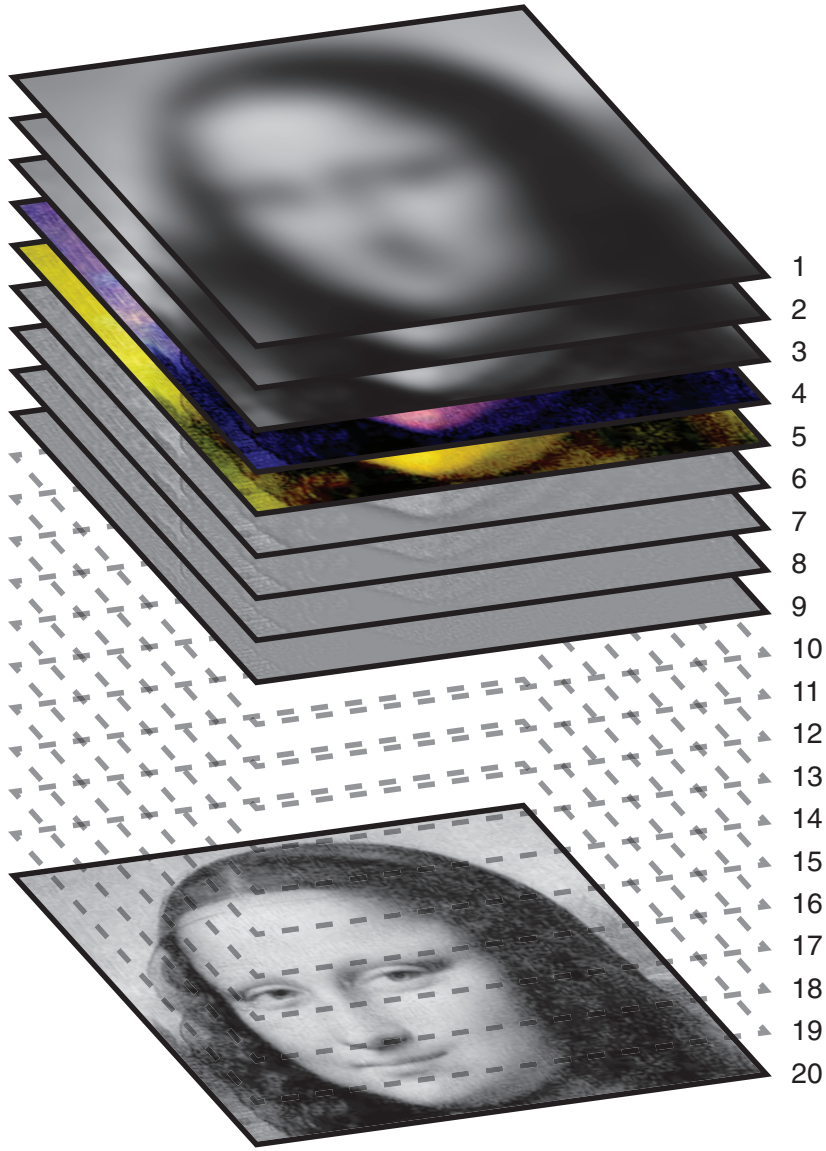

The retina creates 20 neural representations of the “movie” that enters the eye.

Roska and Meister, 2014

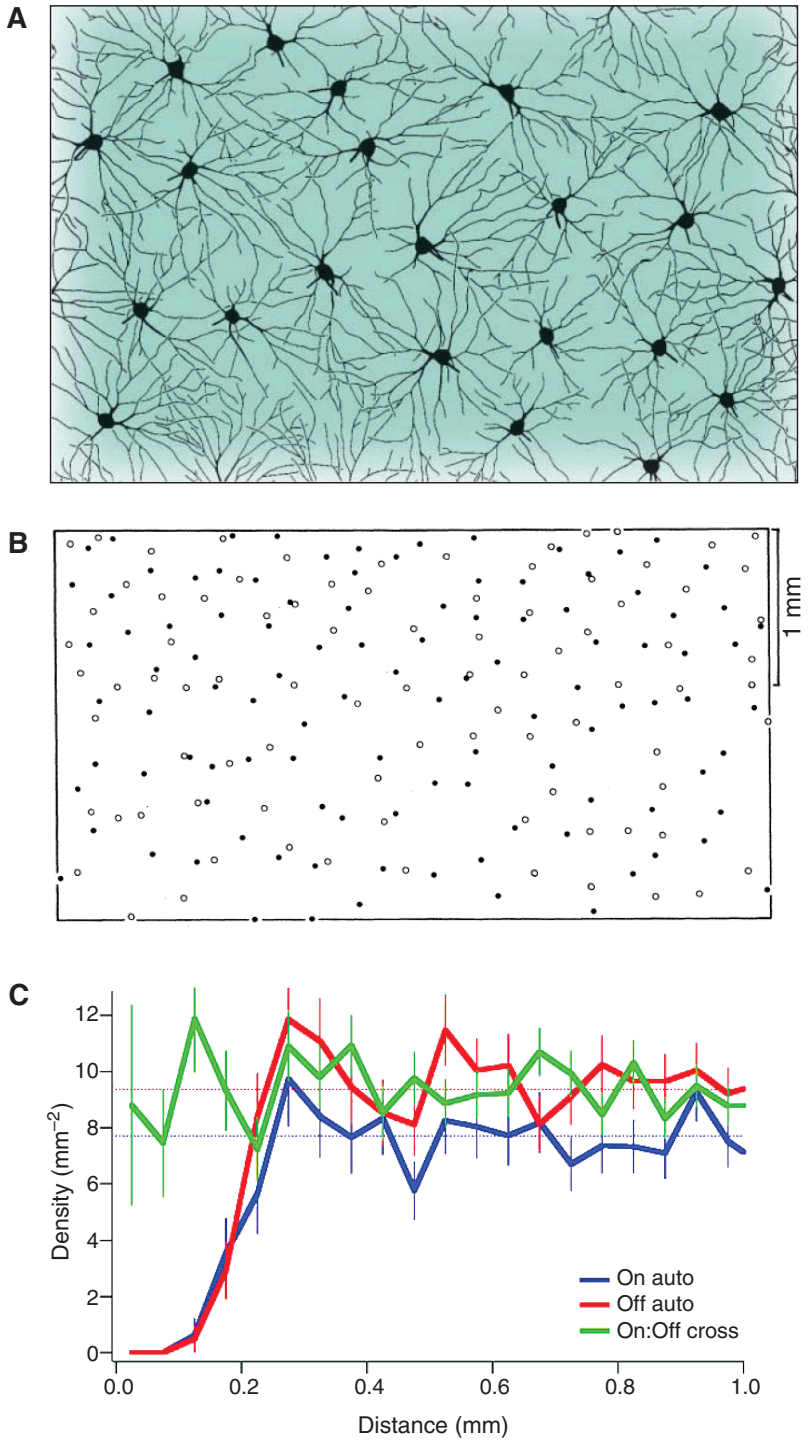

Masland, 2012

Primate Retinal Ganglion Cell Receptive Field Mosaics

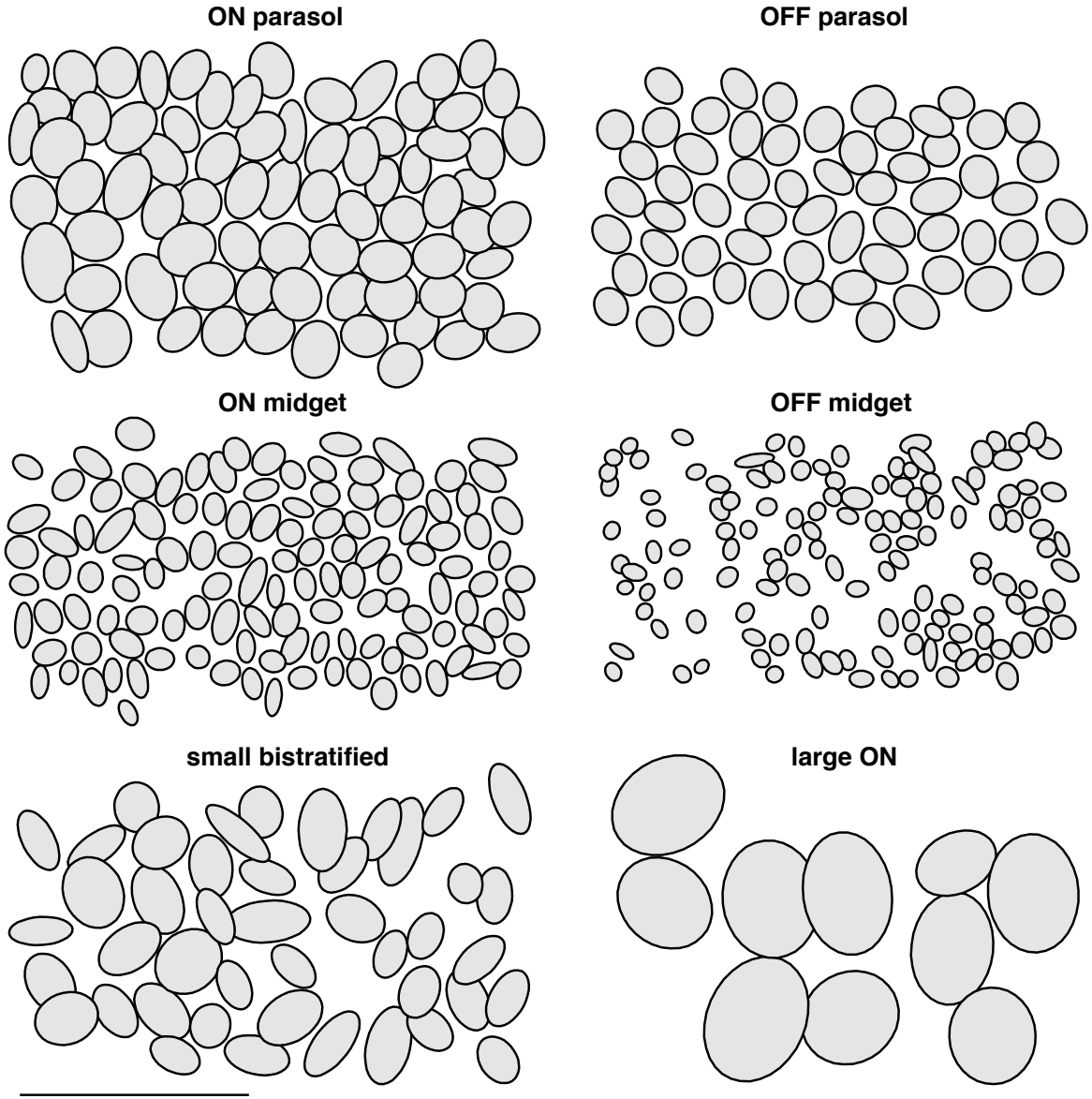

Field & Chichilnisky (2007)

Midget Retinal Ganglion Cell Dendritic Field Mosaic

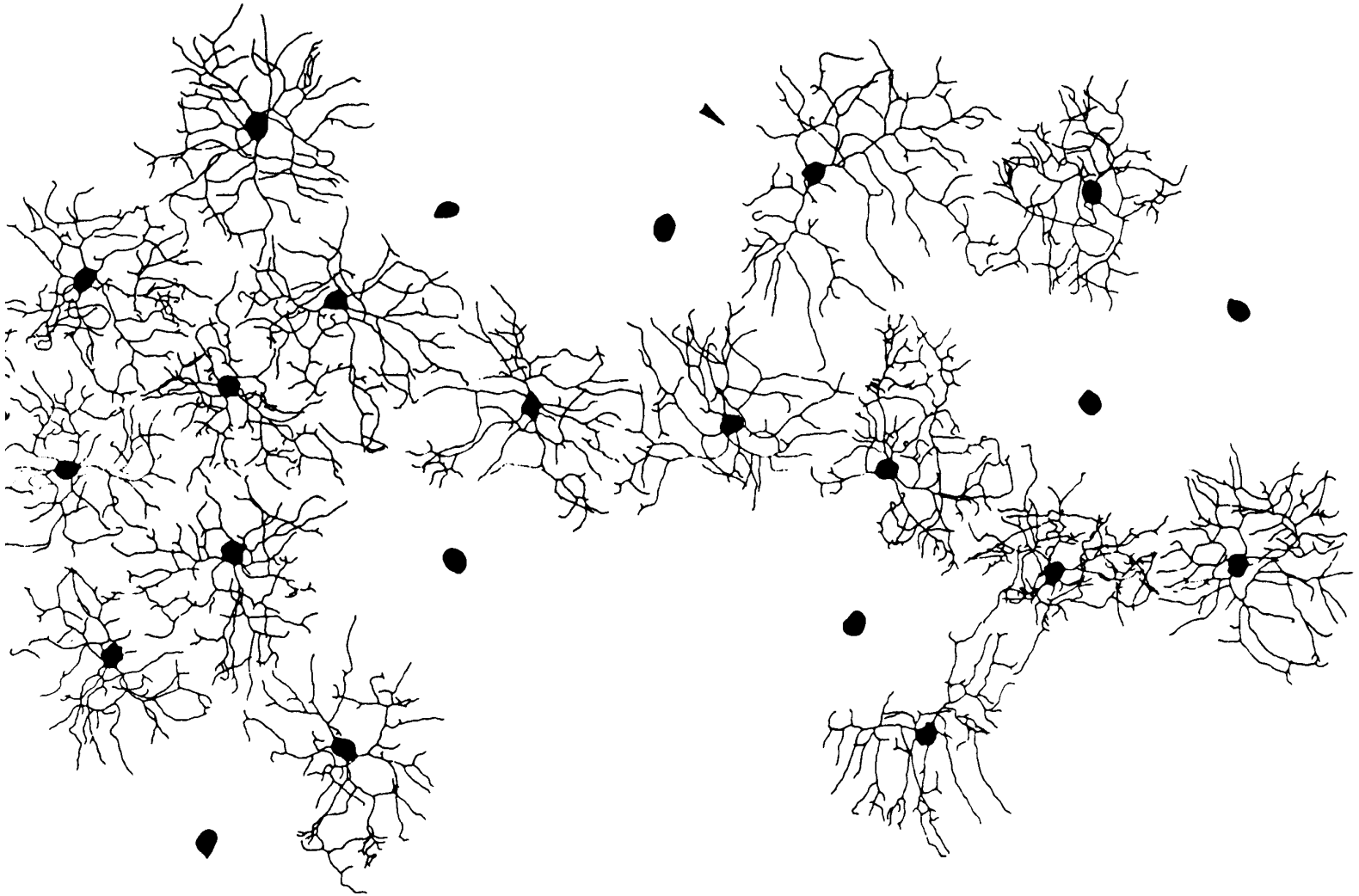

Dacey (1993)

Coordinated Fine Structure of Receptive Fields

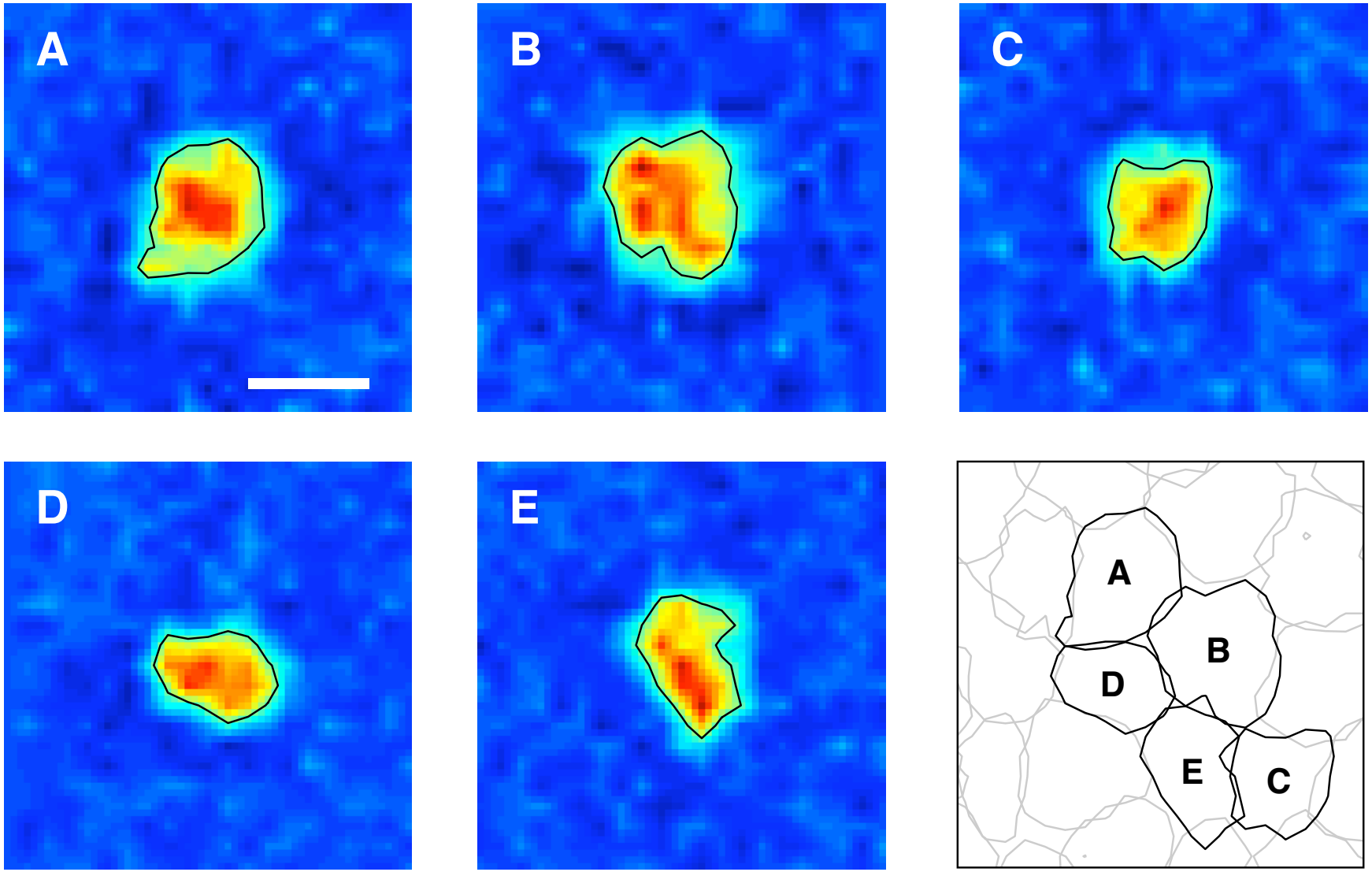

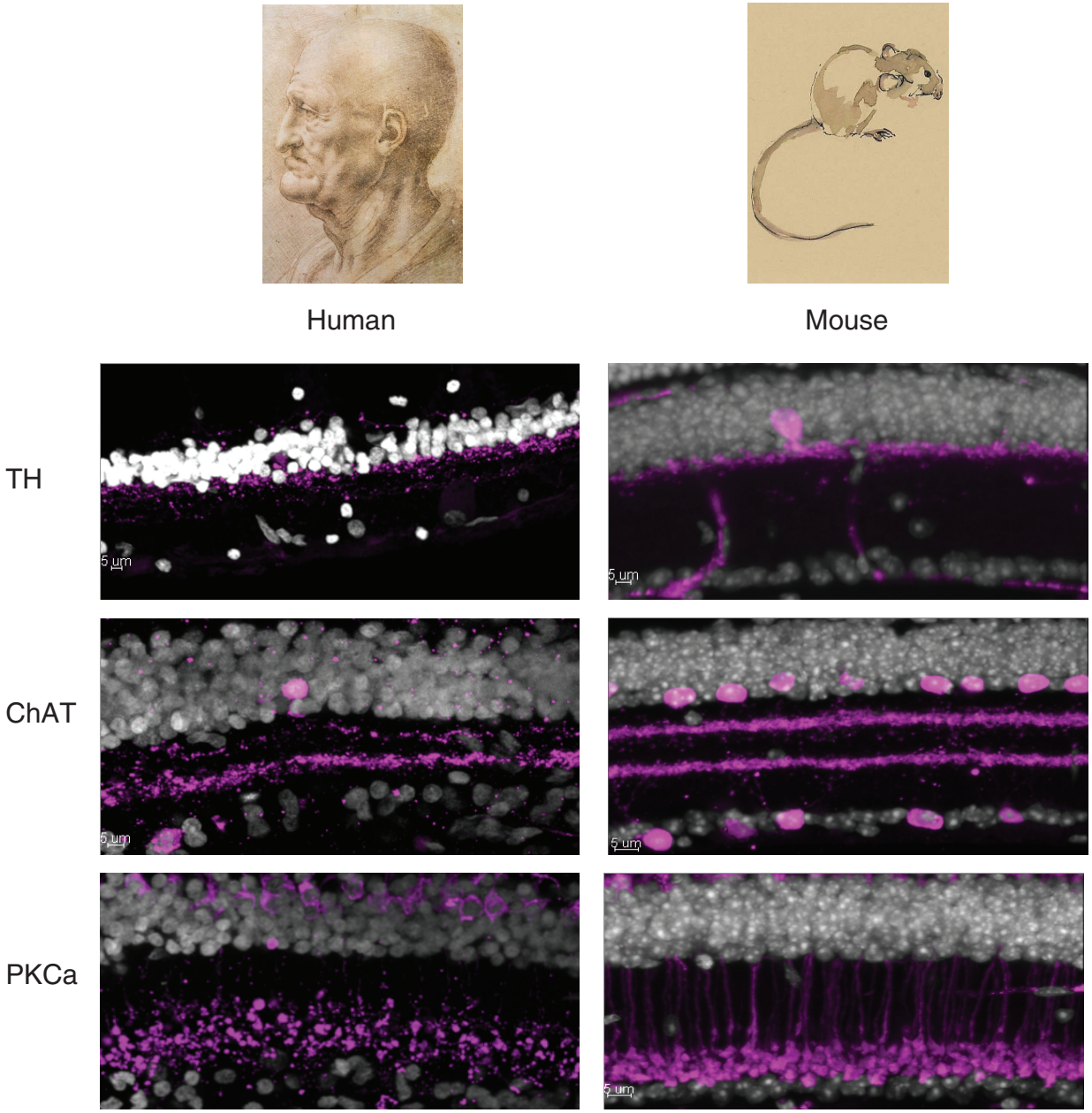

FIGURE 13.5 Comparing the retinas of humans and mice. Vertical sections of human (left) and mouse (right) retinas. Staining with three antibodies against tyrosine hydroxylase (TH), choline acetyl transferase (ChAT), and protein kinase C alpha (PKCa) identifies strata with similar positions in the two species.

Roska & Meister, 2014

Diversity of ganglion cell morphology in macaque retina

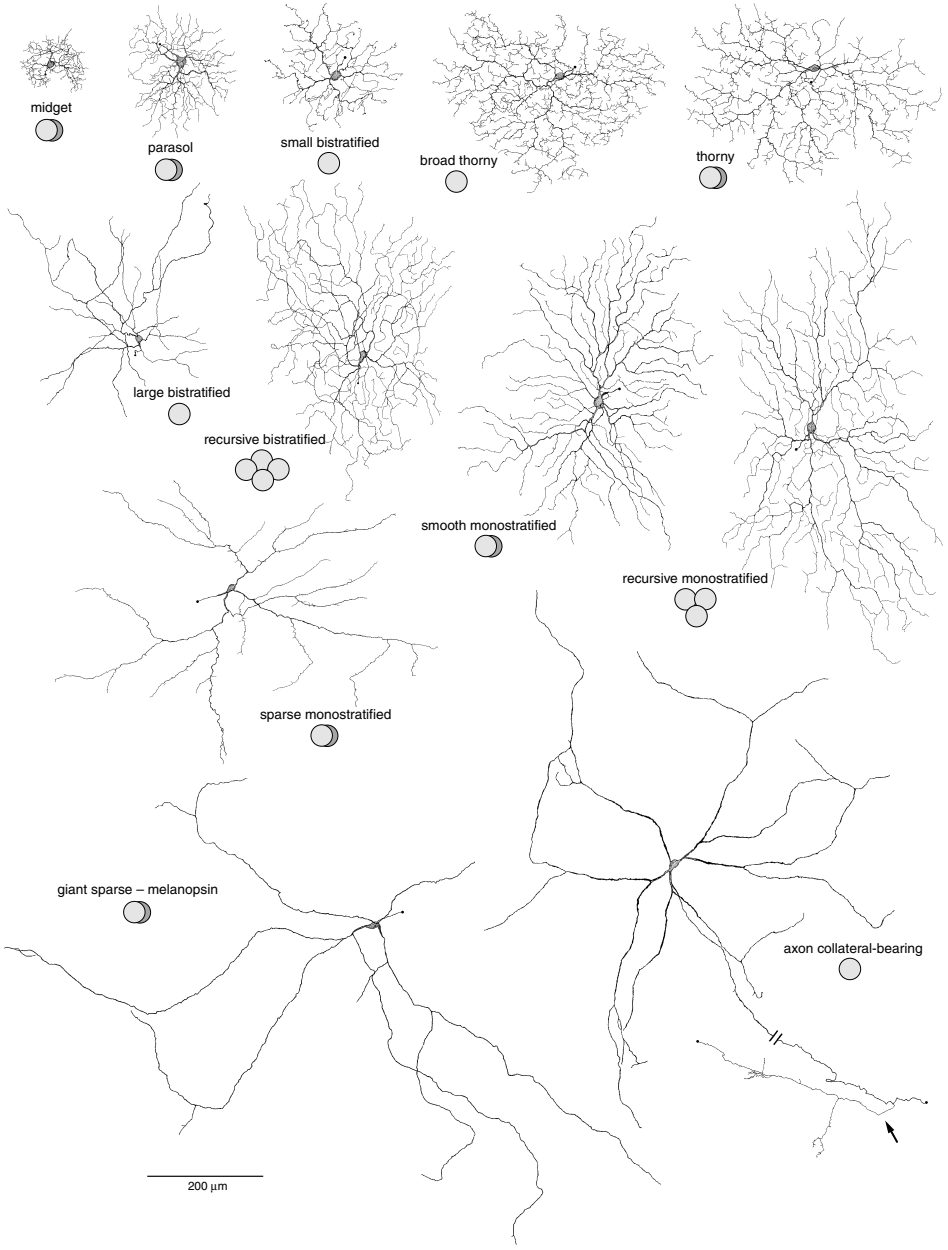

Dacey, 2004

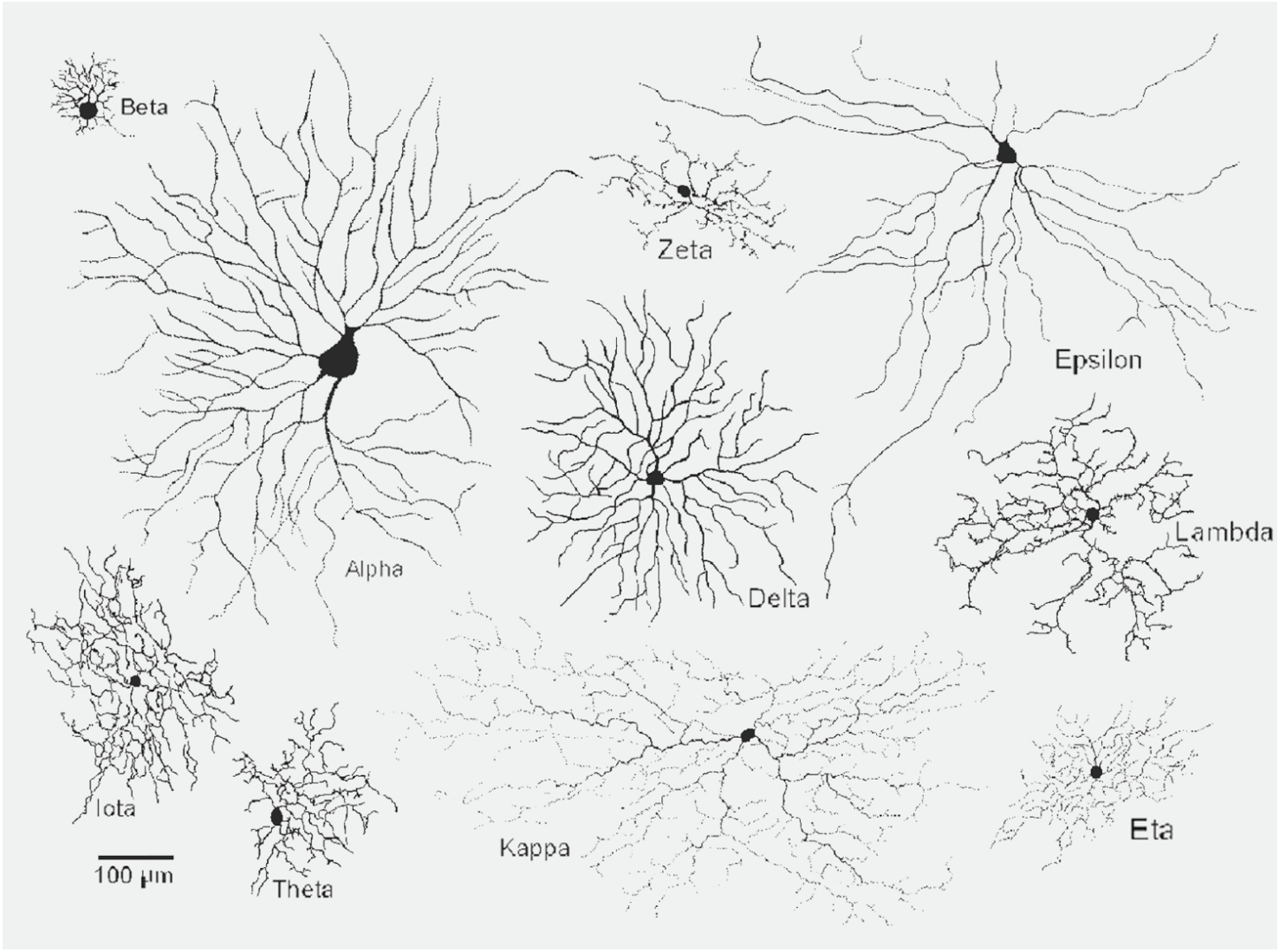

Fig. 5. The types of ganglion cells identified thus far in the retina of the cat. Ongoing work in the rabbit and monkey confirms this diversity, and many of the cells observed are probably homologs of those seen in the cat. Courtesy of D. Berson[77–80].

Masland, 2001

Diversity of ganglion cell morphology in mouse retina

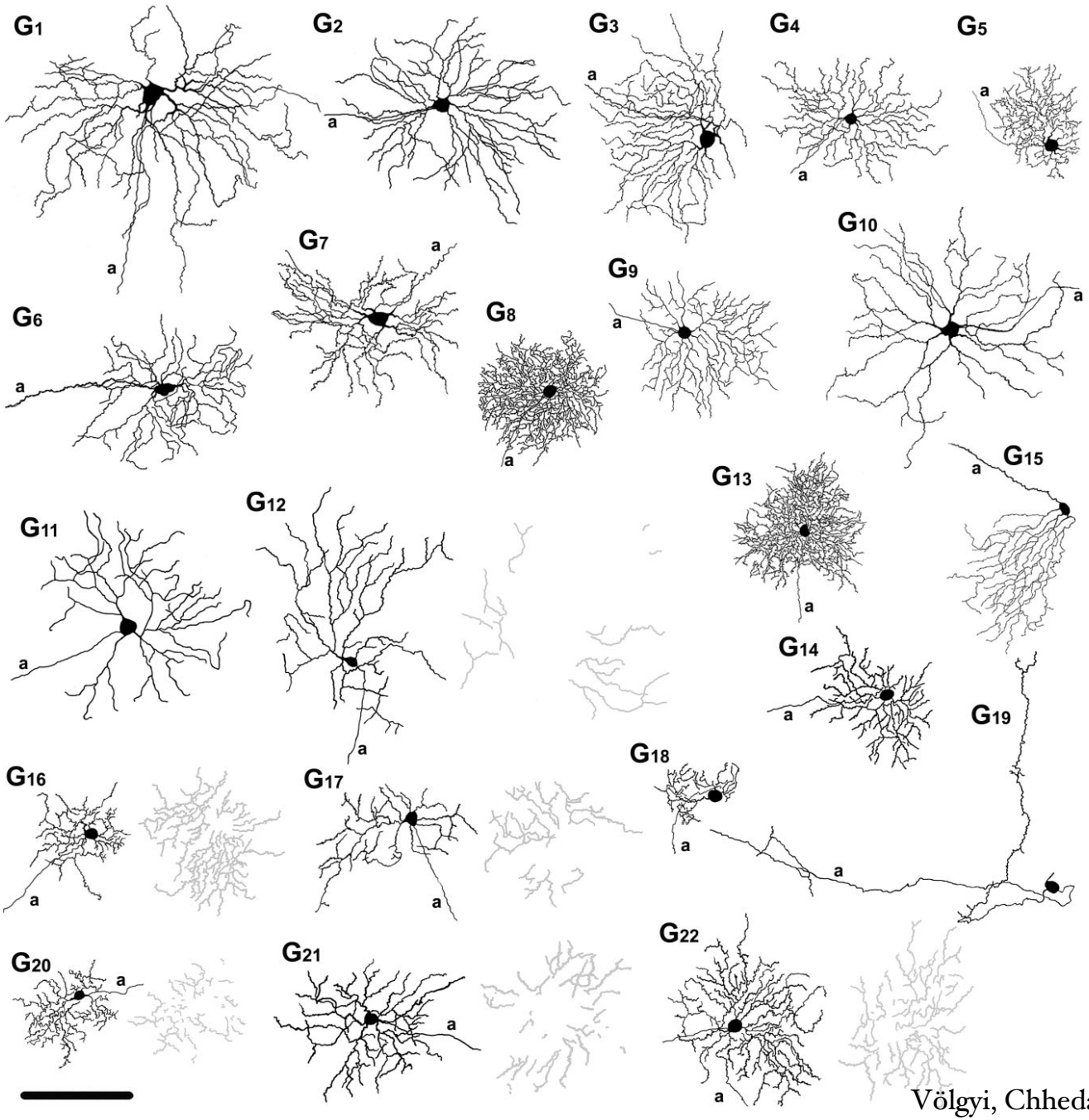

Völgyi, Chheda & Blooomfield, 2009

The distribution of rods and cones in human retina

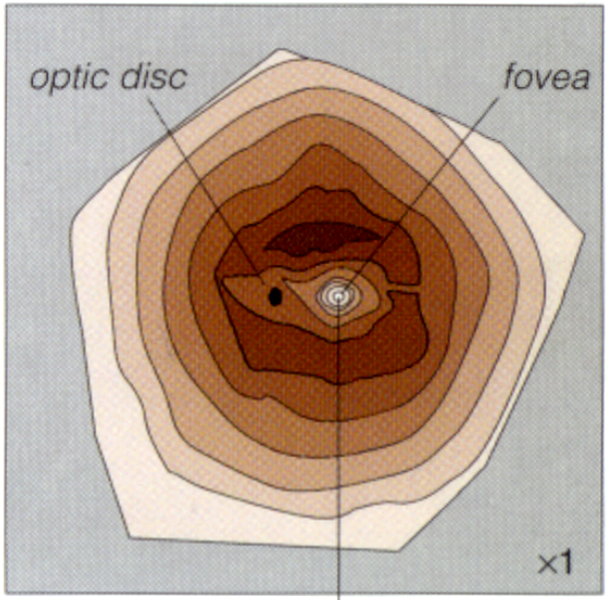

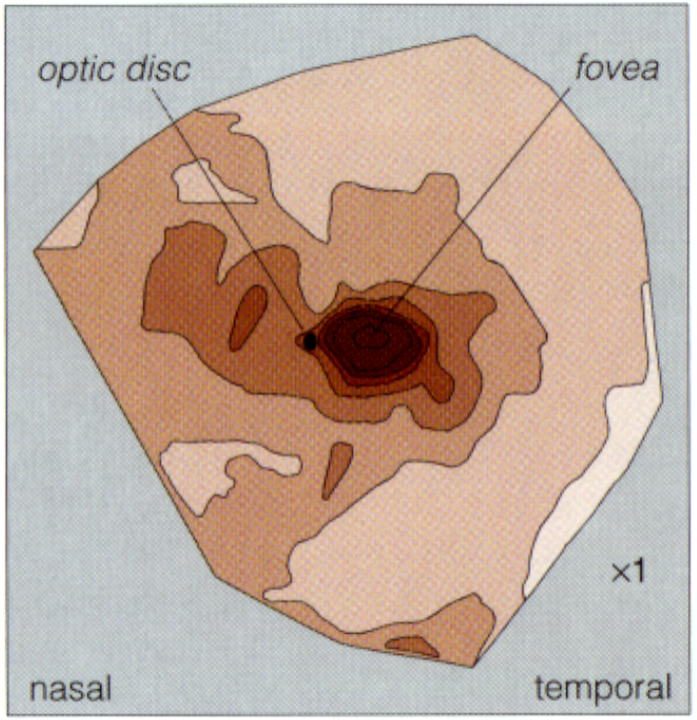

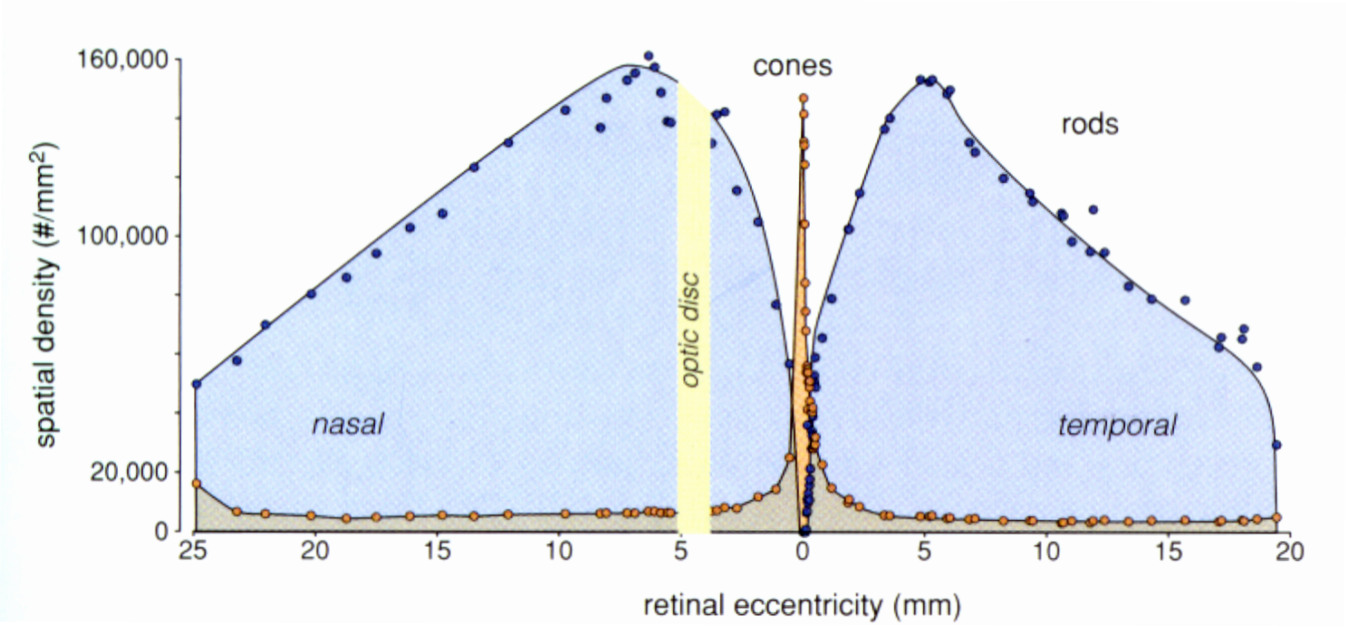

Sampling of visual space by human retinal ganglion cells

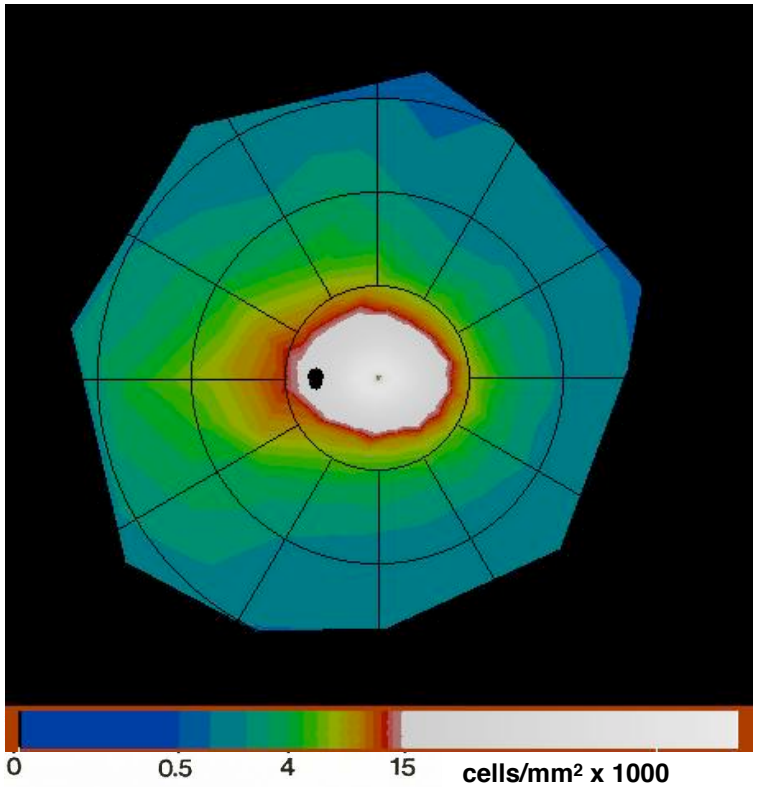

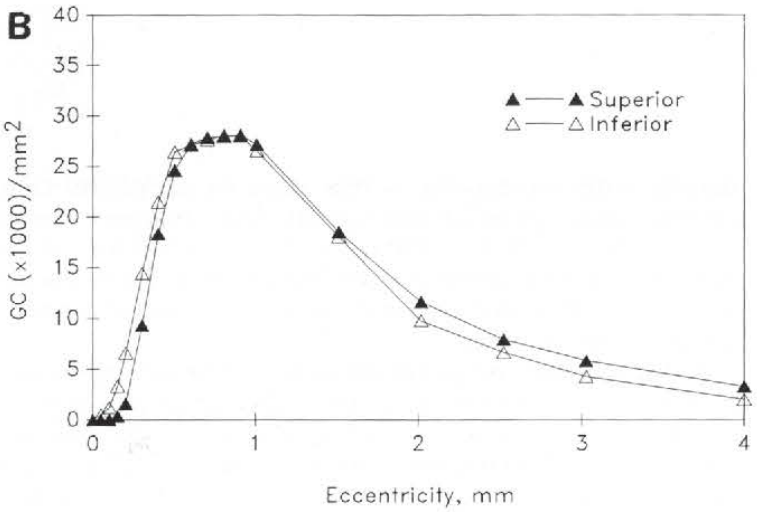

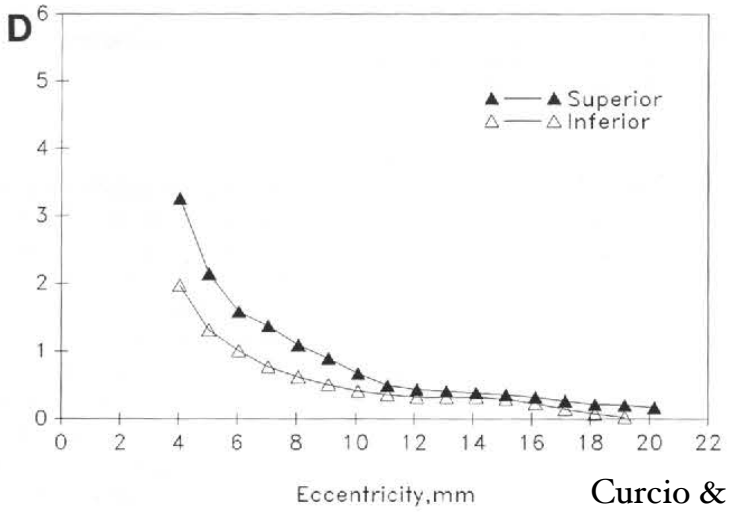

Curcio & Allen, 1990

Sampling of visual space by different mouse ganglion cell types

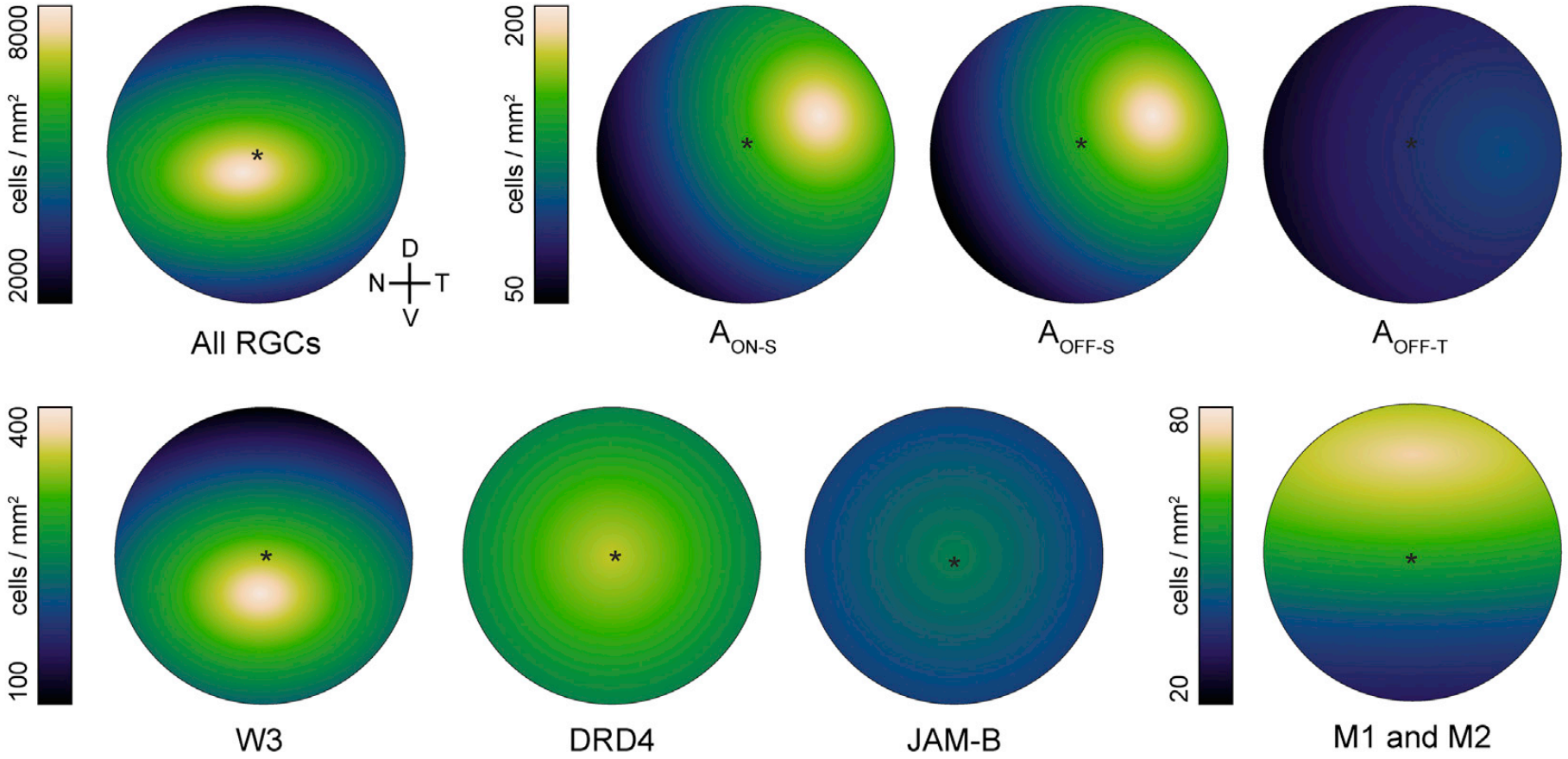

Bleckert et al, 2014

Diversity of ganglion cell morphology in mammalian retina

Icon	Mouse	Rabbit	Cat	Macaque	Properties

A catalog of retinal ganglion cell types in the mammalian retina[a]

Icon	Mouse	Rabbit	Cat	Macaque	Properties
	M1[1,2]			Outer melanopsin[3]	Large sparse dendrites. ON sluggish synaptic response.
	M2[1,2]			Inner melanopsin[3]	Large complex dendrites. ON sluggish synaptic response.
	ON DS temporal[4]	ON DS temporal[5]			ON DS. Preferred direction temporal.
	ON DS ventral,[4] Spig-1 EGFP[6,7]	ON DS ventral[5]			ON DS. Preferred direction ventral.
	ON, DS dorsal[4,6,7]	ON DS dorsal[5]			ON DS. Preferred direction dorsal.
	ON–OFF DS temporal[8]	ON–OFF DS temporal[9]	Theta?[10]	Recursive bistratified?[11]	ON-OFF DS. Preferred direction temporal.
	ON-OFF DS dorsal[8]	ON-OFF DS dorsal[9]	Theta?[10]	Recursive bistratified?[11]	ON-OFF DS. Preferred direction dorsal.
	Drd4-EGFP,[12] W9[8]	ON–OFF, DS nasal[9]	Theta?[10]	Recursive bistratified?[11]	ON-OFF DS. Preferred direction nasal.
	BD-CreER,[8] Hb9-EGFP[13]	ON–OFF, DS ventral[9]	Theta?[10]	Recursive bistratified?[11]	ON-OFF DS. Preferred direction ventral. Asymmetric dendrites in mouse.
	JAM-B[14]	OFF coupled[15], G3[16]			OFF DS. Preferred direction ventral. Highly asymmetric dendrites point ventral.

A catalog of retinal ganglion cell types in the mammalian retina[a] *(Continued)*

Icon	Mouse	Rabbit	Cat	Macaque	Properties
	ON alpha,[17] PV-Cre-1[18]	ON alpha[19]	ON alpha[20,21]		Large dendritic field. ON response.
	PV-Cre-3[18]	ON parasol[15]		ON parasol[22]	Medium dendritic field. ON response.
				ON smooth[23]	
		ON beta[15]	ON beta[24]		Small dendritic field. ON response.
				ON midget[22]	Small dendritic field. ON response.
		OFF beta[15]	OFF beta[24]		Small dendritic field. OFF response.
				OFF midget[22]	Small dendritic field. OFF response.
	PV-Cre-4[18]	OFF parasol[15]	Eta?[25]	OFF parasol[22]	Medium dendritic field. OFF response.
	OFF alpha transient[17], PV-Cre-5[18]	OFF alpha[19]	OFF alpha[24]	OFF smooth[23]	Large dendritic field. OFF response.
	OFF alpha Sustained,[17] PV-Cre-6[18]	OFF delta[15]	OFF delta[10]		Large dendritic field. OFF sustained response.

A catalog of retinal ganglion cell types in the mammalian retina[a] *(Continued)*

Icon	Mouse	Rabbit	Cat	Macaque	Properties
		ON-bistratified?[15]		Small-bistratified[11]	ON excitation, OFF inhibition, blue-yellow opponent in macaque.
				Large-bistratified[11]	Blue-yellow opponent.
	W3[26]	Local edge Detector[5,27]	Zeta[28]	Broad thorny[11]	ON–OFF, strong surround, fast ON–OFF inhibition.
			Epsilon?[29]	Recursive monostratified[11]	
				ON narrow thorny[11]	
				OFF narrow thorny[11]	
		Uniformity Detector[30]	Uniformity Detector[31]		Transiently suppressed by visual stimuli. ON-OFF response. Dendrites just outside the ChAT bands.

[a]Each graphic icon illustrates stratification of the dendritic tree in the IPL, divided into 10 laminae (Siegert et al., 2009). For each type we list the defining morphological and physiological features and identify its plausible correspondences in four species, as supported by the cited literature. For further detail on cross-species comparisons, see Berson (2008). Note that many of these ganglion cell types have only sparse and partial entries, emphasizing the need for future work to round out the catalog of retinal output signals.

References: [1]Hattar et al. (2006). [2]Schmidt et al. (2011b). [3]Dacey et al. (2005). [4]Sun et al. (2006). [5]Barlow, Hill, & Levick (1964), but see Kanjhan & Sivyer (2010) and Hoshi et al. (2011) for finer divisions. [6]Yonehara et al. (2009). [7]Yonehara et al. (2008). [8]Kay et al. (2011). [9]Oyster & Barlow (1967). [10]Isayama, Berson, & Pu (2000). [11]Dacey (2004). [12]Huberman et al. (2009). [13]Trenholm et al. (2011) erroneously identified the preferred direction as temporal. [14]Kim et al. (2008). [15]Roska, Molnar, & Werblin (2006). [16]Hoshi et al. (2011). [17]Pang, Gao, & Wu (2003). [18]Münch et al. (2009). [19]Zhang et al. (2005). [20]Cleland, Levick, & Wässle (1975). [21]Wässle, Peichl, & Boycott (1981). [22]Dacey & Packer (2003). [23]Crook et al. (2008). [24]Wässle, Boycott, & Illing (1981). [25]Berson, Isayama, & Pu (1999). [26]Kim et al. (2010). [27]van Wyk, Taylor, & Vaney (2006). [28]Berson, Pu, & Famiglietti (1998). [29]Pu, Berson, & Pan (1994). [30]Sivyer & Vaney (2010). [31]Cleland & Levick (1974).

Roska and Meister, 2014

Morphology, mosaics and targets of diverse ganglion cell populations in macaque retina: approaching a complete account

D.M. Dacey, H.R. Joo, B.B. Peterson, T.J. Haun
Department of Biological Structure, University of Washington, Seattle WA

Purpose

Our goal is a complete description of primate visual pathway origins, providing an anatomical basis for targeted physiological analysis, dissection of underlying circuitry and for making trans-species comparisons, most notably with the mouse, for which transgenic technology offers increasing access to retinal pathways.

Methods

To observe the morphology of macaque ganglion cells we used the 'fireworks' photostaining technique (Dacey et al., Neuron 2003, 37:15) from central tracer injections made into the lateral geniculate nucleus (LGN) or the superior colliculus-pretectum. Fireworks staining completely reveals the dendritic trees of large numbers of retrogradely labeled ganglion cells. In this way we can measure type-specific stratification depth in the inner plexiform layer and relative density from the mosaics formed by overlapping dendritic trees of the same type. (Right: photostained cells retrogradely tracer labeled from injections in the superior colliculus.)

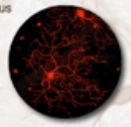

Smooth monostratified

inner ON-center and outer OFF-center types
transient, achromatic, Y-cell receptive field*

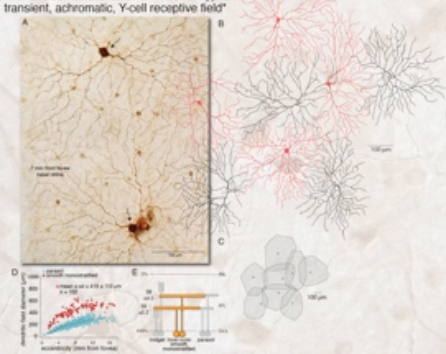

Smooth monostratified cells comprise ~2.5% of total ganglion cells (coverage: inner cells 1.4; outer cells 1.4) and project to the LGN, superior colliculus and pretectum. **A**. Photomicrograph of two smooth cells intracellularly injected with Neurobiotin and processed for HRP histochemistry. The smooth cells are tracer coupled to a population of small- bodied amacrine cells. **B**. Tracings of 8 inner smooth cells ~7 mm from the fovea, tracer labeled from injections in the superior colliculus and processed for HRP histochemistry. **C**. Outlines of the overlapping dendritic fields of the 8 cells shown in *B*. **D**. Dendritic field diameter plotted as a function of eccentricity. **E**. Mean dendritic stratification measured in wholemount retina and plotted as percentage depth in the IPL (inner smooth/parasol cell pairs, n = 4; outer smooth/parasol cell pairs, n = 20). (GCL: ganglion cell layer; IPL: inner plexiform layer; INL: inner nuclear layer.)

*Crook et al., J Neurosci 2008, 28(48):12654

Parasol

inner ON-center and outer OFF-center types
primate correlate of the alpha Y-cell*

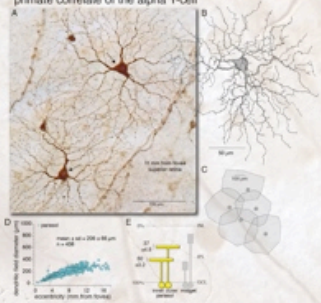

Parasol cells comprise ~14% of total ganglion cells (coverage: inner cells 1.9; outer cells 1.6) and project to the LGN, superior colliculus and pretectum. **A**. Photomicrograph of two photostained cells tracer labeled from injections in the superior colliculus and reacted for HRP histochemistry. **B**. Tracing of an inner parasol cell 8.7 mm from the fovea (dendritic field diameter = 213 µm). Arrow indicates axon. **C**. Outlines of the overlapping dendritic fields of 5 neighboring outer parasol cells ~6 mm from the fovea. **D**. Dendritic field diameter plotted as a function of eccentricity. **E**. Mean dendritic stratification measured in wholemount retina and plotted as percentage depth in the IPL (inner cells, n = 36; outer cells, n = 20).

*Crook et al., J Neurosci 2008, 28(44):11277

Midget

inner ON-center and outer OFF-center types

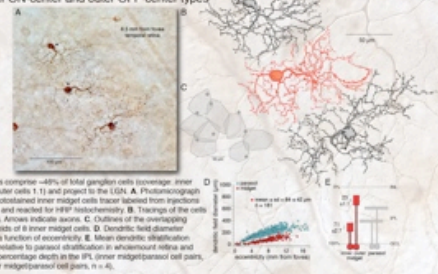

Midget cells comprise ~48% of total ganglion cells (coverage: inner cells 1.1; outer cells 1.1) and project to the LGN. **A**. Photomicrograph of three photostained inner midget cells tracer labeled from injections in the LGN and reacted for HRP histochemistry. **B**. Tracings of the cells shown in *A*. Arrows indicate axons. **C**. Outlines of the overlapping dendritic fields of 8 inner midget cells. **D**. Dendritic field diameter plotted as a function of eccentricity. **E**. Mean dendritic stratification measured relative to parasol stratification in wholemount retina and plotted as percentage depth in the IPL (inner midget/parasol cell pairs, n = 4; outer midget/parasol cell pairs, n = 4).

Small bistratified

'blue-ON' cell; S vs LM cone opponency

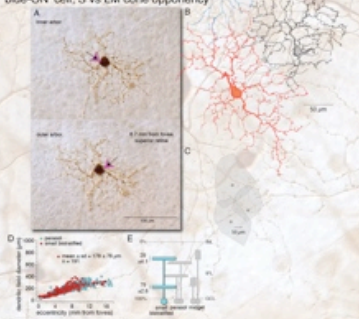

Small bistratified cells make up ~8% of total ganglion cells (coverage = 1.6) and project to the LGN. **A**. Photomicrographs of a small bistratified cell intracellularly injected with Neurobiotin and processed for HRP histochemistry, with the focus on the inner (upper) and outer (lower) dendritic arbors. **B**. Tracings of the inner arbors of 3 neighboring small bistratified cells ~0.8 mm from the fovea, tracer labeled from injections in the LGN and processed for HRP histochemistry. Overlapping dendrites show cofasciculation. Arrows indicate axons. **C**. Outlines of the overlapping dendritic fields of the 3 cells shown in *B*. **D**. Dendritic field diameter plotted as a function of eccentricity. **E**. Mean dendritic stratification measured relative to parasol stratification in wholemount retina and plotted as percentage depth in the IPL (parasol/small bistratified pairs: n = 11).

Large bistratified

second type of S-opponent 'blue-ON' cell

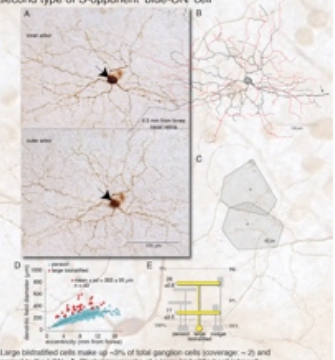

Large bistratified cells make up ~3% of total ganglion cells (coverage: ~ 2) and project to the LGN. **A**. Photomicrographs of a large bistratified cell intracellularly injected with Neurobiotin and processed for HRP histochemistry. Focus is on the inner (upper) and outer (lower) dendritic arbors. **B**. Tracing of the same cell shown in *A*. Outer dendritic arbor is shown in red. Arrow indicates axon. **C**. Outlines of the dendritic fields of two neighboring large bistratified cells with overlapping dendritic fields. **D**. Dendritic field diameter plotted as a function of eccentricity. **E**. Mean dendritic stratification measured relative to parasol stratification in wholemount retina and plotted as percentage depth in the IPL (parasol/large bistratified cell pairs: n = 5).

Recursive bistratified

primate candidate for the ON-OFF direction selective type

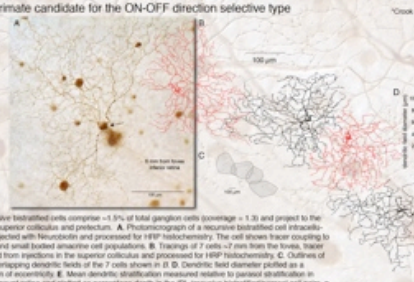

Recursive bistratified cells comprise ~1.5% of total ganglion cells (coverage = 1.3) and project to the LGN, superior colliculus and pretectum. **A**. Photomicrograph of a recursive bistratified cell intracellularly injected with Neurobiotin and processed for HRP histochemistry. The cell shows tracer coupling to large and small bodied amacrine cell populations. **B**. Tracings of 7 cells ~7 mm from the fovea, tracer labeled from injections in the superior colliculus and processed for HRP histochemistry. **C**. Outlines of the overlapping dendritic fields of the 7 cells shown in *B*. **D**. Dendritic field diameter plotted as a function of eccentricity. **E**. Mean dendritic stratification measured relative to parasol stratification in wholemount retina and plotted as percentage depth in the IPL (recursive bistratified/parasol cell pairs, n = 3).

Narrow thorny

inner and outer types, transient, achromatic

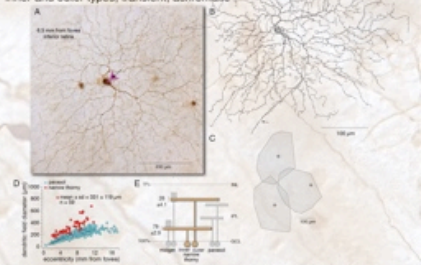

Narrow thorny cells comprise ~3% of total ganglion cells (coverage: inner cells 1.0; outer cells 1.0) and project to the LGN, superior colliculus and pretectum. **A**. Photomicrograph of an outer narrow thorny cell intracellularly injected with Neurobiotin and processed for HRP histochemistry. **B**. Tracing of the same cell shown in *A*. Arrow indicates axon. **C**. Outlines of the overlapping dendritic fields of 3 neighboring outer narrow thorny cells tracer labeled from injections in the superior colliculus. **D**. Dendritic field diameter plotted as a function of eccentricity. **E**. Mean dendritic stratification measured relative to parasol stratification in wholemount retina and plotted as percentage depth in the IPL (inner narrow thorny/parasol cell pairs, n = 4; outer narrow thorny/parasol cell pairs, n = 4).

Melanopsin-expressing

inner and outer types, inherently photosensitive; S-OFF opponency

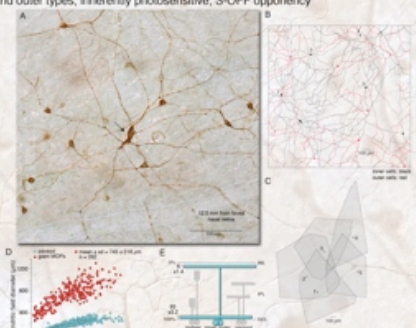

Giant melanopsin cells comprise ~1% of total ganglion cells (coverage: inner cells 1.5; outer cells 2.0) and project to the LGN, superior colliculus and pretectum. **A**. Photomicrograph of a giant melanopsin cell intracellularly injected with Neurobiotin and processed for HRP histochemistry. The cell shows tracer coupling to several populations of amacrine cells. **B**. Tracings of 7 inner (black) and 8 outer (red) giant cells ~10 mm from the fovea, melanopsin immunolabeled and processed for HRP histochemistry. **C**. Outlines of the overlapping dendritic fields of 5 inner giant cells. Numbers correspond to cells shown in *B*. **D**. Dendritic field diameter plotted as a function of eccentricity. **E**. Mean dendritic stratification measured relative to parasol stratification in wholemount retina and plotted as percentage depth in the IPL (inner giant melanopsin/parasol cell pairs, n = 3; outer giant melanopsin/parasol cell pairs, n = 5).

Broad thorny

ON-OFF receptive field
primate candidate for the local edge detector

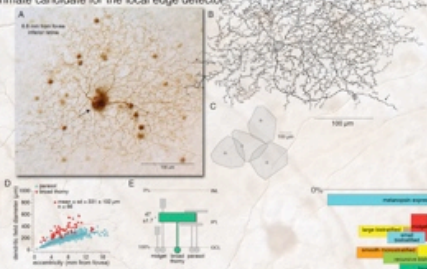

Broad thorny cells make up ~1.5% of total ganglion cells (coverage = 1.2) and project to the LGN, superior colliculus and pretectum. **A**. Photomicrograph of a broad thorny cell intracellularly injected with Neurobiotin and processed for HRP histochemistry. **B**. Tracing of the same cell shown in *A*. Arrow indicates axon. **C**. Outlines of the overlapping dendritic fields of 4 neighboring broad thorny cells ~5 mm from the fovea, tracer labeled from injections in the superior colliculus. **D**. Dendritic field diameter plotted as a function of eccentricity. **E**. Mean dendritic stratification measured relative to parasol stratification in wholemount retina and plotted as percentage depth in the IPL (broad thorny/parasol cell pairs: n = 8).

Recursive monostratified

primate candidate for the ON direction selective type

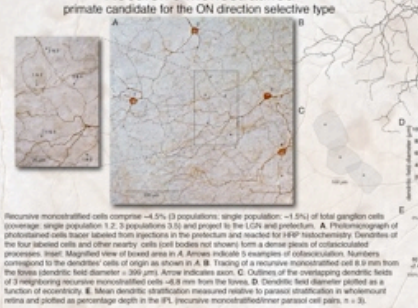

Recursive monostratified cells comprise ~4.5% (3 populations; single population: ~1.5%) of total ganglion cells (coverage: single population 1.2; 3 populations 3.5) and project to the LGN and pretectum. **A**. Photomicrograph of photostained cells tracer labeled from injections in the pretectum and reacted for HRP histochemistry. Dendrites of the four labeled cells and other nearby cells (cell bodies not shown) form a dense plexus of collasiculated processes. Inset: Magnified view of boxed area in *A*. Arrows indicate 5 examples of collasiculation. Numbers correspond to the dendrites' cells of origin as shown in *B*. **B**. Tracing of a recursive monostratified cell 6.9 mm from the fovea (dendritic field diameter = 366 µm). Arrow indicates axon. **C**. Outlines of the overlapping dendritic fields of 3 neighboring recursive monostratified cells ~6.8 mm from the fovea. **D**. Dendritic field diameter plotted as a function of eccentricity. **E**. Mean dendritic stratification measured relative to parasol stratification in wholemount retina and plotted as percentage depth in the IPL (recursive monostratified/inner parasol cell pairs, n = 3).

Conclusions

- The 17 cell populations shown here represent ~ 85% of the total number of ganglion cells.*
- At least 3 other cell types have been identified:
  axon collateral-bearing ganglion cells
  (Peterson & Dacey, Vis Neurosci 1998, 15:377)
  large, sparsely branched monostratified cells
  (inner and outer types).
- Taken together, and assuming ~ 2% density for the remaining 3 cell types, the 20 types account for ~ 90% of the ganglion cells. If multiple ON-OFF direction selective mosaics exist in primate (as found in other mammals) another ~5% would be accounted for.

*Total ganglion cell density is from Wässle et al., Nature 1989, 341:643. Density estimates for individual cell types were derived from the mosaics.

Schematic summary of dendritic stratification. Lengths of colored bars are proportional to dendritic field diameter for each cell type relative to parasol cell diameter. Vertical positioning of each bar is centered on the mean stratification depth for that cell type (values not shown). Widths of the bars are arbitrary for all cell types except midget and broad thorny cells, where it represents the mean innermost and outermost dendrites for these broadly stratifying cell types.

Midget

inner ON-center and outer OFF-center types

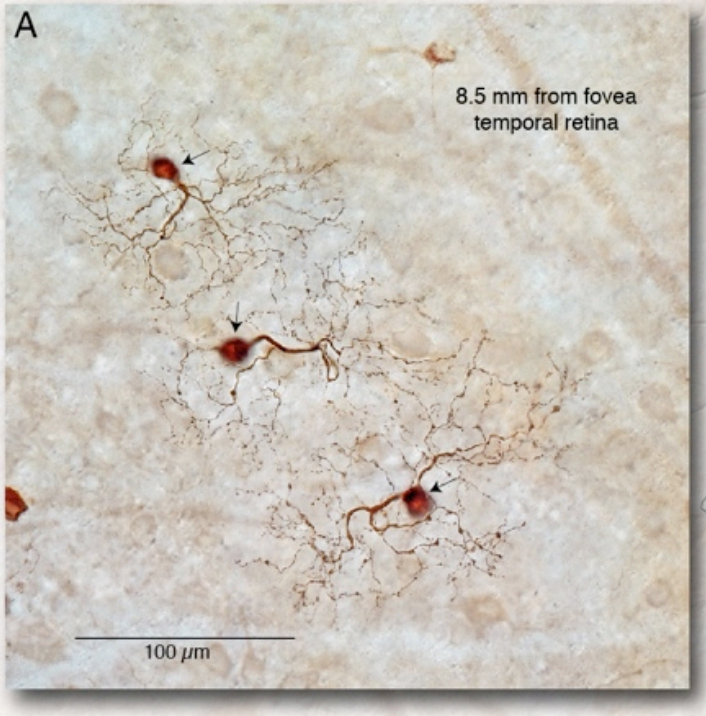

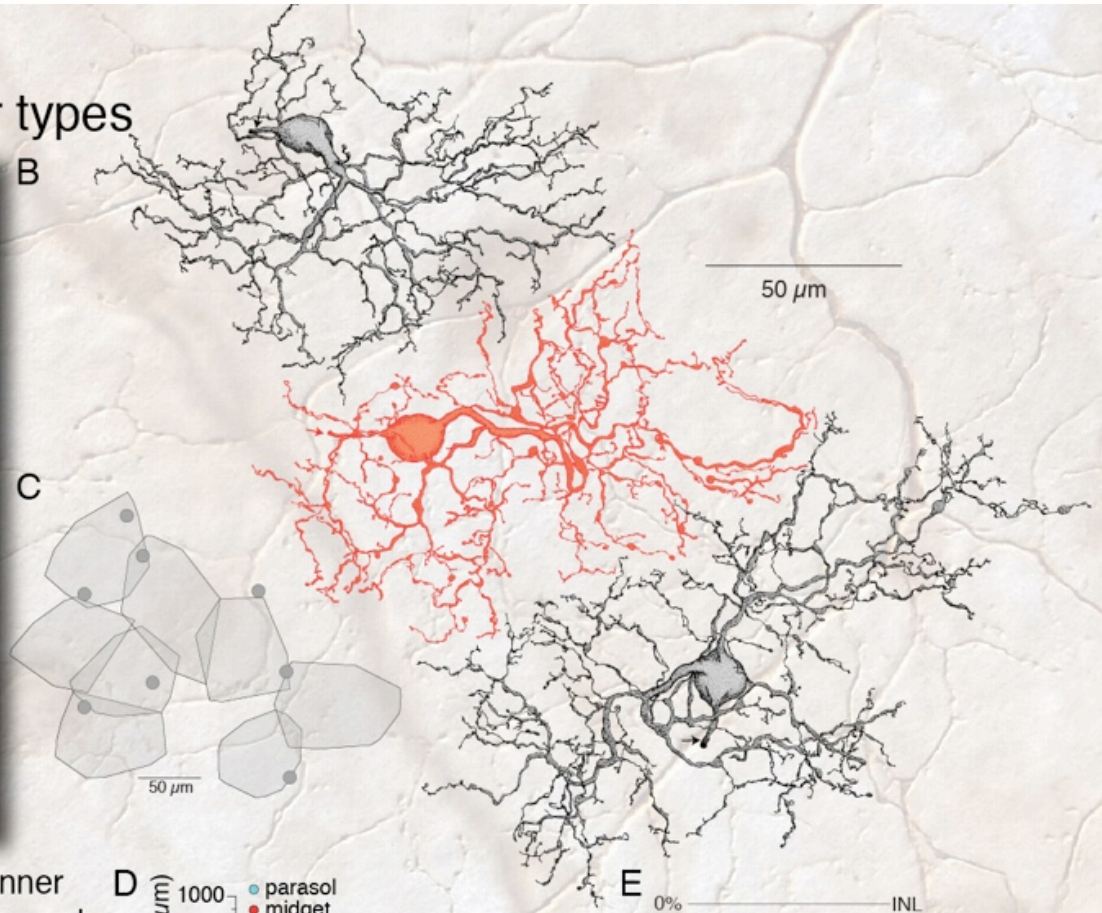

Midget cells comprise ~46% of total ganglion cells (coverage: inner cells 1.1; outer cells 1.1) and project to the LGN. **A**. Photomicrograph of three photostained inner midget cells tracer labeled from injections in the LGN and reacted for HRP histochemistry. **B**. Tracings of the cells shown in *A*. Arrows indicate axons. **C**. Outlines of the overlapping dendritic fields of 8 inner midget cells. **D**. Dendritic field diameter plotted as a function of eccentricity. **E**. Mean dendritic stratification measured relative to parasol stratification in wholemount retina and plotted as percentage depth in the IPL (inner midget/parasol cell pairs, n = 4; outer midget/parasol cell pairs, n = 4).

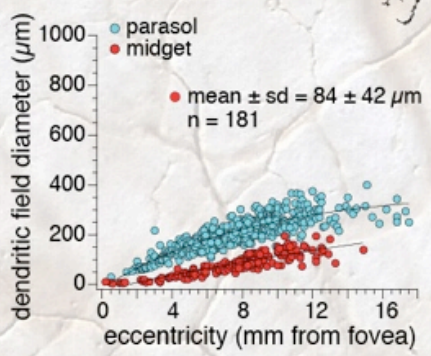

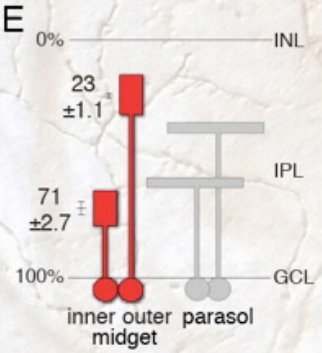

Parasol

inner ON-center and outer OFF-center types
primate correlate of the alpha Y-cell*

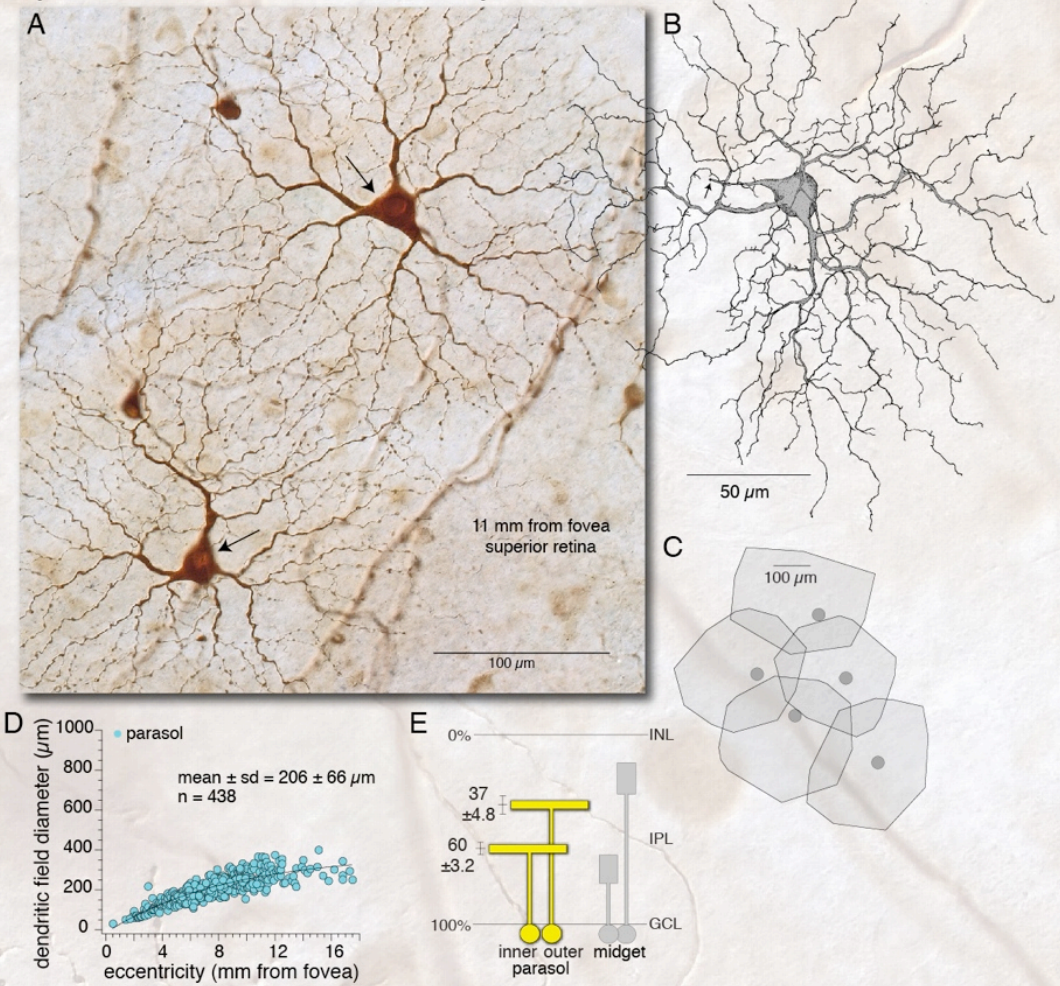

Parasol cells comprise ~14% of total ganglion cells (coverage: inner cells 1.9; outer cells 1.6) and project to the LGN, superior colliculus and pretectum. **A**. Photomicrograph of two photostained cells tracer labeled from injections in the superior colliculus and reacted for HRP histochemistry. **B**. Tracing of an inner parasol cell 8.7 mm from the fovea (dendritic field diameter = 213 μm). Arrow indicates axon. **C**. Outlines of the overlapping dendritic fields of 5 neighboring outer parasol cells ~6 mm from the fovea. **D**. Dendritic field diameter plotted as a function of eccentricity. **E**. Mean dendritic stratification measured in wholemount retina and plotted as percentage depth in the IPL (inner cells, n = 36; outer cells, n = 20).

*Crook et al., J Neurosci 2008, 28(44):11277

Smooth monostratified

inner ON-center and outer OFF-center types
transient, achromatic, Y-cell receptive field*

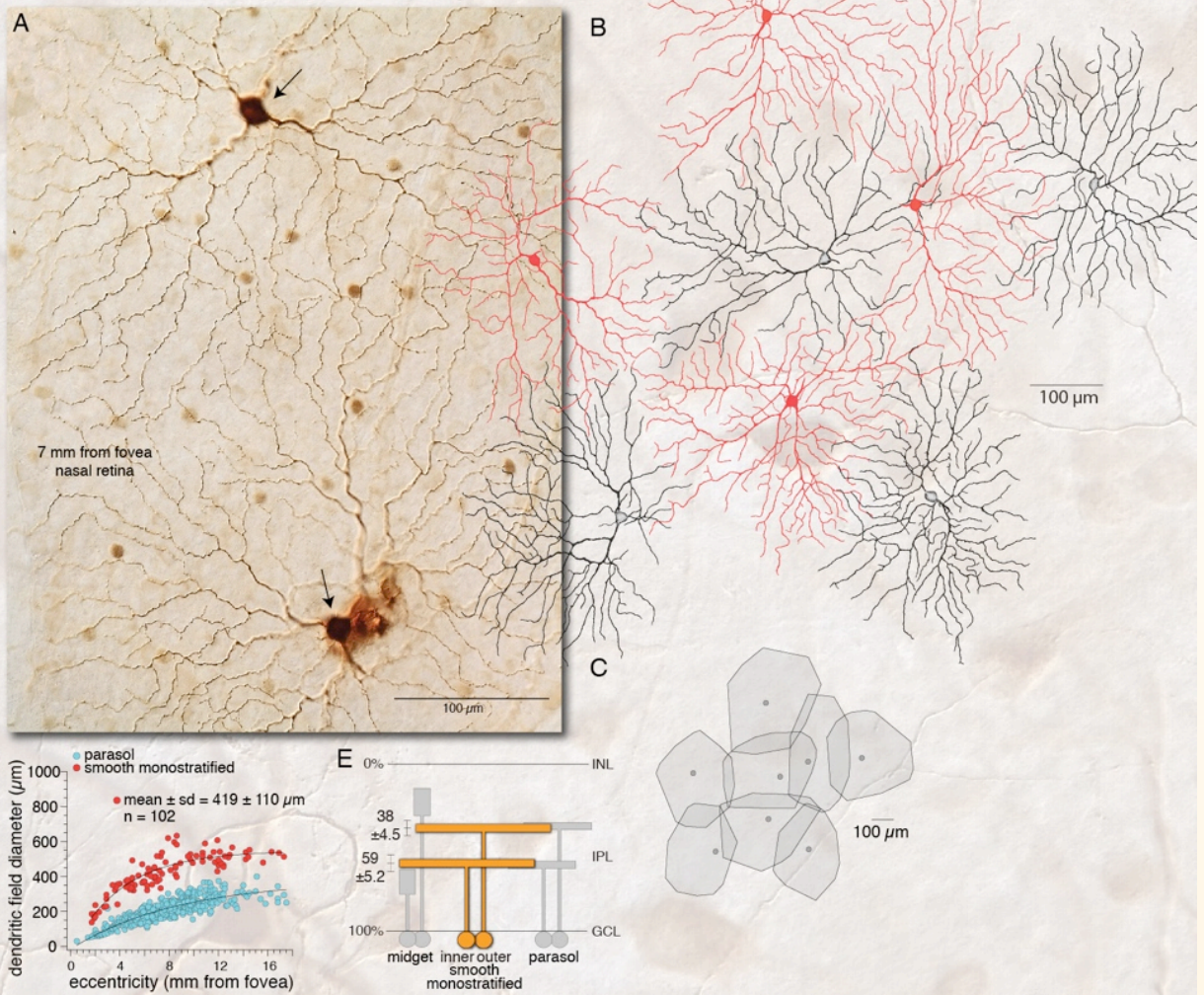

Smooth monostratified cells comprise ~2.5% of total ganglion cells (coverage: inner cells 1.4; outer cells 1.4) and project to the LGN, superior colliculus and pretectum. **A**. Photomicrograph of two smooth cells intracellularly injected with Neurobiotin and processed for HRP histochemistry. The smooth cells are tracer coupled to a population of small bodied amacrine cells. **B**. Tracings of 8 inner smooth cells ~7 mm from the fovea, tracer labeled from injections in the superior colliculus and processed for HRP histochemistry. **C**. Outlines of the overlapping dendritic fields of the 8 cells shown in *B*. **D**. Dendritic field diameter plotted as a function of eccentricity. **E**. Mean dendritic stratification measured relative to parasol stratification in wholemount retina and plotted as percentage depth in the IPL (inner smooth/parasol cell pairs, n = 4; outer smooth/parasol cell pairs, n = 20). (GCL, ganglion cell layer; IPL, inner plexiform layer; INL, inner nuclear layer.)

*Crook et al., J Neurosci 2008, 28(48):12654

Recursive monostratified

primate candidate for the ON direction selective type

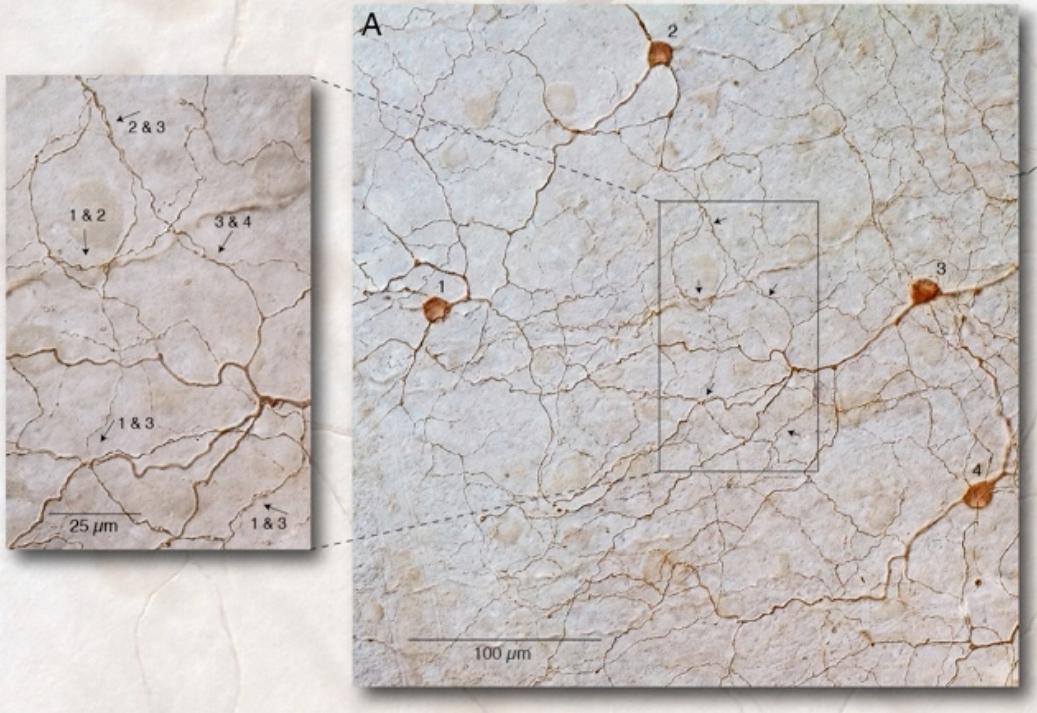

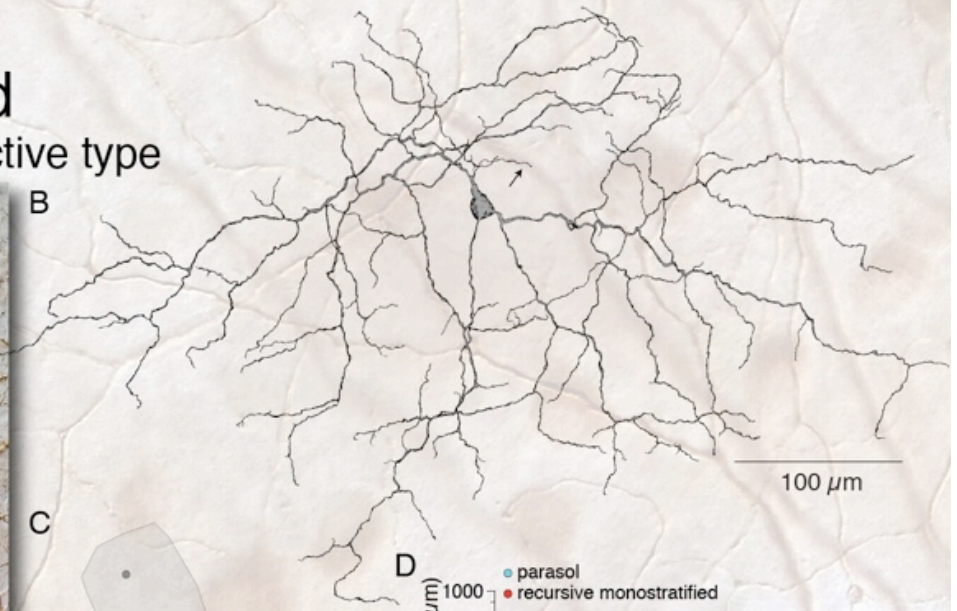

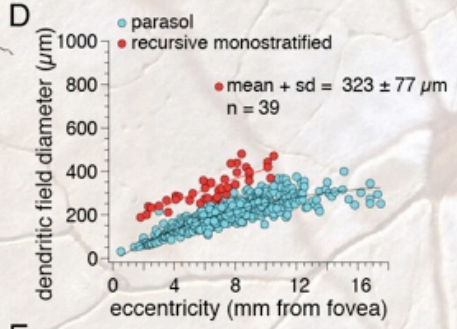

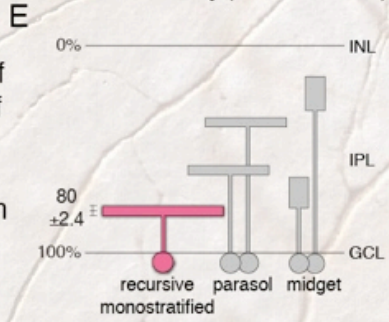

Recursive monostratified cells comprise ~4.5% (3 populations; single population: ~1.5%) of total ganglion cells (coverage: single population 1.2; 3 populations 3.5) and project to the LGN and pretectum. **A**. Photomicrograph of photostained cells tracer labeled from injections in the pretectum and reacted for HRP histochemistry. Dendrites of the four labeled cells and other nearby cells (cell bodies not shown) form a dense plexis of cofasciculated processes. Inset: Magnified view of boxed area in *A*. Arrows indicate 5 examples of cofasciculation. Numbers correspond to the dendrites' cells of origin as shown in *A*. **B**. Tracing of a recursive monostratified cell 8.9 mm from the fovea (dendritic field diameter = 399 μm). Arrow indicates axon. **C**. Outlines of the overlapping dendritic fields of 3 neighboring recursive monostratified cells ~6.8 mm from the fovea. **D**. Dendritic field diameter plotted as a function of eccentricity. **E**. Mean dendritic stratification measured relative to parasol stratification in wholemount retina and plotted as percentage depth in the IPL (recursive monostratified/inner parasol cell pairs, n = 3).

Recursive bistratified

primate candidate for the ON-OFF direction selective type

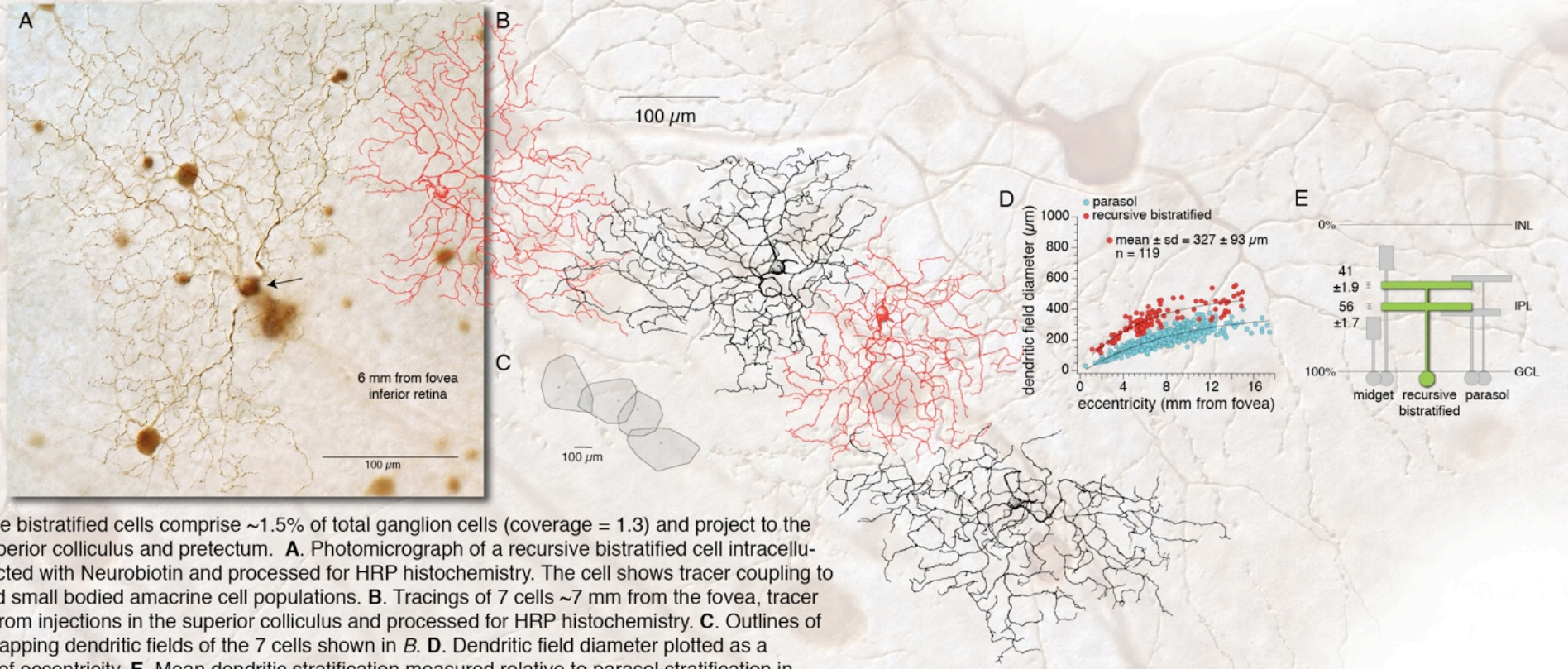

Recursive bistratified cells comprise ~1.5% of total ganglion cells (coverage = 1.3) and project to the LGN, superior colliculus and pretectum. **A**. Photomicrograph of a recursive bistratified cell intracellularly injected with Neurobiotin and processed for HRP histochemistry. The cell shows tracer coupling to large and small bodied amacrine cell populations. **B**. Tracings of 7 cells ~7 mm from the fovea, tracer labeled from injections in the superior colliculus and processed for HRP histochemistry. **C**. Outlines of the overlapping dendritic fields of the 7 cells shown in *B*. **D**. Dendritic field diameter plotted as a function of eccentricity. **E**. Mean dendritic stratification measured relative to parasol stratification in wholemount retina and plotted as percentage depth in the IPL (recusive bistratified/parasol cell pairs, n = 3).

Small bistratified

‘blue-ON’ cell; S vs LM cone opponency

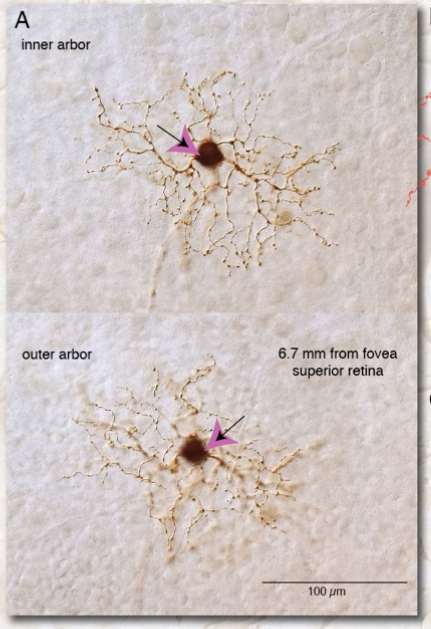

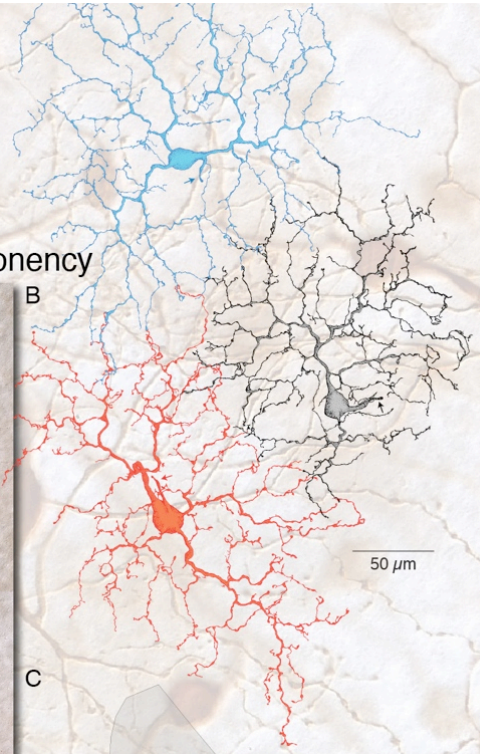

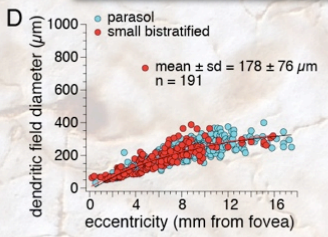

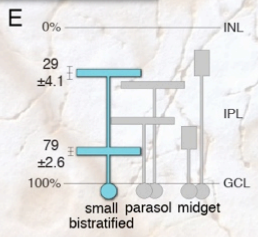

Small bistratified cells make up ~6% of total ganglion cells (coverage = 1.6) and project to the LGN. **A**. Photomicrographs of a small bistratified cell intracellularly injected with Neurobiotin and processed for HRP histochemistry, with the focus on the inner (upper) and outer (lower) dendritic arbors. **B**. Tracings of the inner arbors of 3 neighboring small bistratified cells ~9.8 mm from the fovea, tracer labeled from injections in the LGN and processed for HRP histochemistry. Overlapping dendrites show cofasciculation. Arrows indicate axons. **C**. Outlines of the overlapping dendritic fields of the 3 cells shown in *B*. **D**. Dendritic field diameter plotted as a function of eccentricity. **E**. Mean dendritic stratification measured relative to parasol stratification in wholemount retina and plotted as percentage depth in the IPL (parasol/small bistratified pairs: n = 11).

Large bistratified

second type of S-opponent 'blue-ON' cell

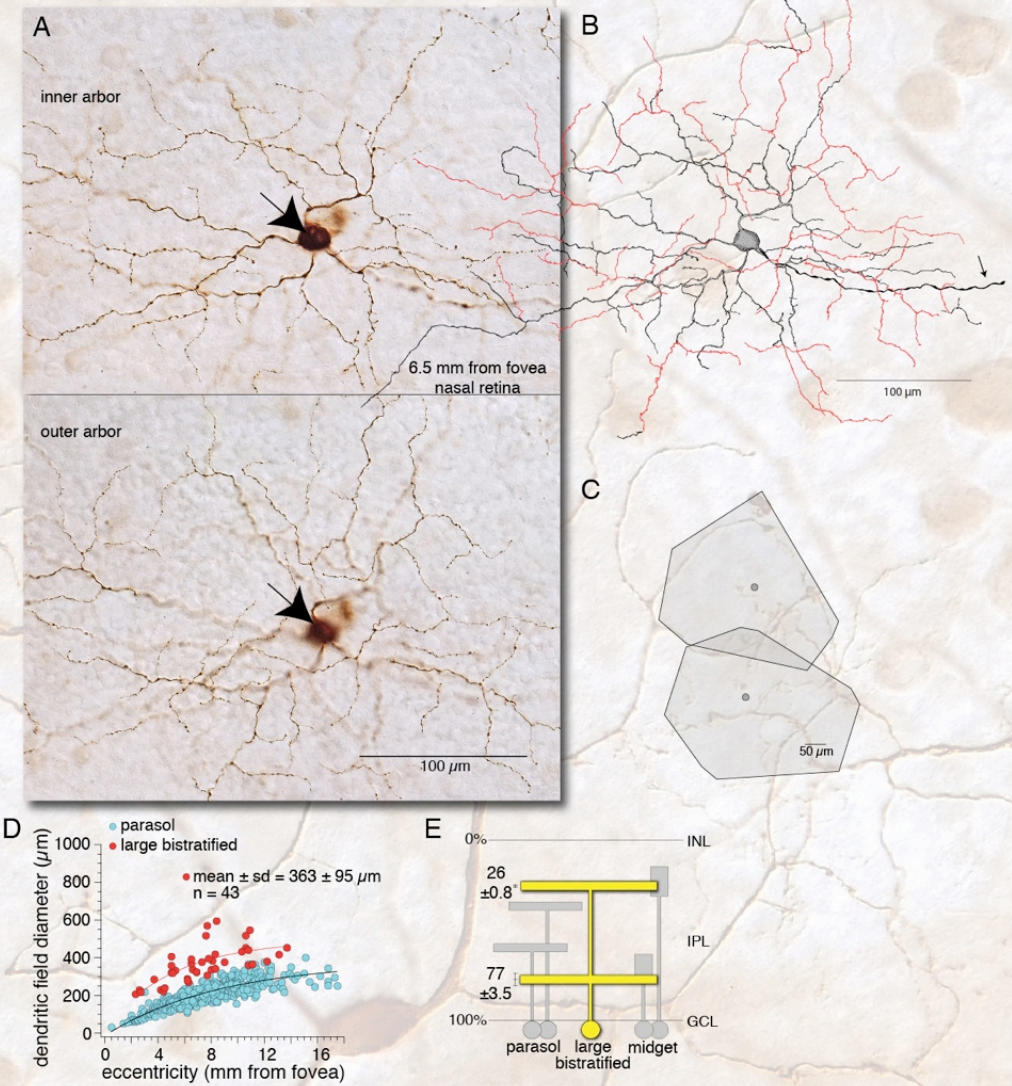

Large bistratified cells make up ~3% of total ganglion cells (coverage: ~ 2) and project to the LGN. **A**. Photomicrographs of a large bistratified cell intracellularly injected with Neurobiotin and processed for HRP histochemistry. Focus is on the inner (upper) and outer (lower) dendritic arbors. **B**. Tracing of the same cell shown in *A*. Outer dendritic arbor is shown in red. Arrow indicates axon. **C**. Outlines of the dendritic fields of two neighboring large bistratified cells with overlapping dendritic fields. **D**. Dendritic field diameter plotted as a function of eccentricity. **E**. Mean dendritic stratification measured relative to parasol stratification in wholemount retina and plotted as percentage depth in the IPL (parasol/large bistratified cell pairs: n = 5).

Narrow thorny

inner and outer types, transient, achromatic

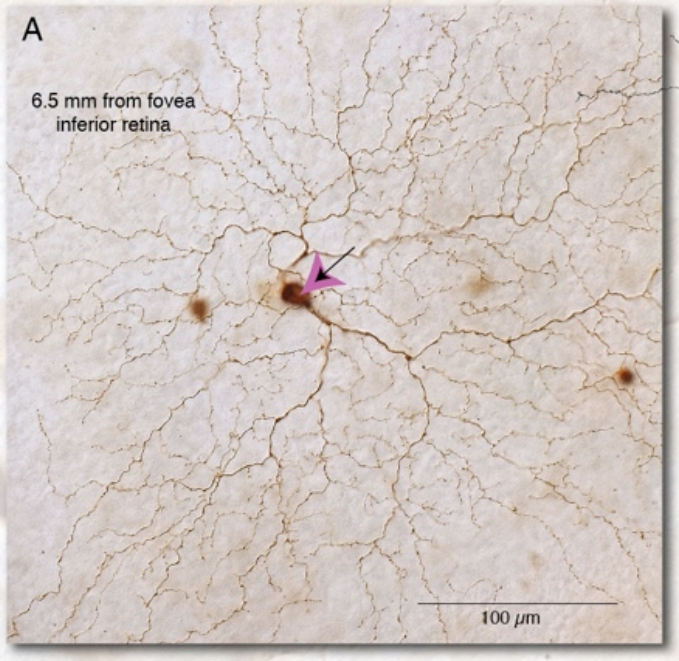

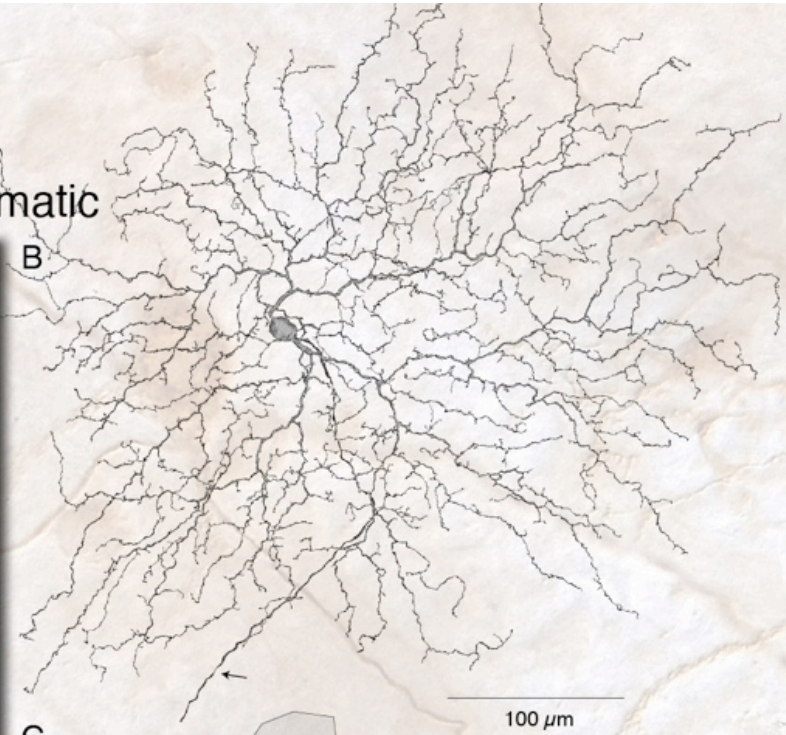

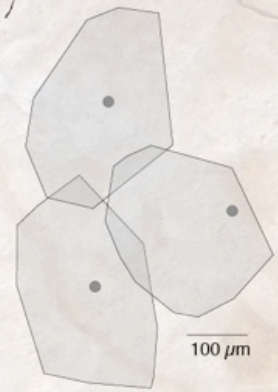

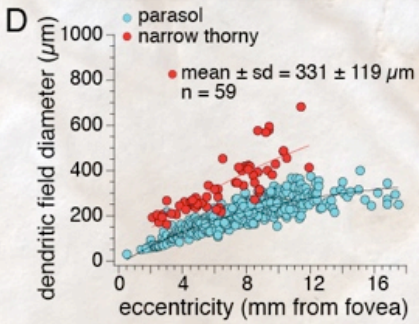

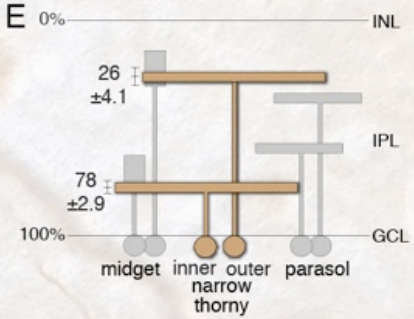

Narrow thorny cells comprise ~3% of total ganglion cells (coverage: inner cells 1.0; outer cells 1.0) and project to the LGN, superior colliculus and pretectum. **A**. Photomicrograph of an outer narrow thorny cell intracellularly injected with Neurobiotin and processed for HRP histochemistry. **B**. Tracing of the same cell shown in *A*. Arrow indicates axon. **C**. Outlines of the overlapping dendritic fields of 3 neighboring outer narrow thorny cells tracer labeled from injections in the superior colliculus. **D**. Dendritic field diameter plotted as a function of eccentricity. **E**. Mean dendritic stratification measured relative to parasol stratification in wholemount retina and plotted as percentage depth in the IPL (inner narrow thorny/parasol cell pairs, n = 4; outer narrow thorny/parasol cell pairs, n = 4).

Broad thorny

ON-OFF receptive field
primate candidate for the local edge detector

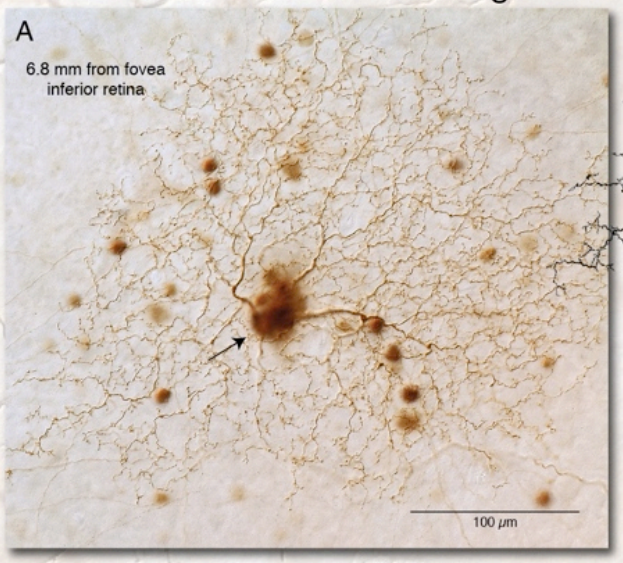

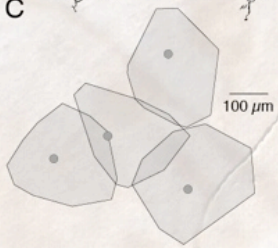

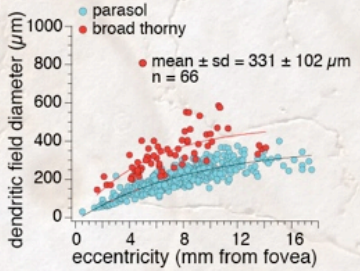

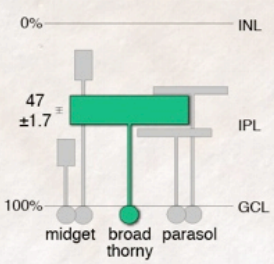

Broad thorny cells make up ~1.5% of total ganglion cells (coverage = 1.2) and project to the LGN, superior colliculus and pretectum. **A**. Photomicrograph of a broad thorny cell intracellularly injected with Neurobiotin and processed for HRP histochemistry. **B**. Tracing of the same cell shown in *A*. Arrow indicates axon. **C**. Outlines of the overlapping dendritic fields of 4 neighboring broad thorny cells ~5 mm from the fovea, tracer labeled from injections in the superior colliculus. **D**. Dendritic field diameter plotted as a function of eccentricity. **E**. Mean dendritic stratification measured relative to parasol stratification in wholemount retina and plotted as percentage depth in the IPL (broad thorny/parasol cell pairs: n = 8).

Melanopsin-expressing

inner and outer types, inherently photosensitive; S-OFF opponency

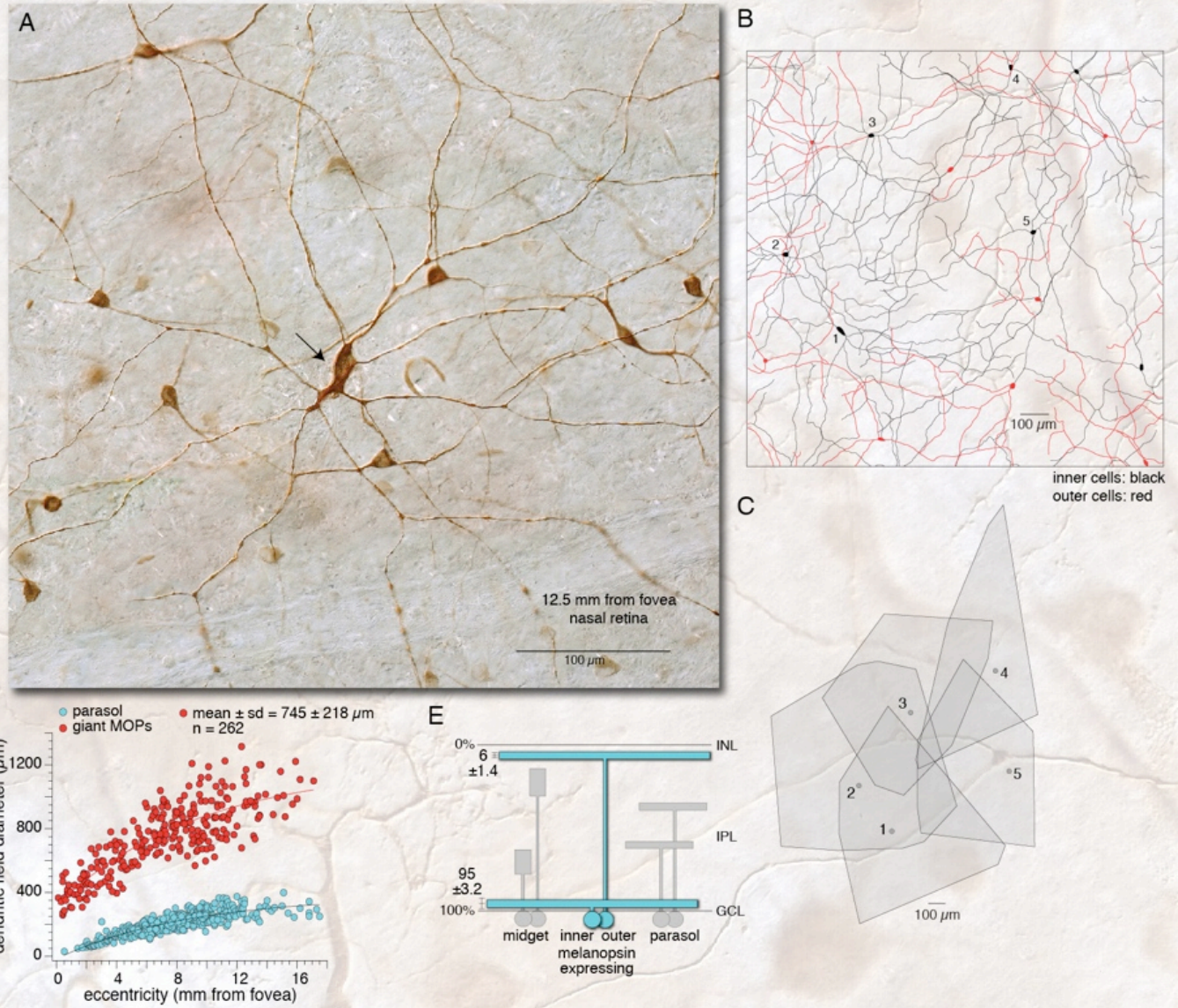

Giant melanopsin cells comprise ~1% of total ganglion cells (coverage: inner cells 1.5; outer cells 2.0) and project to the LGN, superior colliculus and pretectum. **A**. Photomicrograph of a giant melanopsin cell intracellularly injected with Neurobiotin and processed for HRP histochemistry. The cell shows tracer coupling to several populations of amacrine cells. **B**. Tracings of 7 inner (black) and 8 outer (red) giant cells ~10 mm from the fovea, melanopsin immunolabeled and processed for HRP histochemistry. **C**. Outlines of the overlapping dendritic fields of 5 inner giant cells. Numbers correspond to cells shown in *B*. **D**. Dendritic field diameter plotted as a function of eccentricity. **E**. Mean dendritic stratification measured relative to parasol stratification in wholemount retina and plotted as percentage depth in the IPL (inner giant melanopsin/parasol cell pairs, n = 3; outer giant melanopsin/parasol cell pairs, n = 5).

midget cells - 46 % - coverage inner 1.1, outer 1.1
parasol cels - 14% - coverage inner 1.9 outer 1.6
smooth monostratified cells- 2.5% - coverage inner 1.4 outer 1.4
recursive monostratified - 4.5% (3 populations each 1.5%, coverage 1.2)(on ds?)
recursive bistratified - 1.5% - coverage 1.3 (on-off ds?)
small bistratified - 6% - coverage 1.6 - blue on yellow off
large bistratified - 3% - coverage 2 - blue on yellow off
narrow thorny - 3% - coverage inner 1.0, outer 1.0 - transient achromatic
broad thorny - 1.5% - coverage 1.2 - on-off "local edge detector"
melanopsin - 1% - coverage inner 1.5, outer 2.0 - S off

17 populations, 85% of cells

Summary of ganglion cell types in macaque retina

	Morphological type	% of ganglion cell population	Central projections	Some physiological properties
1	Midget Inner	26%	LGN parvo 5, 6	ON-center; OFF-surround Achromatic/chromatic L vs M cone opponent
2	Midget Outer	26%	LGN parvo 3, 4	OFF center; ON surround Achromatic/chromatic L vs M cone opponent S cone OFF opponent group?
3	Parasol Inner	8.0%	LGN magno 1, 2	ON-center; OFF-surround Achromatic L+M cone input S cone input controversial
4	Parasol Outer	8.0%	LGN magno 1, 2	OFF-center; ON-surround Achromatic L+M cone input S cone input controversial
5	Small bistratified	6.2%	LGN konio 3	S ON; L+M OFF opponent
6	Large bistratified	2.7%	LGN	S ON opponent details unknown
7	Thorny monostratified Inner	1.2%	LGN Superior colliculus	Unknown
8	Thorny monostratified Outer	1.2%	LGN Superior colliculus	Unknown
9	Broad thorny monostratified	1.2%	LGN Superior colliculus	Unknown
10	Recursive bistratified	4.2%	Superior colliculus	Possible correlate of ON-OFF direction selective
11	Recursive monostratified	1.9%	Superior colliculus LGN? Pretectal area (NOT?)	Possible correlate of ON direction selective
12	Moderate monostratified Inner	1.3%	Superior colliculus	Unknown
13	Moderate monostratified Outer	1.3%	Superior colliculus	Unknown
14	Sparse monostratified Inner	2.0 %	LGN	L+M ON; S OFF opponent
15	Sparse monostratified Outer	1.2%	LGN	Unknown
16	Giant monostratified Melanopsin-containing Inner/outer Weakly bistratified	1.0%	LGN Pretectal area, PON SCN?	Sustained ON response S OFF; L+M ON opponent Strong rod input Intrinsically photosensitive via novel photopigment
17	Giant monostratified intrinsic axon-collaterals	1.0%	Unknown	Unknown

*Total ganglion cell density is from Wässle et al., 1989, for temporal retina ~ 8 mm from the fovea. Individual cell type densities were determined from celldensity at ~8 mm (parasol cells, Perry & Cowey, 1985) or from dendritic field area at ~ 8 mm and coverage factor where known (thorny and giant monostratified cells, Dacey, unpublished; midget cells Dacey, 1993). All other cell type densities were determined from measured dendritic field area at ~8 mm and estimated coverage. For abbreviations, see Figure 1.

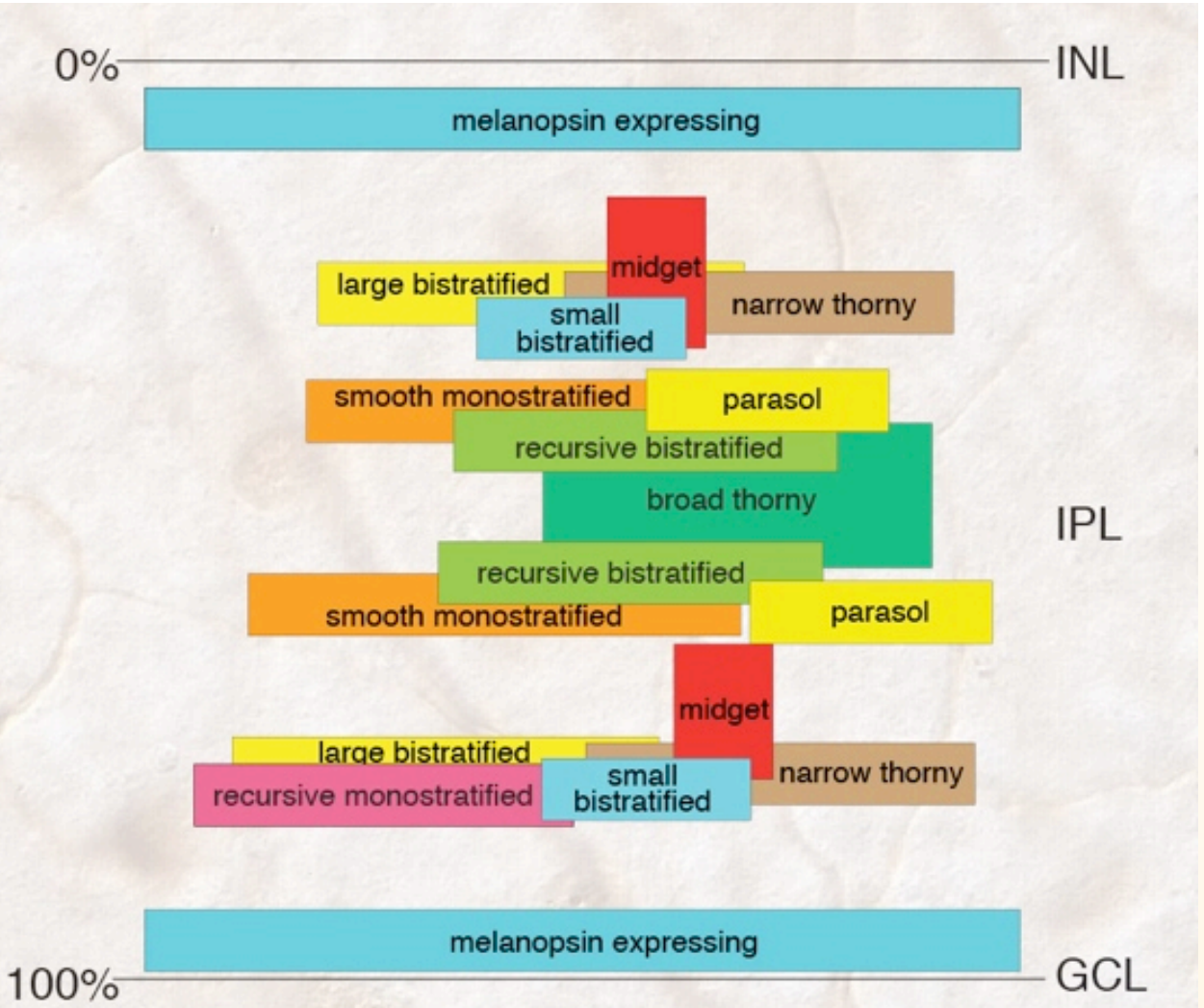

Schematic summary of dendritic stratification. Lengths of colored bars are proportional to dendritic field diameter for each cell type relative to parasol cell diameter. Vertical positioning of each bar is centered on the mean stratification depth for that cell type (values not shown). Widths of the bars are arbitrary for all cell types except midget and broad thorny cells, where it represents the mean innermost and outermost dendrites for these broadly stratifying cell types.

Conclusions

- The 17 cell populations shown here represent ~ 85% of the total number of ganglion cells.*

- At least 3 other cell types have been identified:
  axon collateral-bearing ganglion cells
  (Peterson & Dacey, Vis Neurosci 1998, 15;377)
  large, sparsely branched monostratified cells
  (inner and outer types).

- Taken together, and assuming ~ 2% density for the remaining 3 cell types, the 20 types account for ~ 90% of the ganglion cells. If multiple ON-OFF direction selective mosaics exist in primate (as found in other mammals) another ~5% would be accounted for.

*Total ganglion cell density is from Wässle et al., Nature 1989, 341;643. Density estimates for individual cell types were derived from the mosaics.

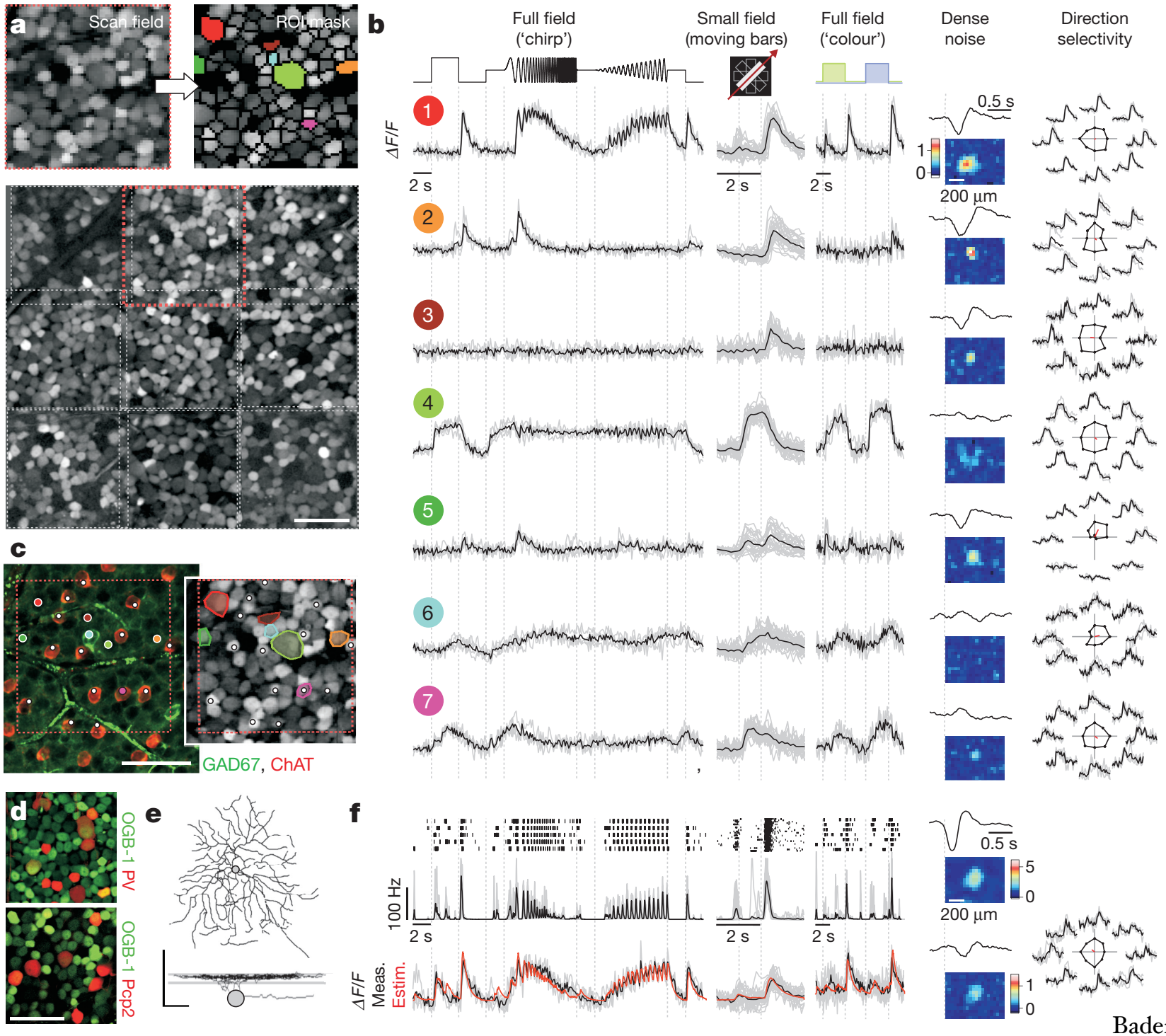

Baden et al, 2016

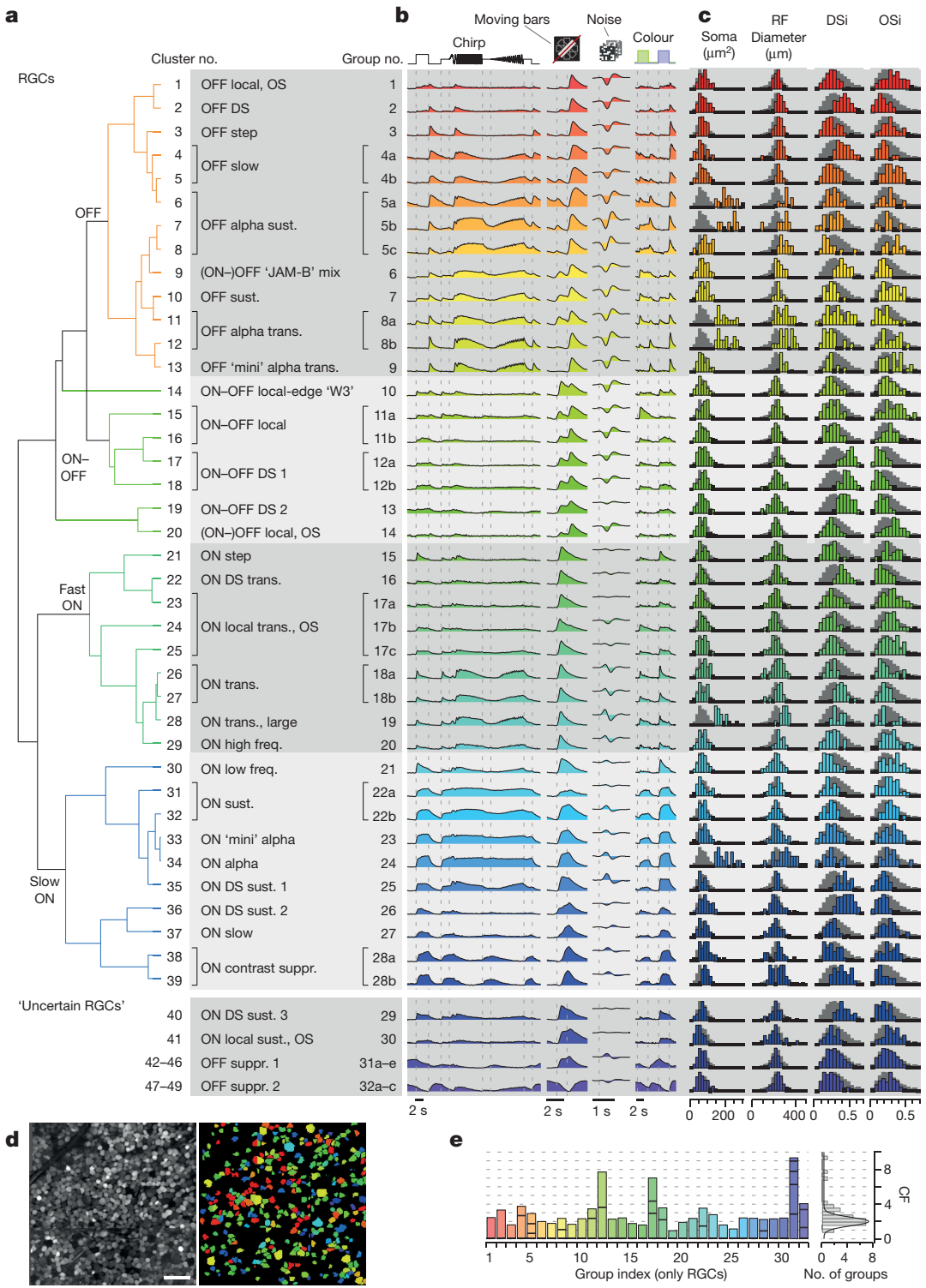

Figure 2 | Functional RGC types of the mouse retina. a, Cluster-dendrogram (Methods) with groups indicated: $n = 28$ RGC and $n = 4$ 'uncertain' RGC groups. **b**, Cluster-mean Ca^{2+} responses to the four stimuli. **c**, Selected metrics, from left to right: region of interest (soma) area, receptive field (RF) diameter (2 s.d. of Gaussian), direction-selectivity index (DSi) and orientation-selectivity index (OSi) (Methods). Background-histograms demarcate all RGCs. **d**, Experiment (left, from Fig. 1a, bottom) with RGCs colour-coded by group (right). dACs and discarded cells not shown. **e**, Coverage factor (CF) calculated from receptive field area of RGC groups, with horizontal divisions delineating individual clusters (left) and distribution of coverage factors across groups (right). Scale bar in **d**, 50 µm.

Baden et al, 2016

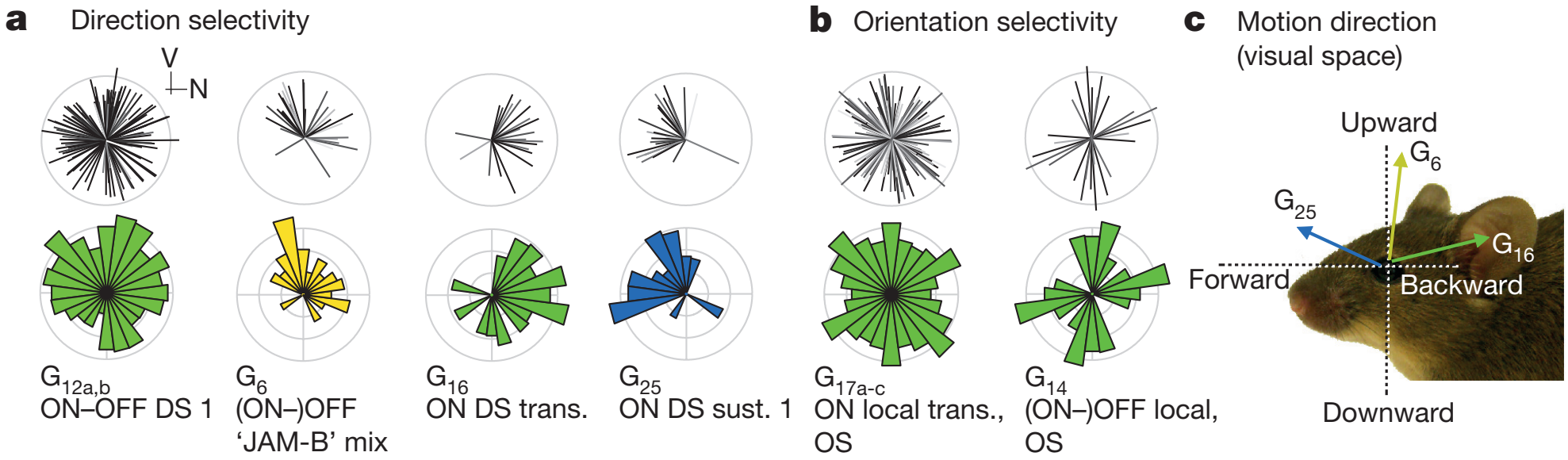

Figure 4 | Direction and orientation selectivity. a, Pairs of retinocentric polar plots showing distributions of preferred motion directions of selected direction-selective (DS) RGC groups (V, ventral; N, nasal). Top plot of each pair: preferred directions, with length representing direction-selective index and grey level p_{DS} (Methods). Bottom plot of each pair: circular area-normalized histogram. **b**, As for **a**, but for selected orientation-selective (OS) RGCs. Further direction-selective/orientation-selective groups detailed in Extended Data Fig. 7. **c**, Motion directions in the visual space of the mouse.

Physiologically **and morphologically characterized ganglion cell types that project to the macaque LGN**

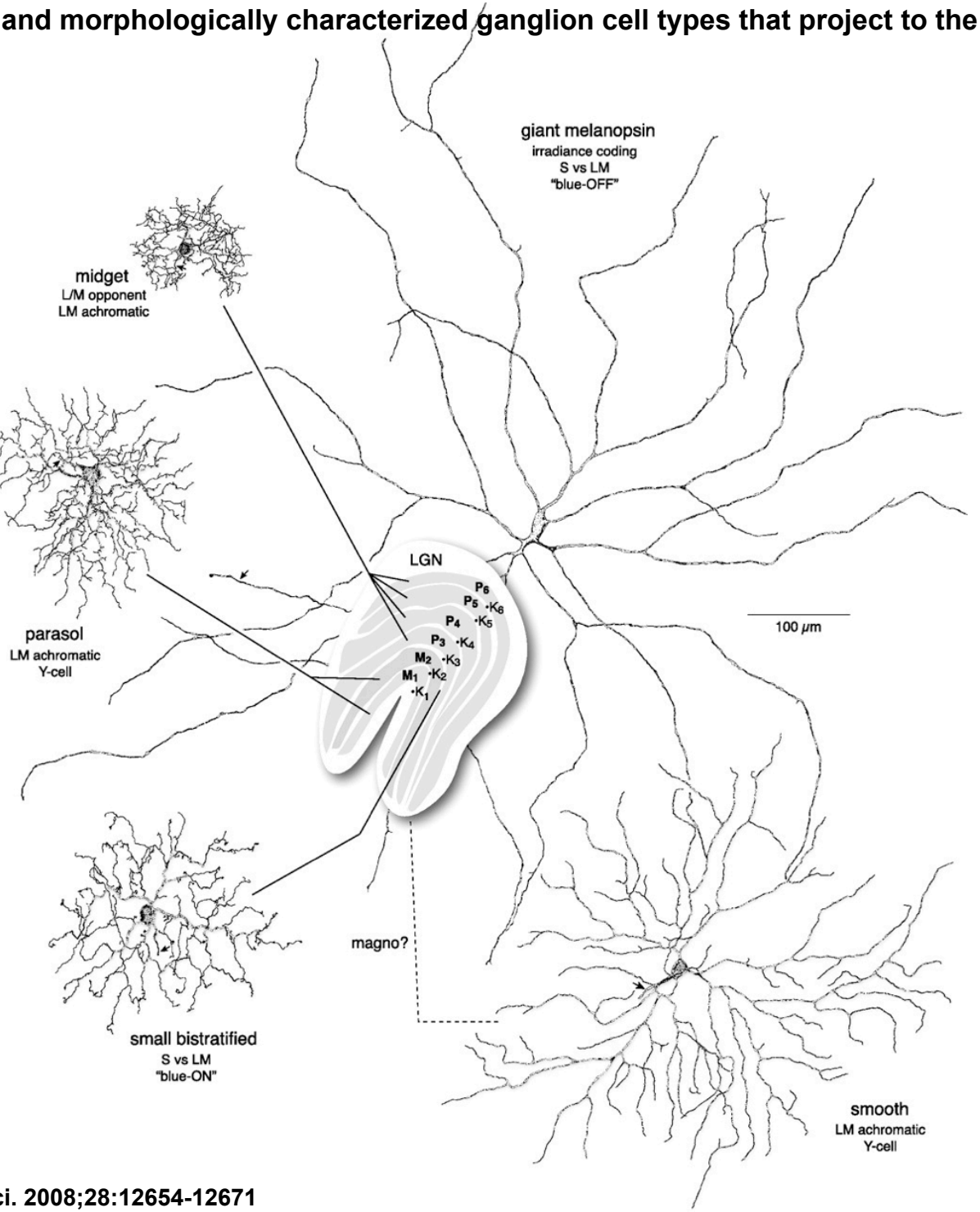

Crook, J. D. et al. J. Neurosci. 2008;28:12654-12671

Figure 5. Parasol cells have Y-cell physiology

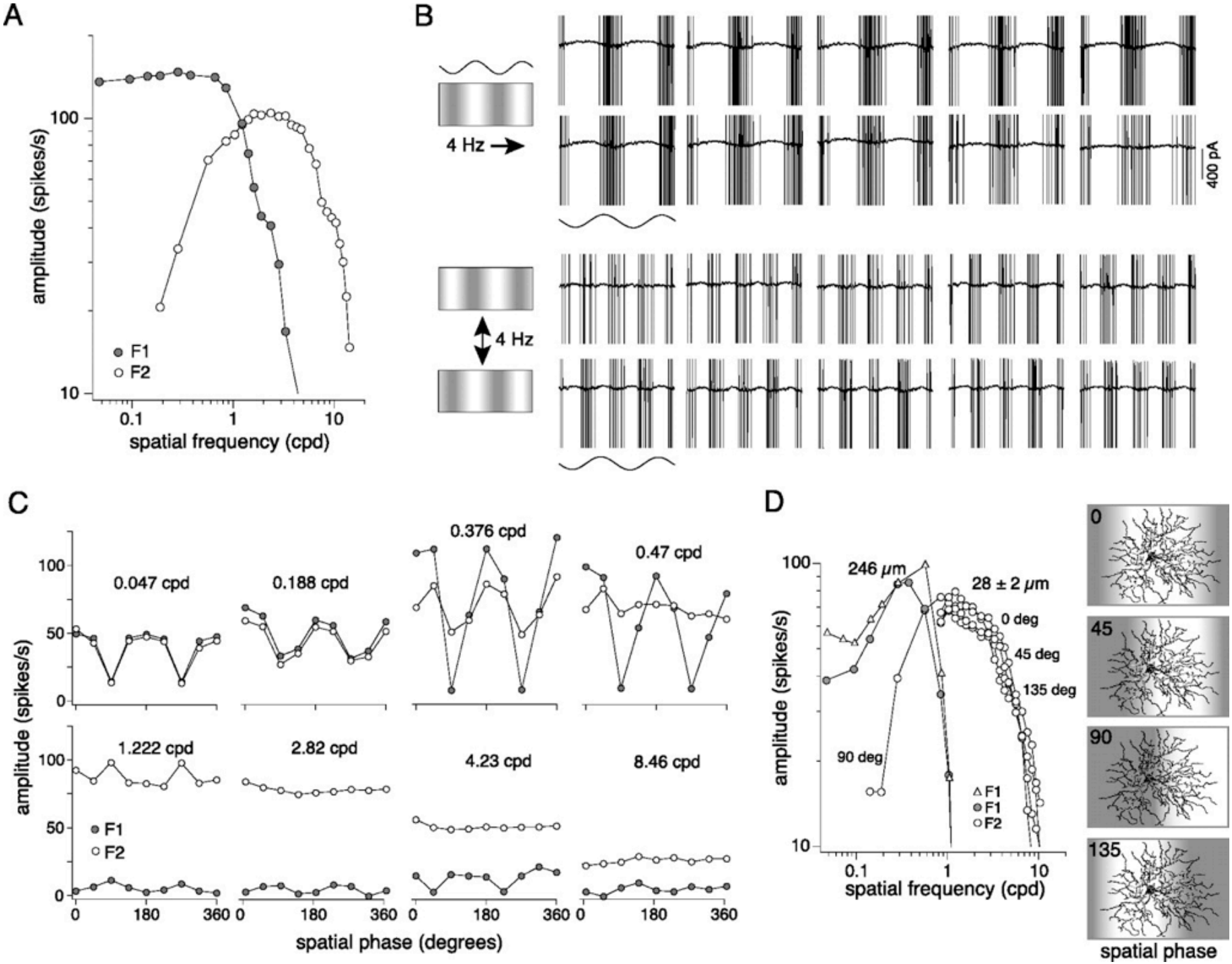

Crook, J. D. et al. J. Neurosci. 2008;28:11277-11291

Figure 6. Parasol cells of all eccentricities exhibit Y-like second harmonic responses to counterphase gratings

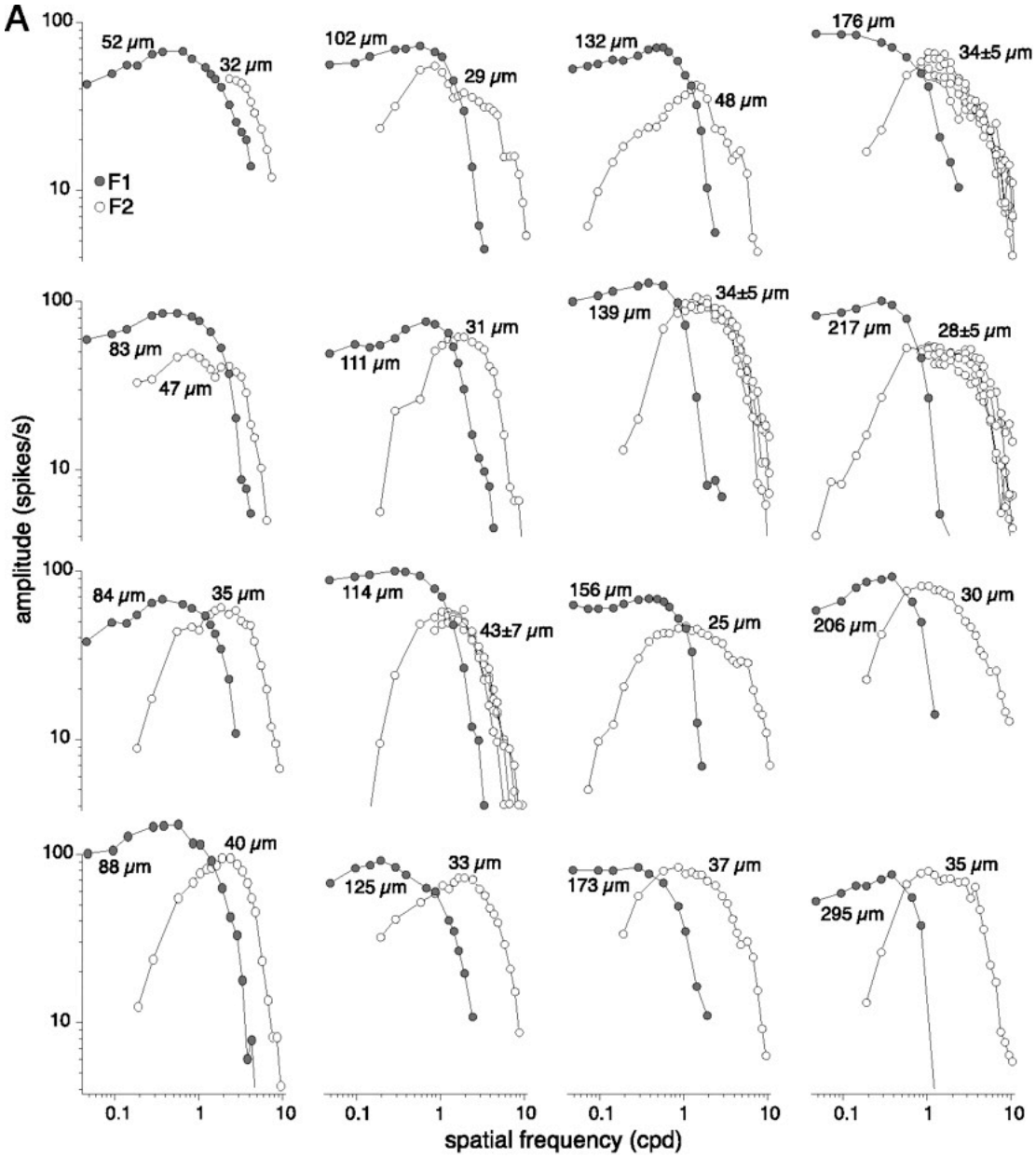

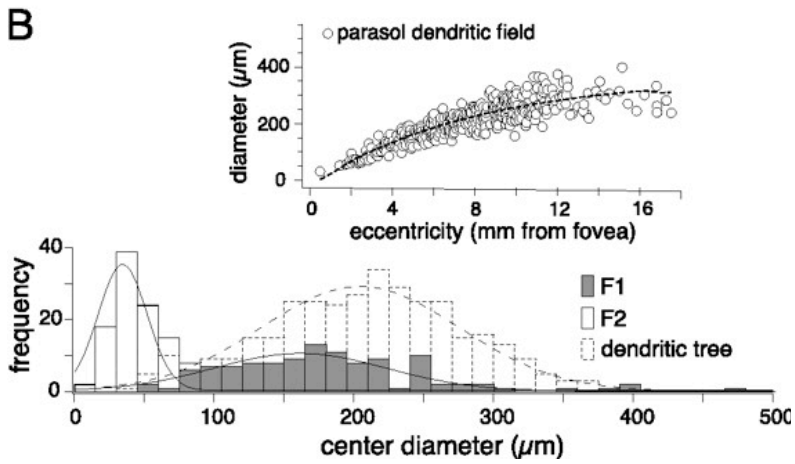

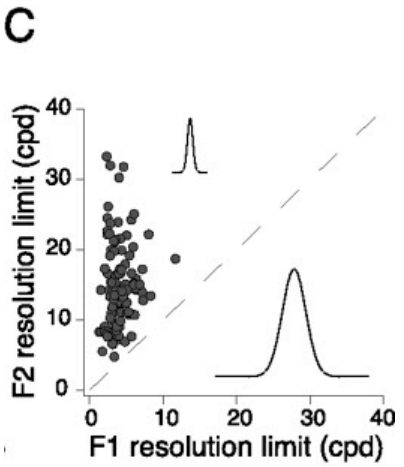

Crook, J. D. et al. J. Neurosci. 2008;28:11277-11291

Figure 10. Summary and hypothesis for the origin of the F2 receptive field component in parasol cells

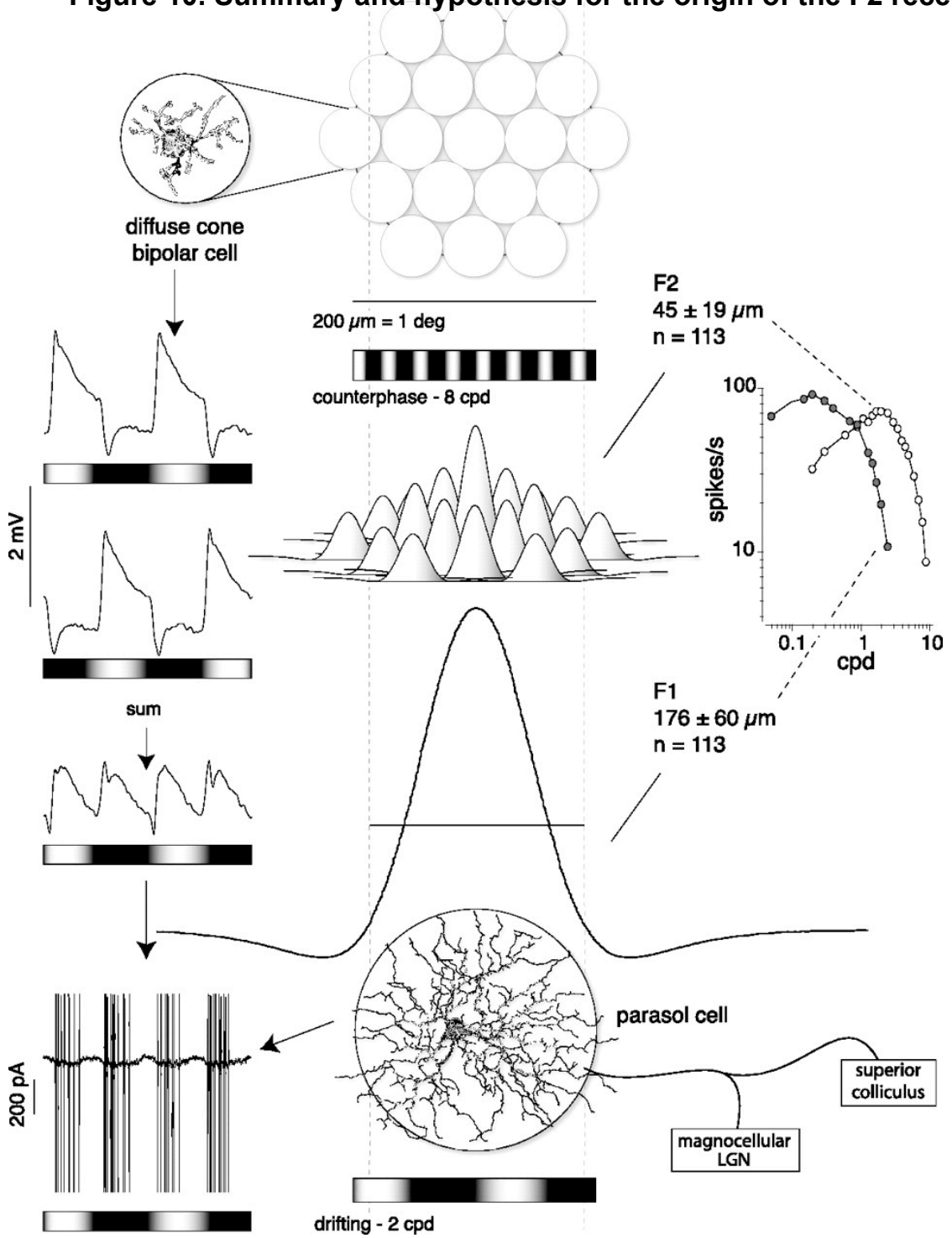

Crook, J. D. et al. J. Neurosci. 2008;28:11277-11291

Figure 4. Morphology of inner and outer smooth cells and parasol cells

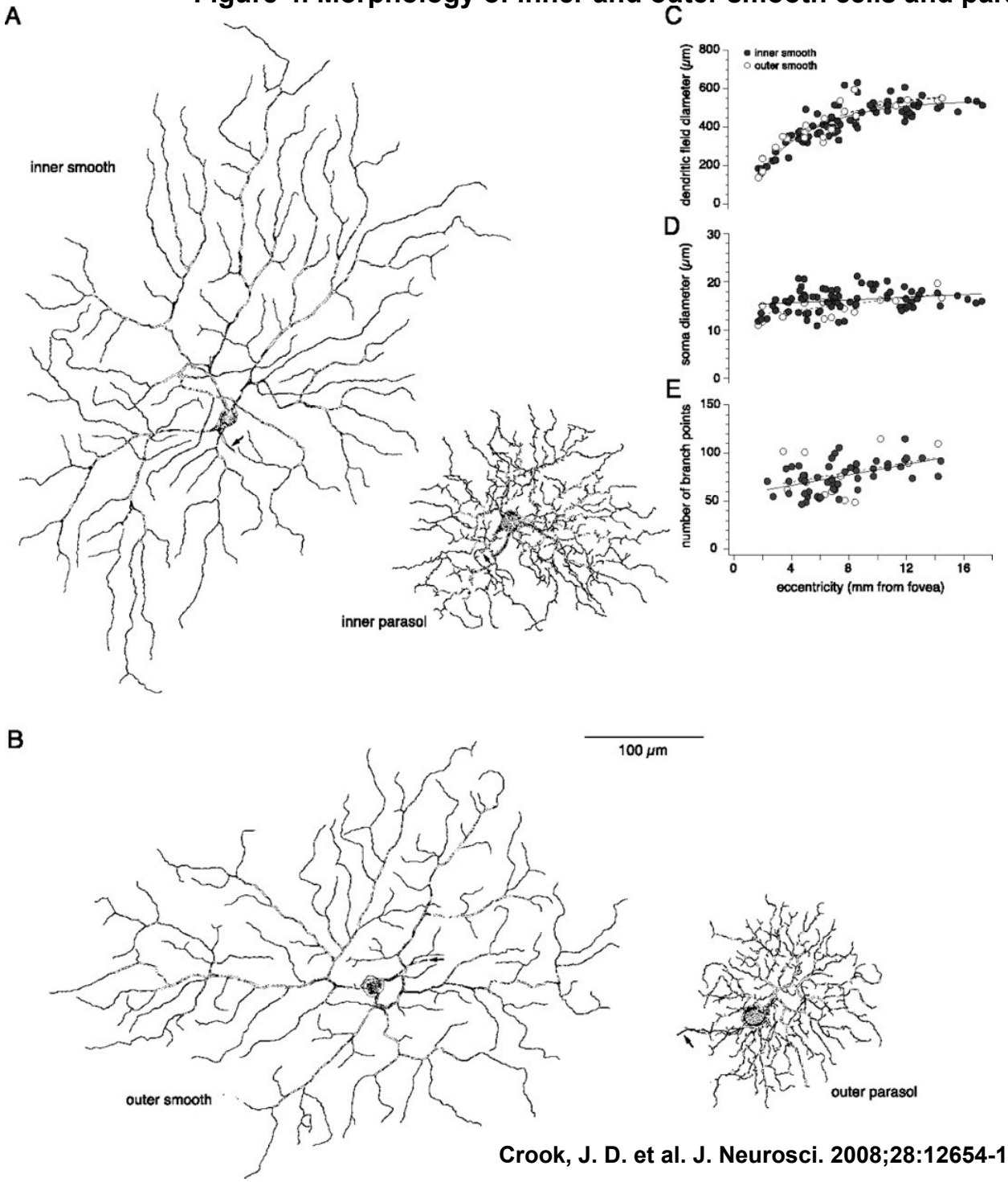

Crook, J. D. et al. J. Neurosci. 2008;28:12654-12671

Figure 6. Smooth cell dendritic diameter increases with increasing eccentricity and is twice the size of parasol cells

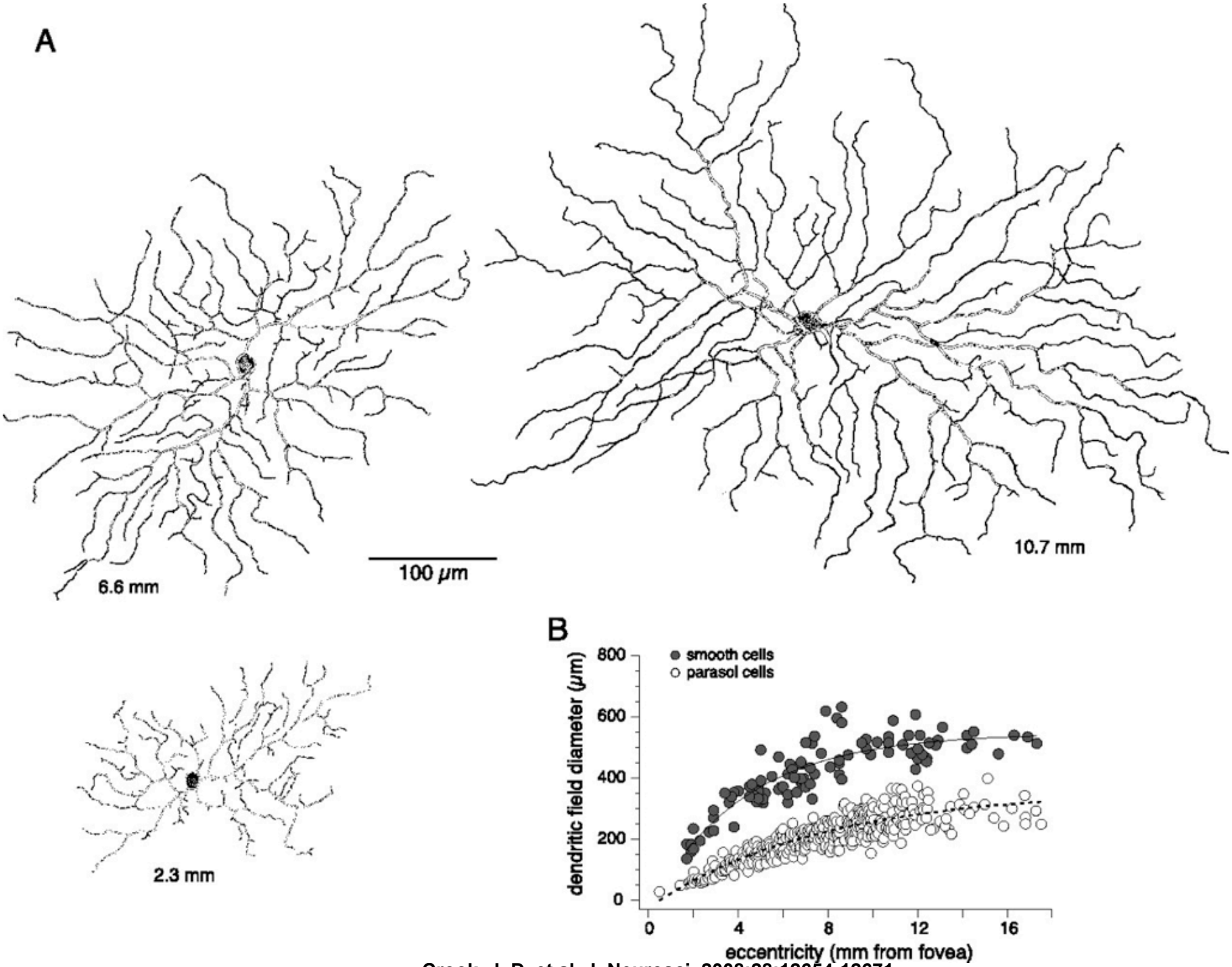

Crook, J. D. et al. J. Neurosci. 2008;28:12654-12671

Figure 7. Smooth and parasol dendritic trees costratify within the IPL

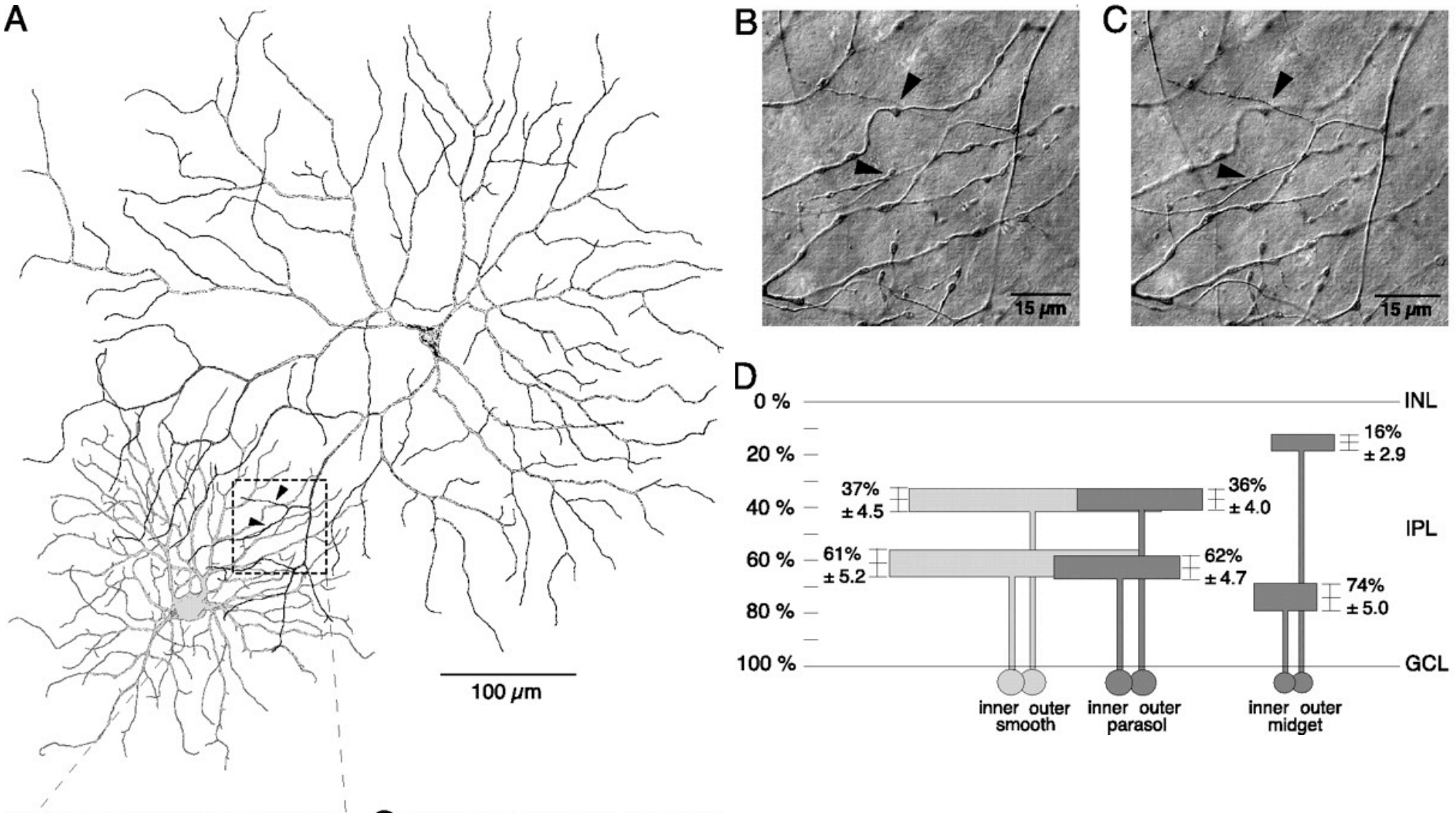

Crook, J. D. et al. J. Neurosci. 2008;28:12654-12671

Figure 9. Smooth cells have large receptive fields with center and surround organization

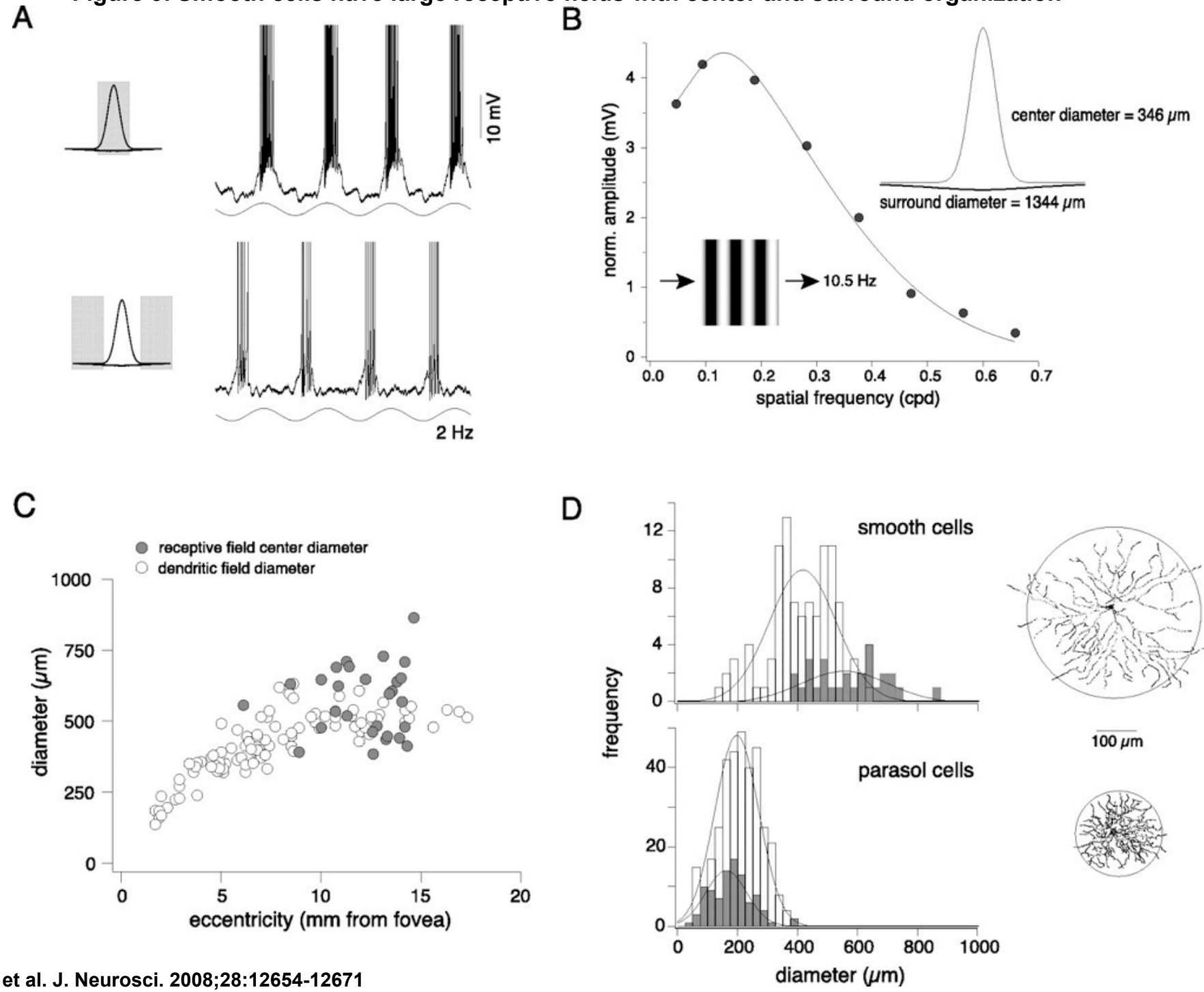

Crook, J. D. et al. J. Neurosci. 2008;28:12654-12671

Figure 11. Smooth cells, like parasol cells, have transient responses and encode high temporal frequencies

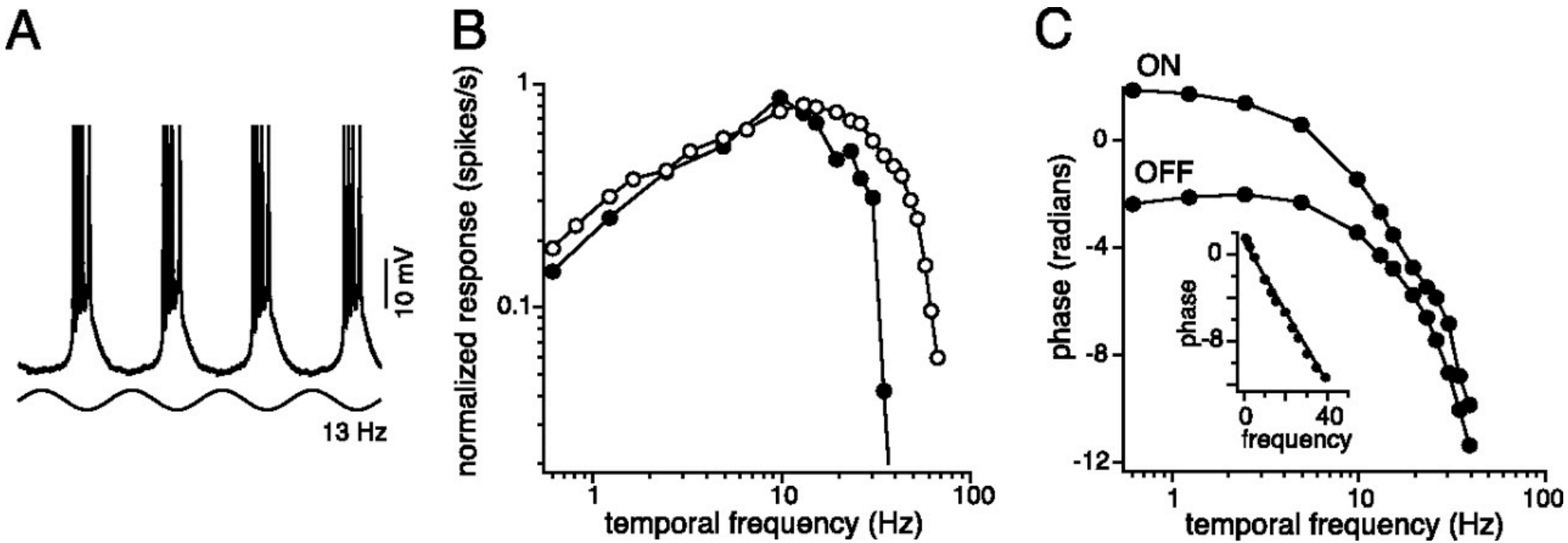

Crook, J. D. et al. J. Neurosci. 2008;28:12654-12671

Figure 13. Smooth cells have Y-cell like physiology

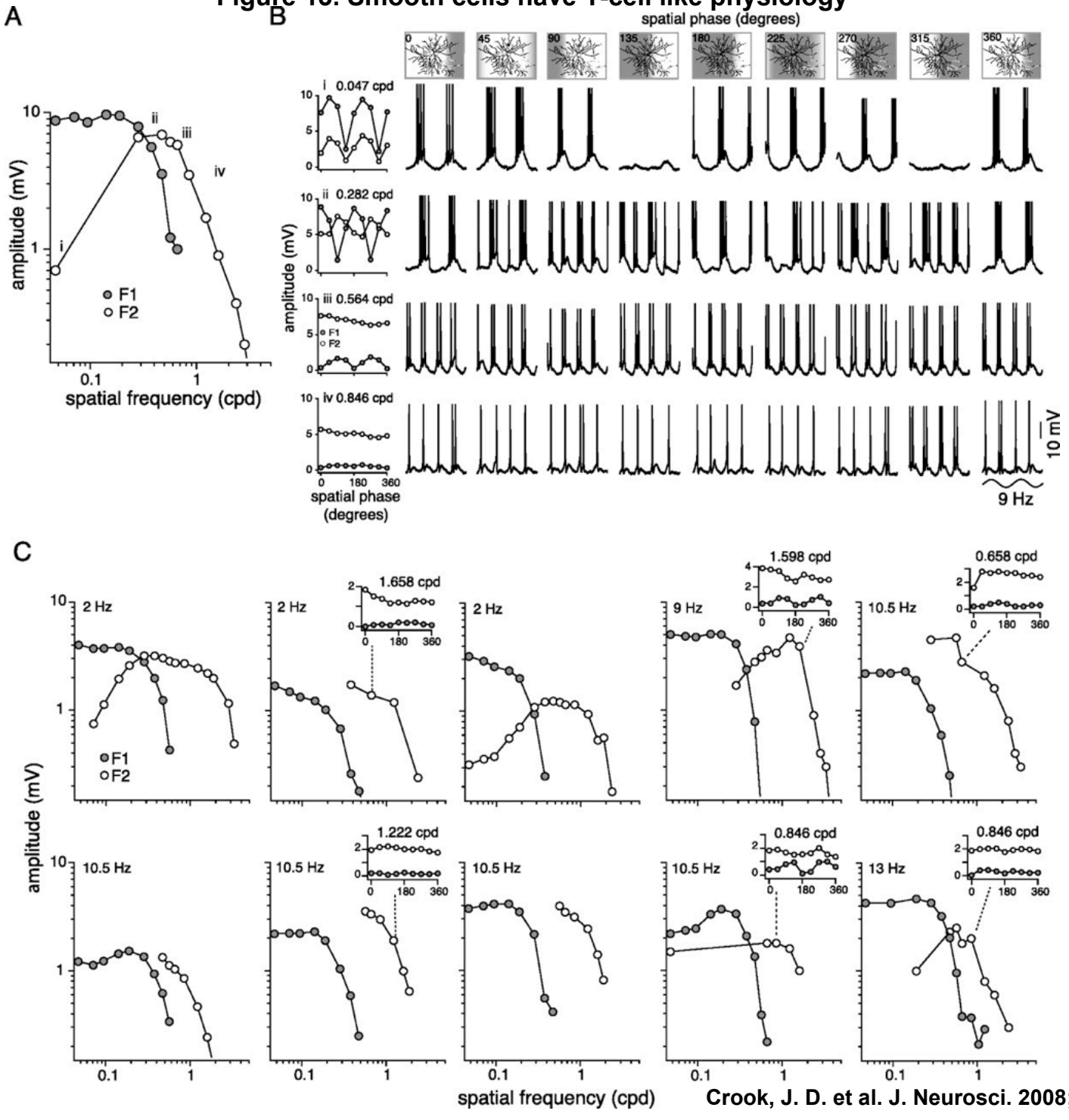

Crook, J. D. et al. J. Neurosci. 2008;28:12654-12671

Figure 15. Summary of the central projections, dendritic morphology and receptive field spatial structure for smooth and parasol ganglion cell classes of the macaque retina found in this and a companion study (Crook et al., 2008)

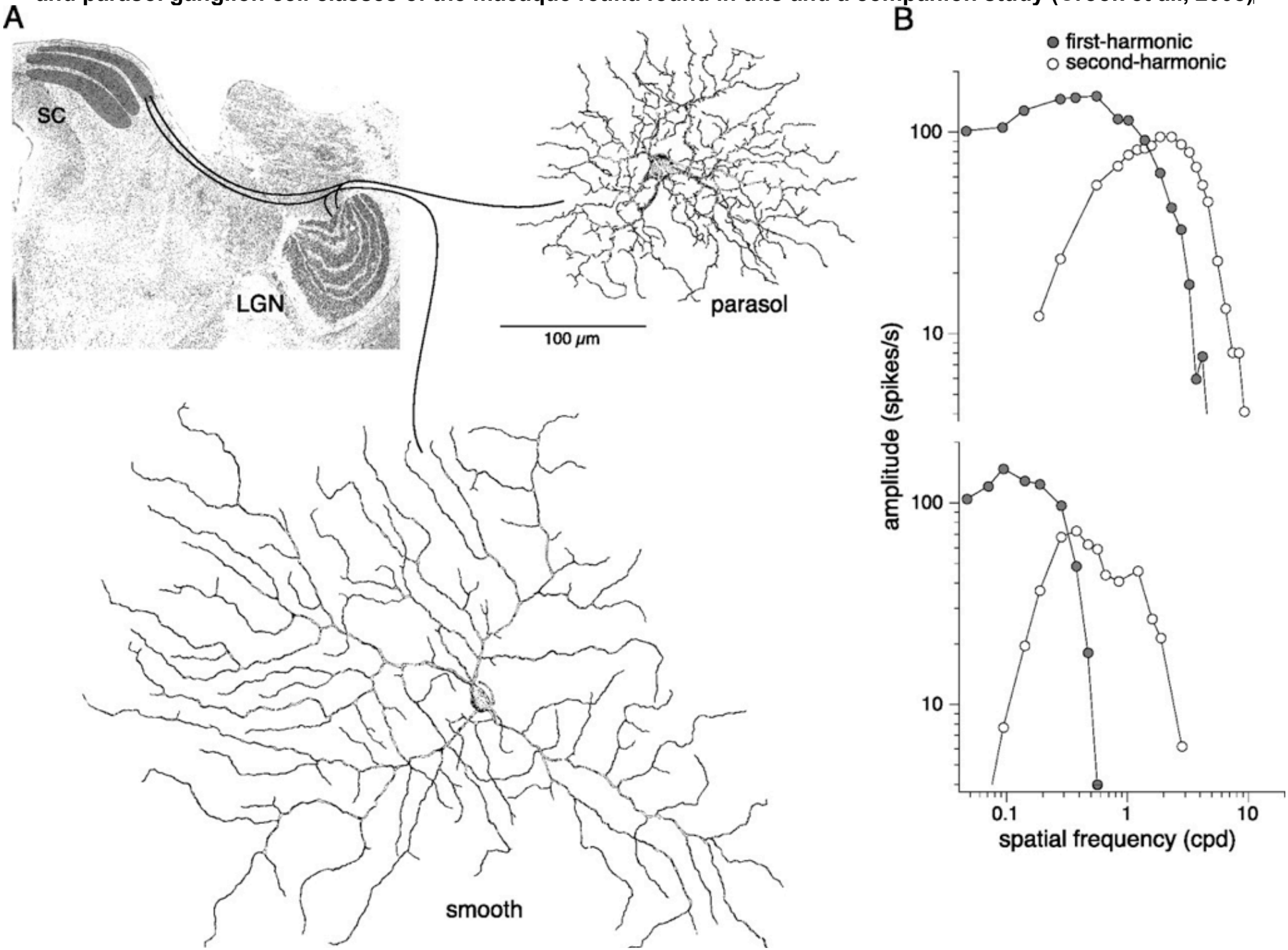

Figure 16. Physiologically and morphologically characterized ganglion cell types that project to the macaque LGN

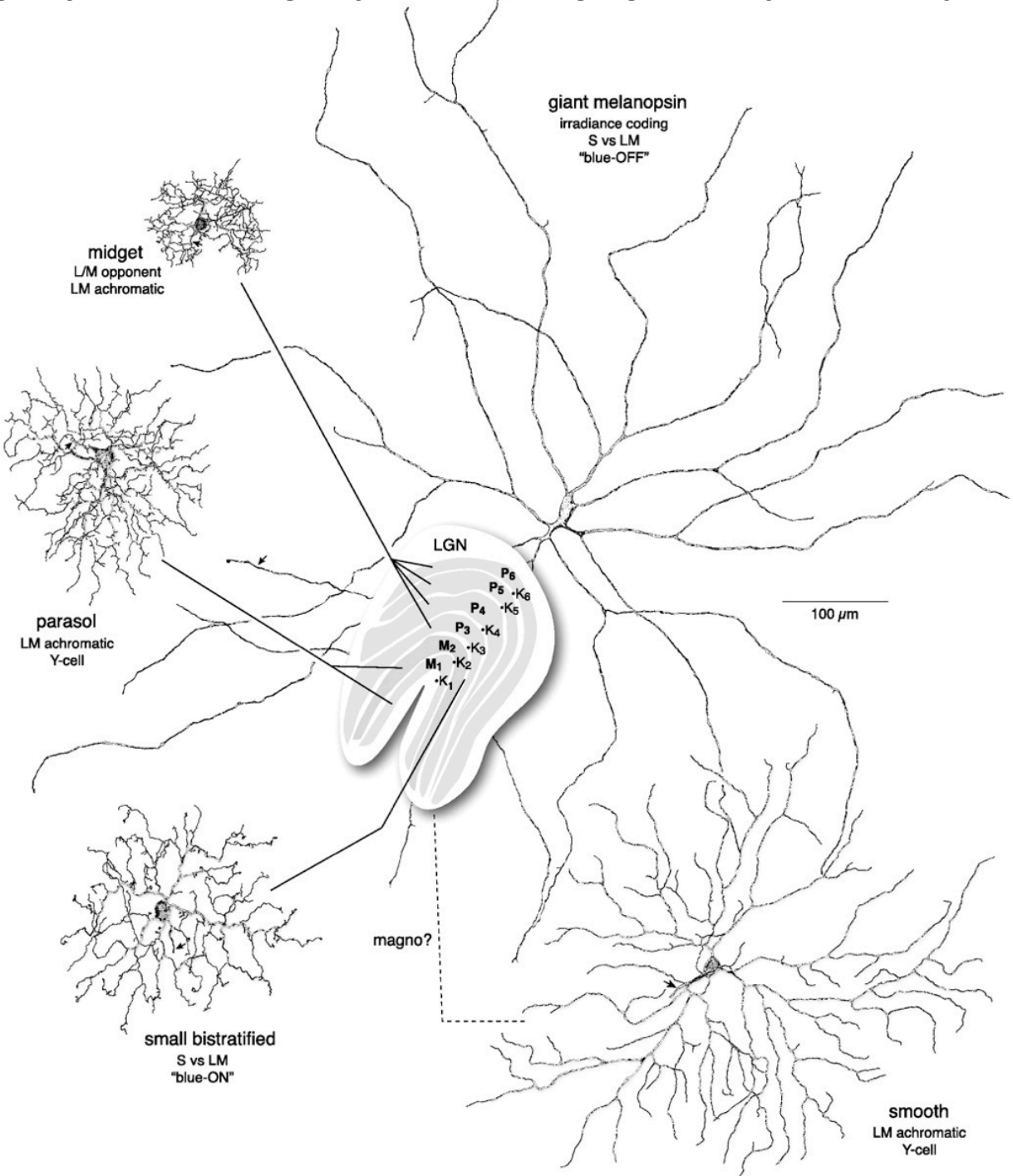

Crook, J. D. et al. J. Neurosci. 2008;28:12654-12671

Diversity of ganglion cell morphology in mammalian retina

Icon	Mouse	Rabbit	Cat	Macaque	Properties
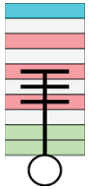				ON midget[22]	Small dendritic field. ON response.
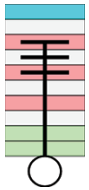				OFF midget[22]	Small dendritic field. OFF response.

Roska and Meister, 2014

Color-opponent midget cells: a primate specialization

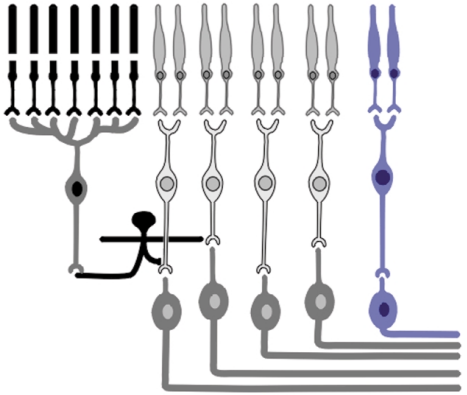

Primates →

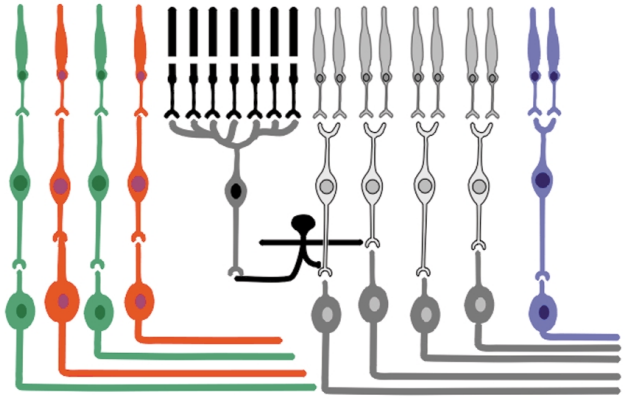

Generic mammalian retina

Primate Color Opponent Ganglion Cells

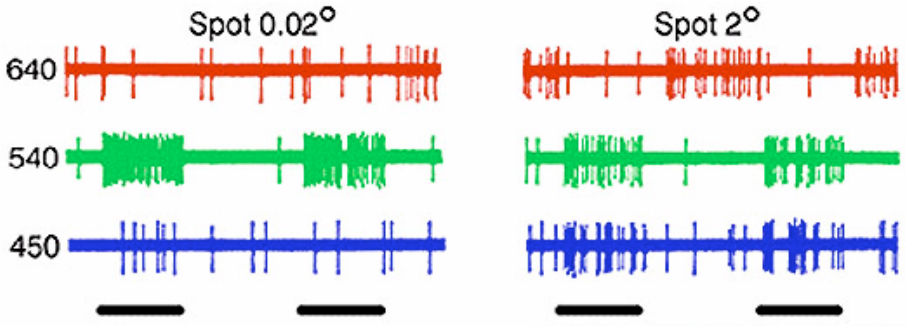

DeMonasterio & Gouras (1975)

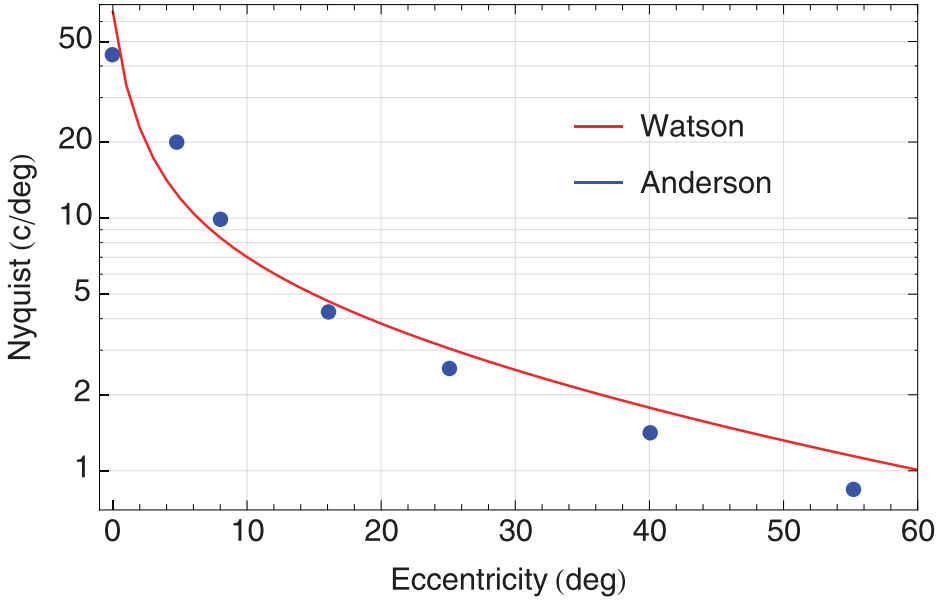

Inferred Receptive Field Description

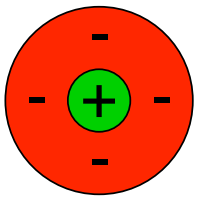

Masland, 2001;
DeMonasterios & Gouras, 1975;
Watson, 2014

Midget ganglion cells show red-green L vs M cone opponency

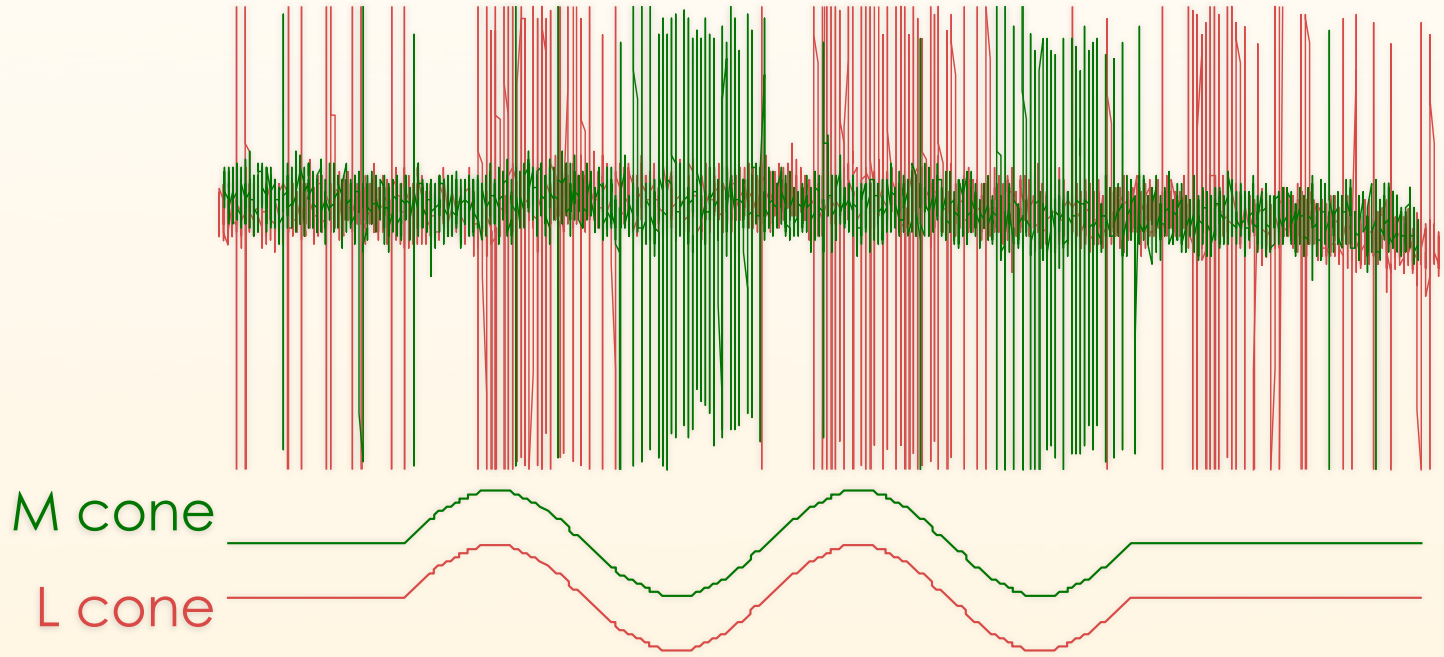

Jo Crook & Dennis Dacey

random-wiring
achromatic-chromatic

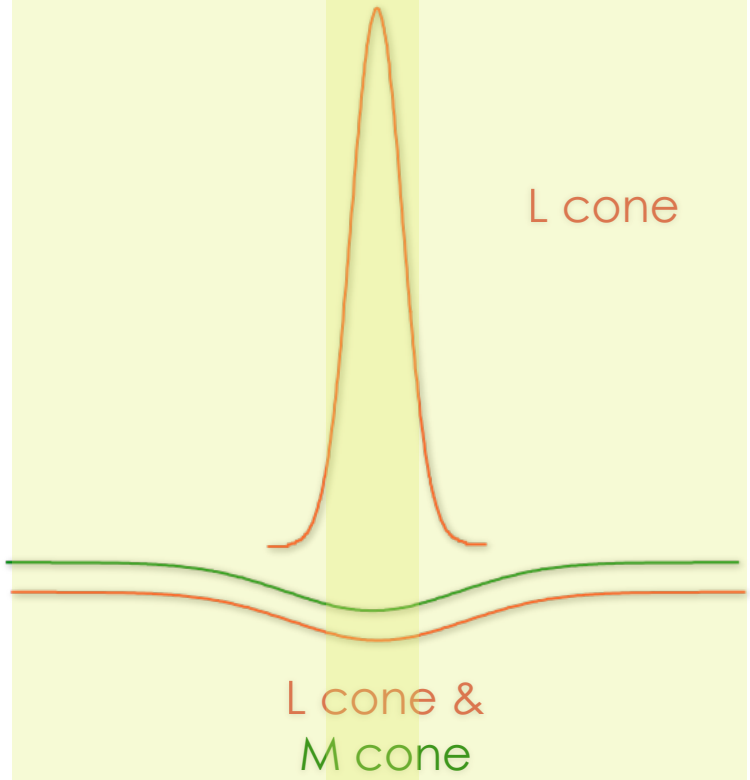

e.g. Paulus & Kroger-Paulus, 1983
Lennie et al., 1991

cone-selective
pure color

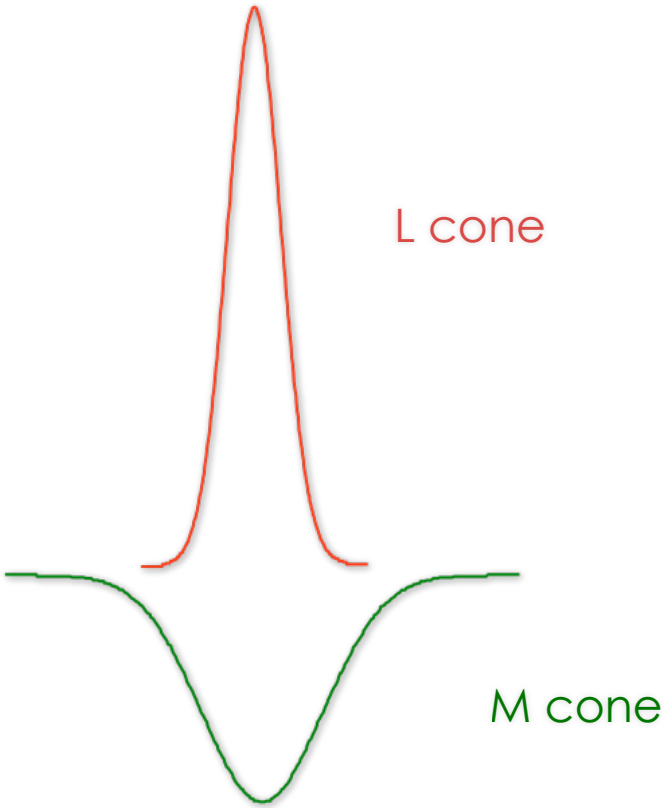

Shapley & Perry, 1986
Lee, 1999
Reid & Shapley, 2002
Shapley, 2006
Buzas et al., 2006

Jo Crook & Dennis Dacey

Record from midget cells with multiple cone inputs to the receptive field center

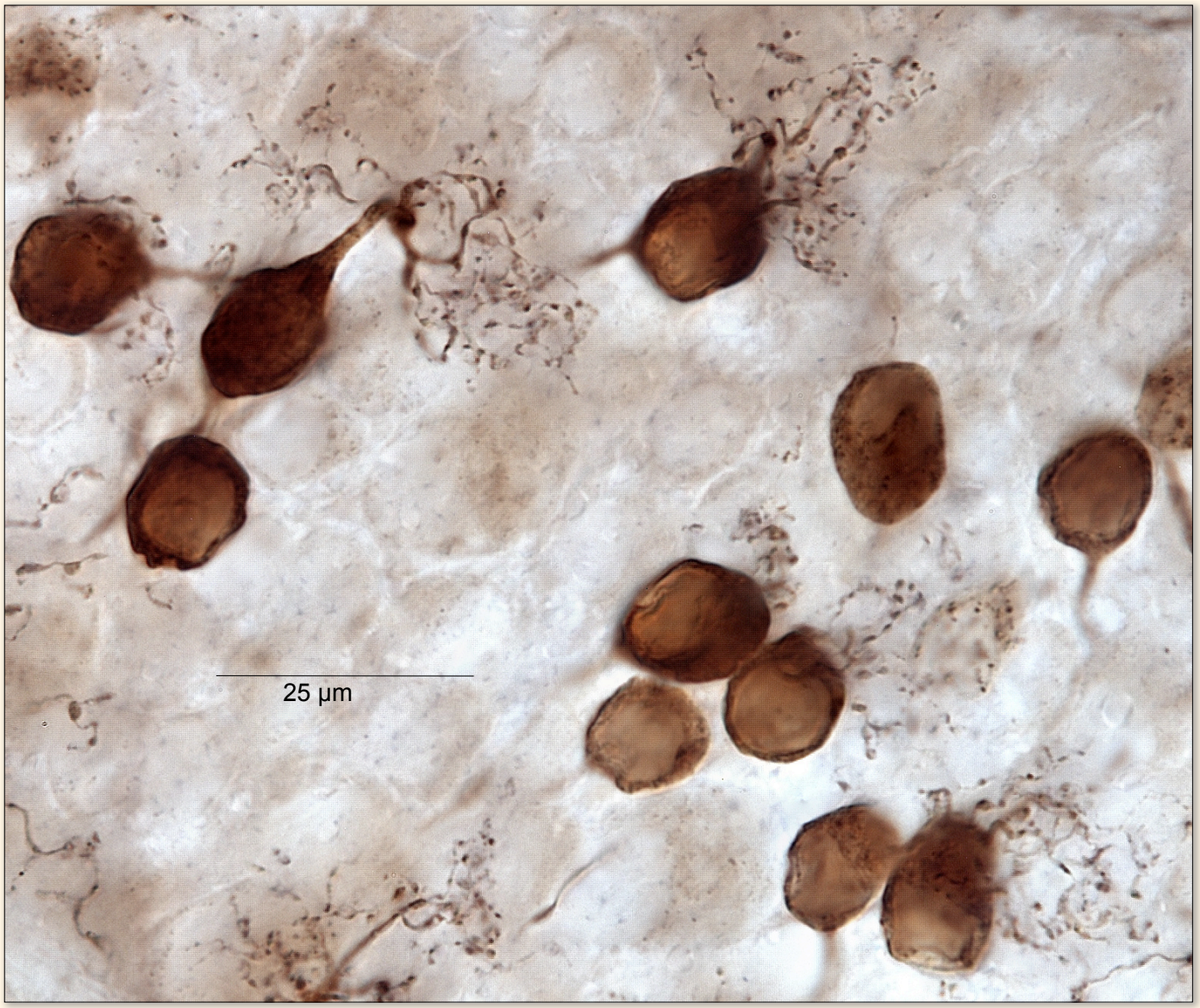

Jo Crook & Dennis Dacey

Record from midget cells with multiple cone inputs to the receptive field center

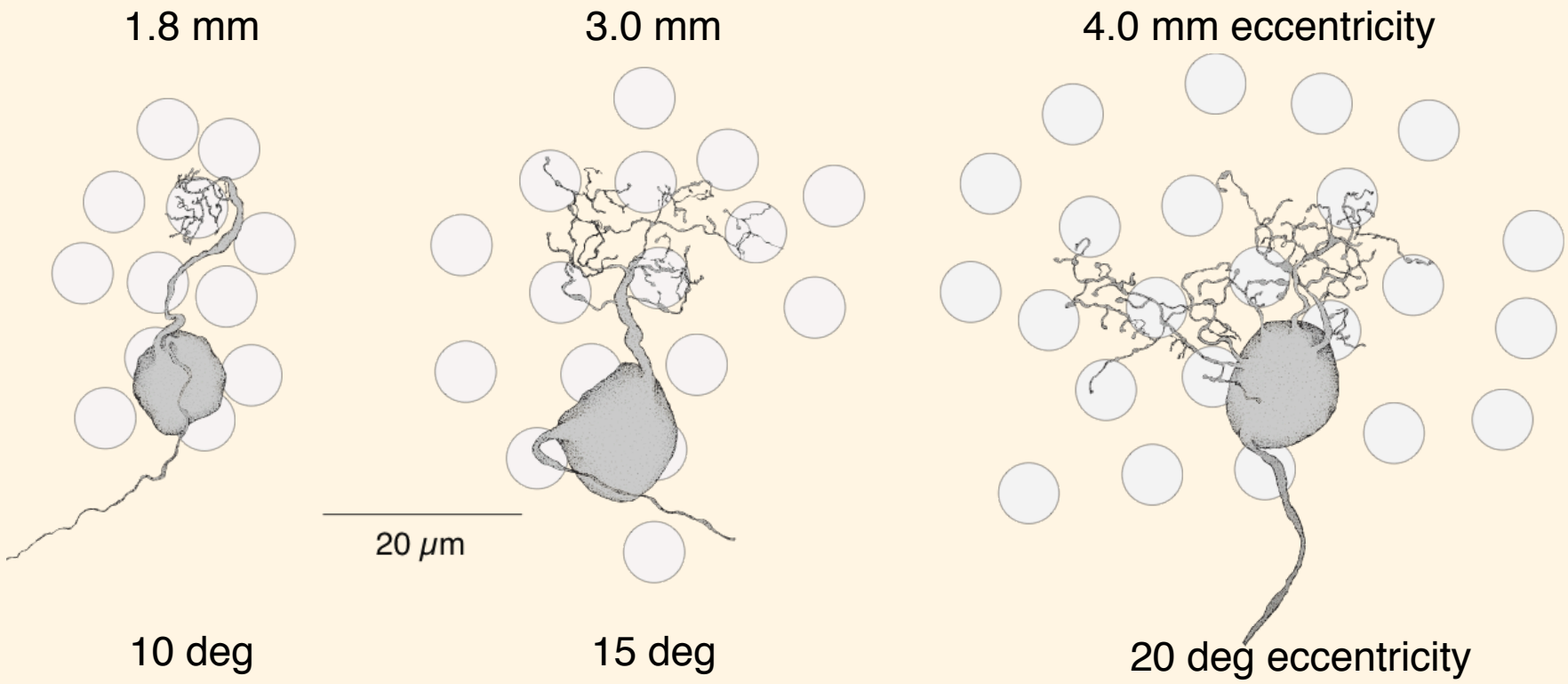

Martin et al., 2001
Solomon et al., 2005
Buzas et al., 2006

Jo Crook & Dennis Dacey

Mixed L and M cone input weights to midget center and surround supports random wiring

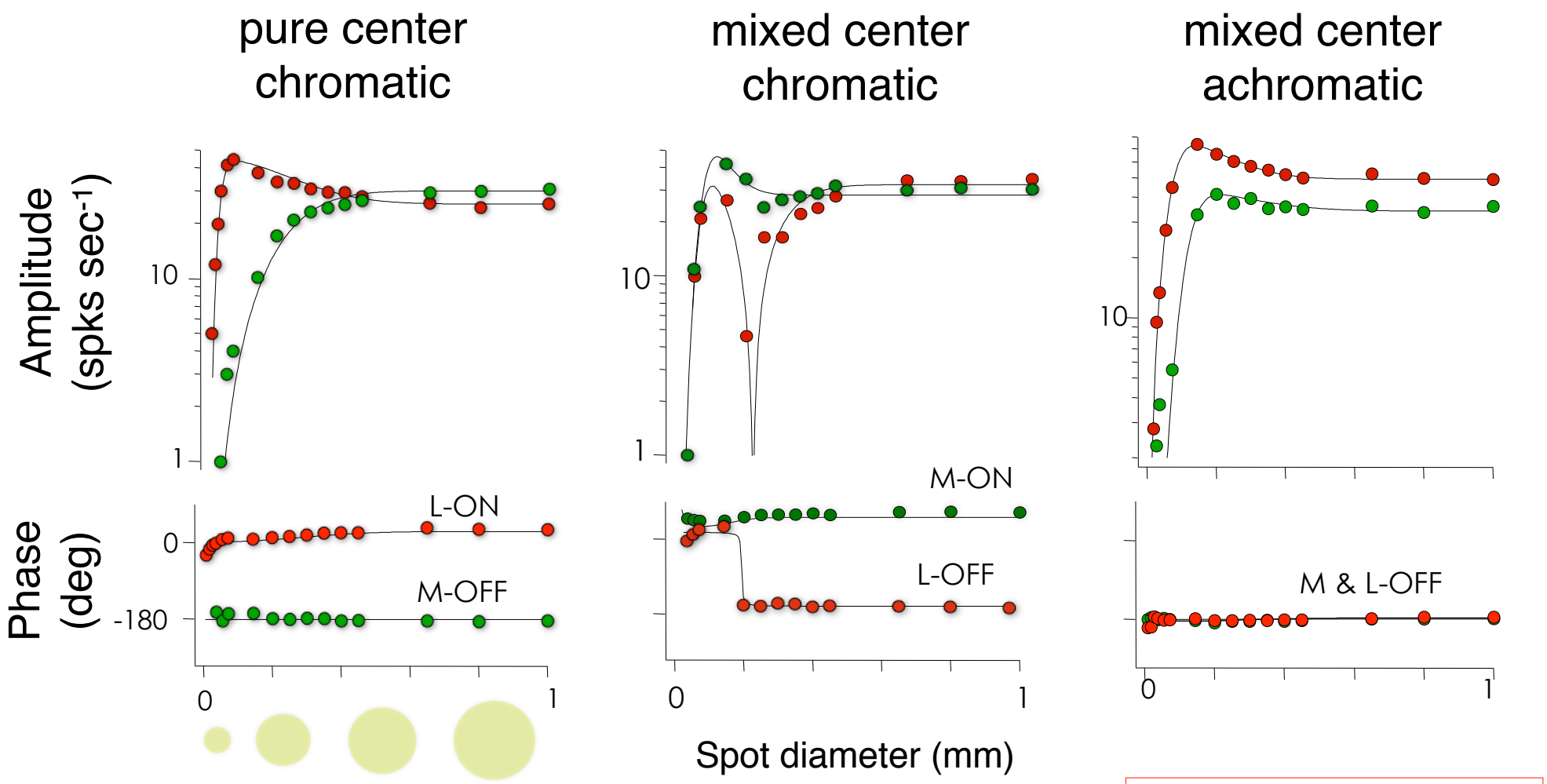

Chromatic midgets (n = 109)

Achromatic midgets (n = 74)

Jo Crook & Dennis Dacey

Mosaic of Red, Green and Blue Cones of the Living Human Retina

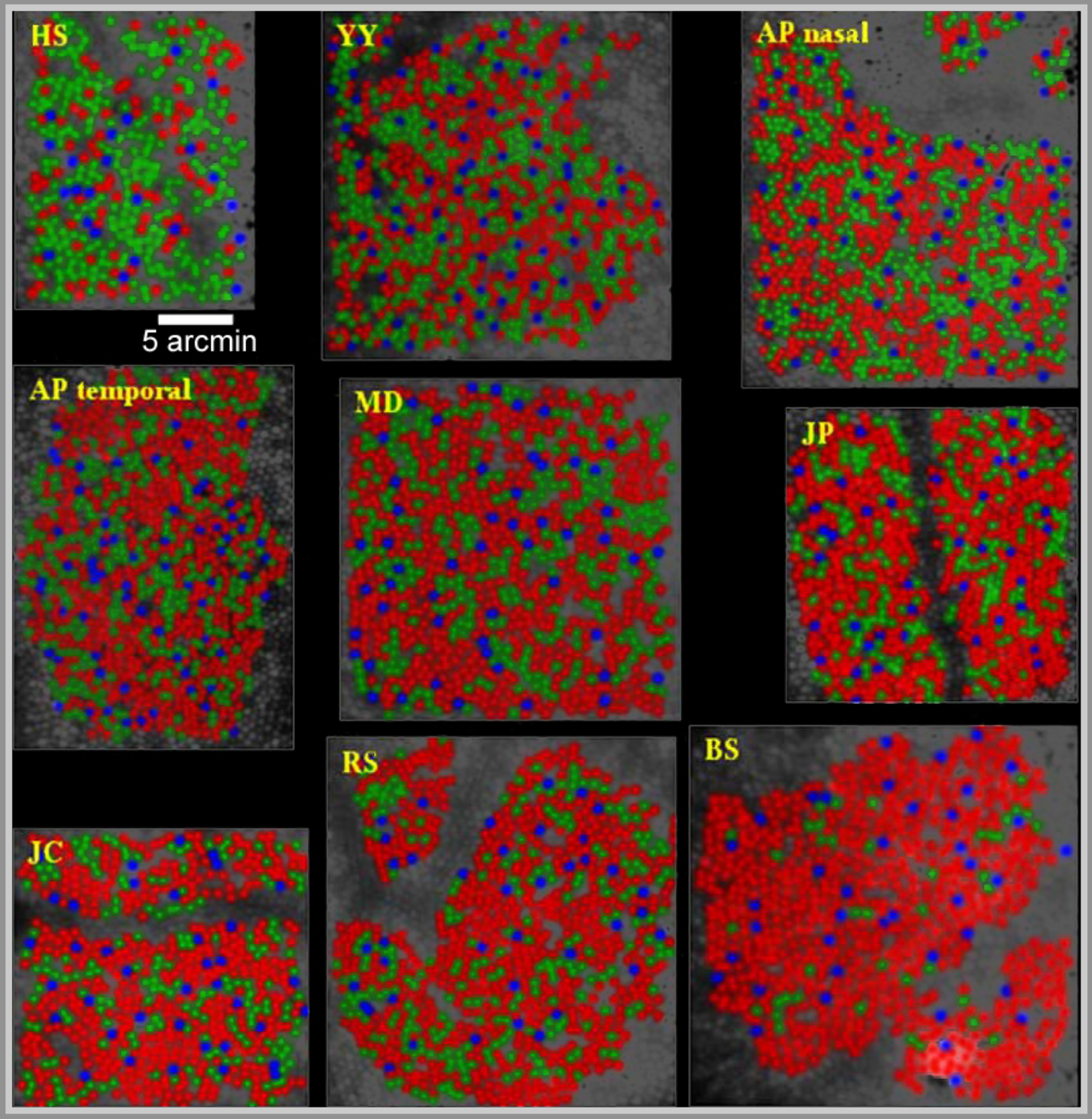

Hofer et al. (2005)

Mixed L and M cone input weights to midget center & surround supports random wiring

Chromatic midgets
(n = 109)

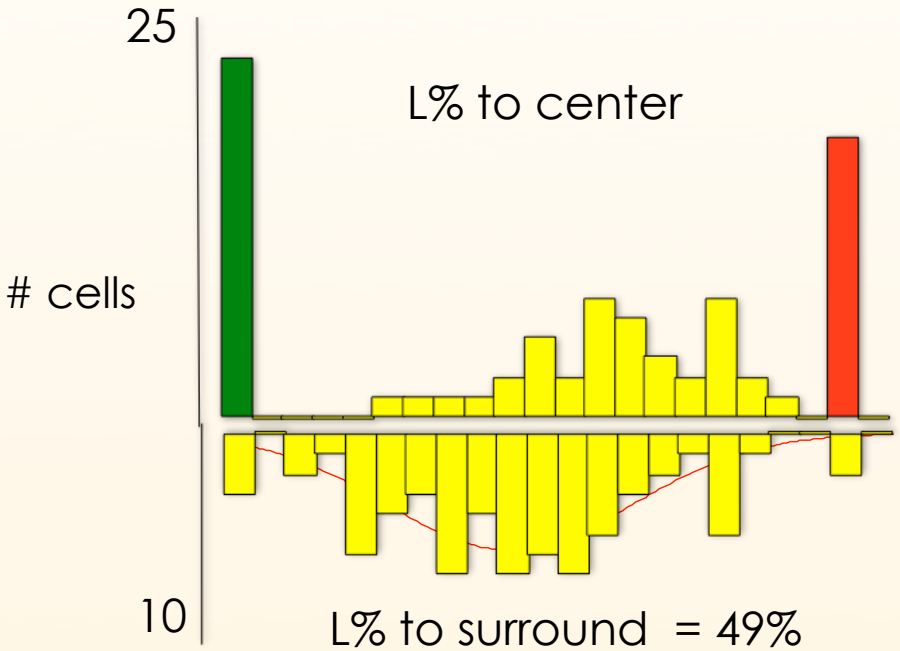

Achromatic midgets
(n = 74)

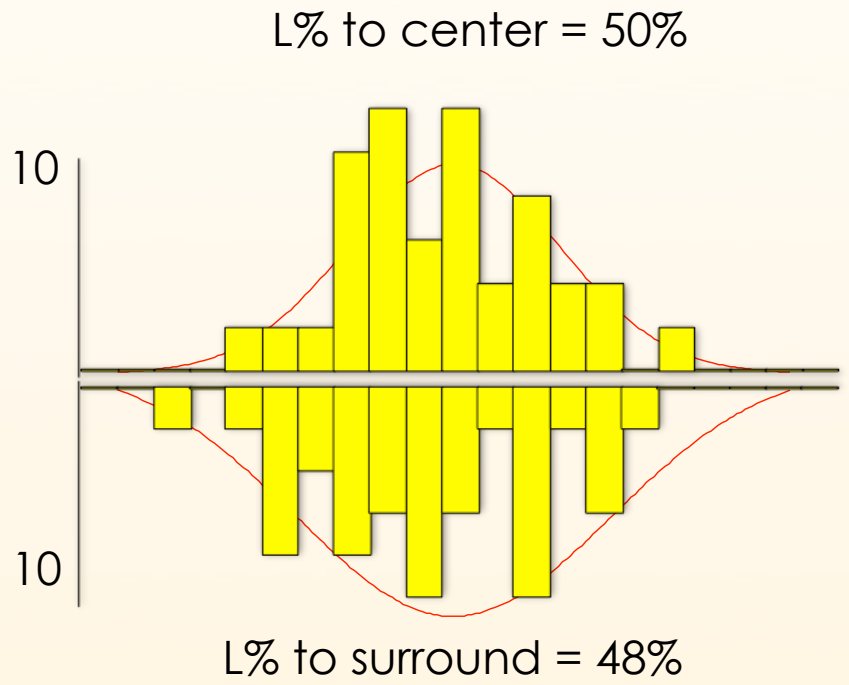

L% input L/(L+M)

Jo Crook & Dennis Dacey

Cone inputs to the receptive field suggest random wiring

- *inputs to the midget center are variable*
- *all midgets show mixed cone input to the surround*
- *all midgets are achromatic to narrow stimuli*
- *many midgets are purely achromatic*

Jo Crook & Dennis Dacey

Primate H1 Horizontal Cell Mosaic

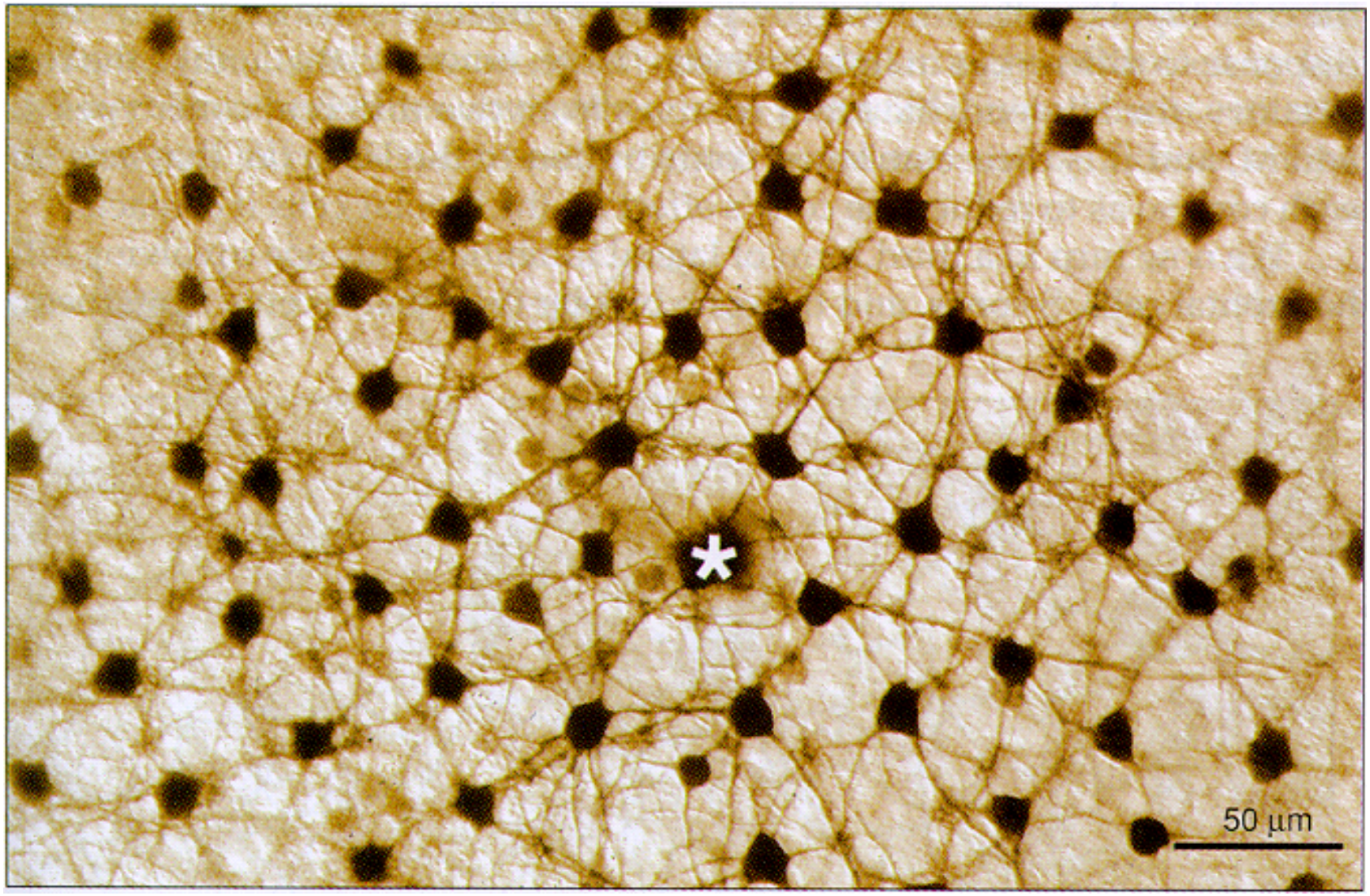

Dacey et al (1996)

As predicted by random-wiring the surround arises by indiscriminate horizontal cell feedback to cones

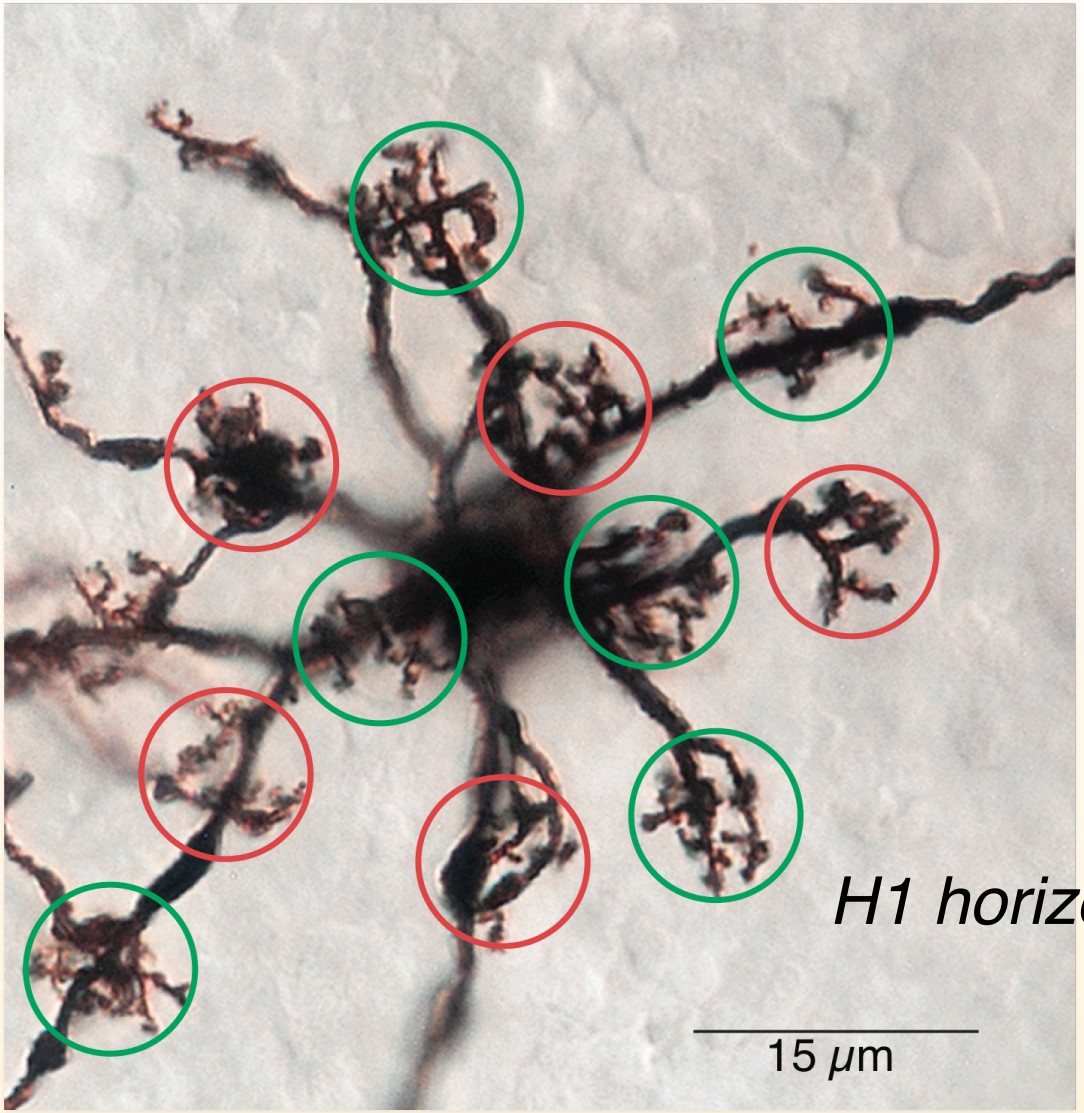

H1 horizontal cell

Dacey et al., 1996

Cell-type classification and receptive fields at single-cone resolution.

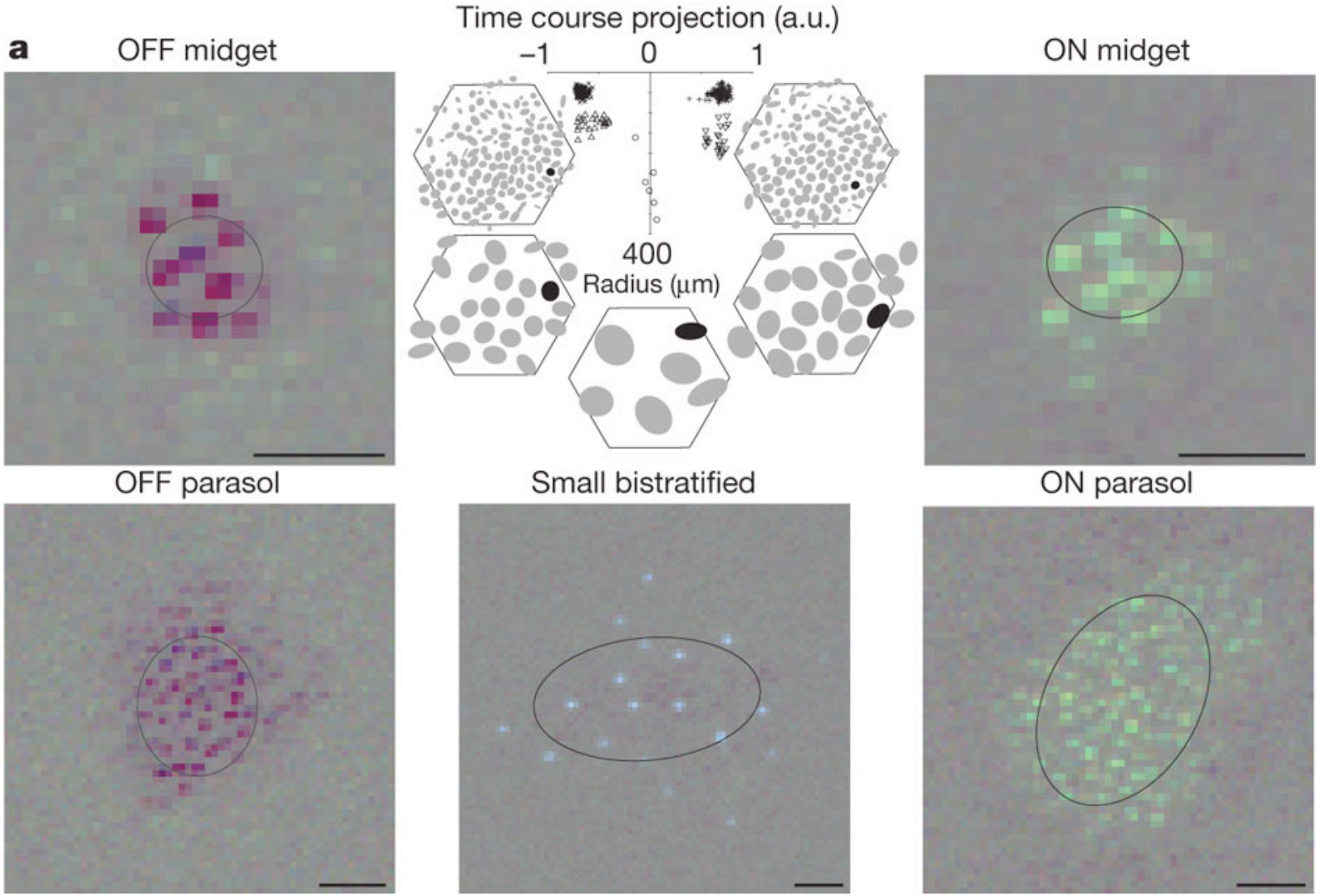

a, Receptive fields of 323 RGCs recorded simultaneously from isolated macaque retina were measured using reverse correlation with white noise stimuli. Centre panel shows receptive-field radius versus first principal component of response time course; clusters reveal distinct cell types. a.u., arbitrary units. Hexagons surrounding centre panel show outline of electrode array and ellipses show Gaussian fits to receptive fields of cells from each cluster. The outer panels show fine-grained spatial receptive-field profiles for highlighted cells. Scale bars, 50 μm

nature
GD Field *et al. Nature* **467**, 673-677 (2010)
doi:10.1038/nature09424

Cone-type identification and inputs to RGCs.

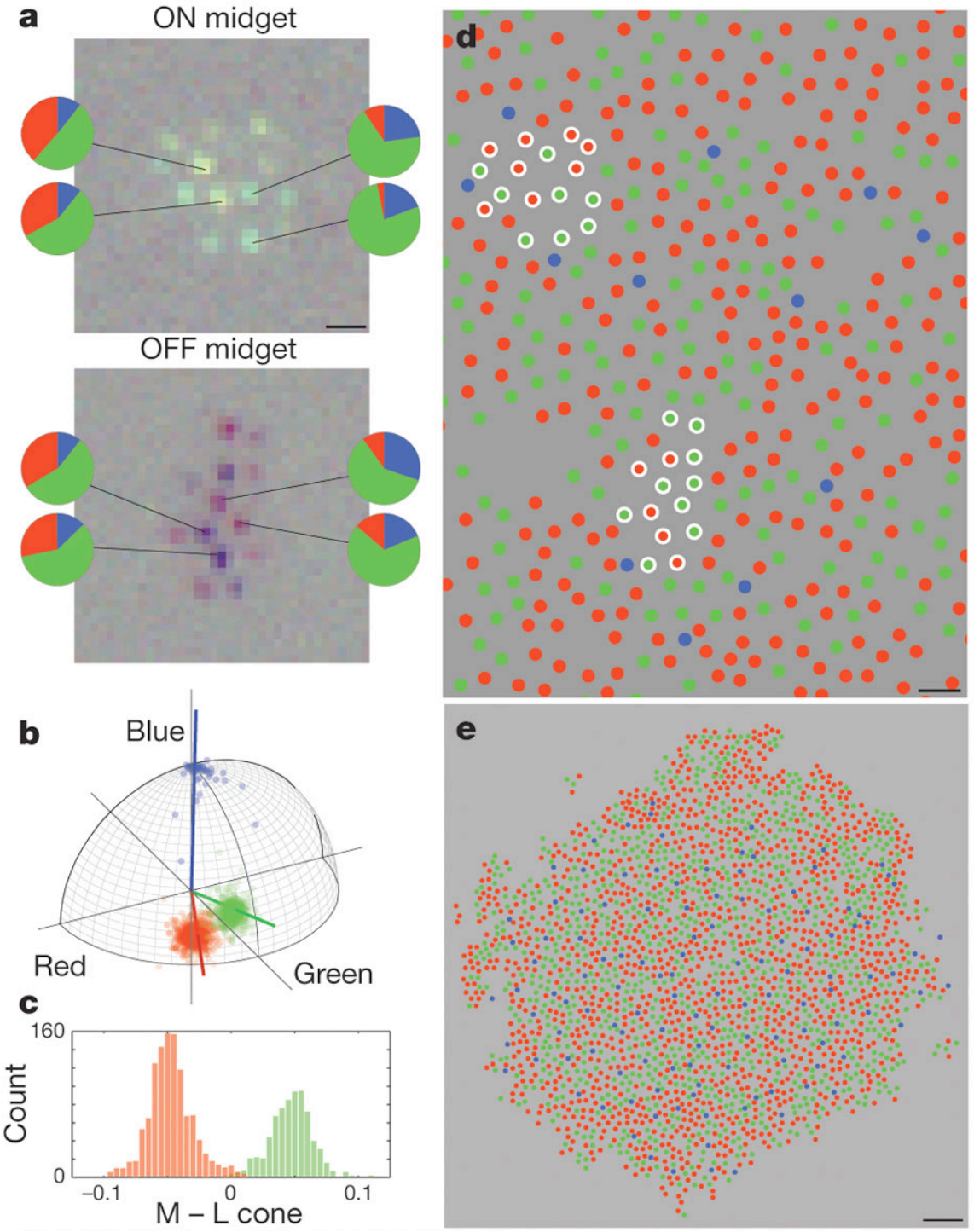

a, The spectral sensitivity of cones providing input to two cells is represented by the relative magnitude of the red, green and blue spike-triggered average values (a.u.) at their locations.

b, For every cone in one recording, these values are shown as points on a sphere. Coloured lines indicate spectral sensitivity of macaque cones. Point colour indicates classification as L (red), M (green), or S (blue).

c, L- and M-cone discriminability quantified by projection along the line joining L- and M-cone loci. Bar colour indicates classification. S cones excluded.

d, Assembled cone mosaic from all RGCs over a region. Cones from **a** are circled.

e, Full mosaic of 2,373 cones from one recording

nature
GD Field *et al. Nature* **467**, 673-677 (2010)
doi:10.1038/nature09424

Full functional sampling of cone lattice by four RGC types

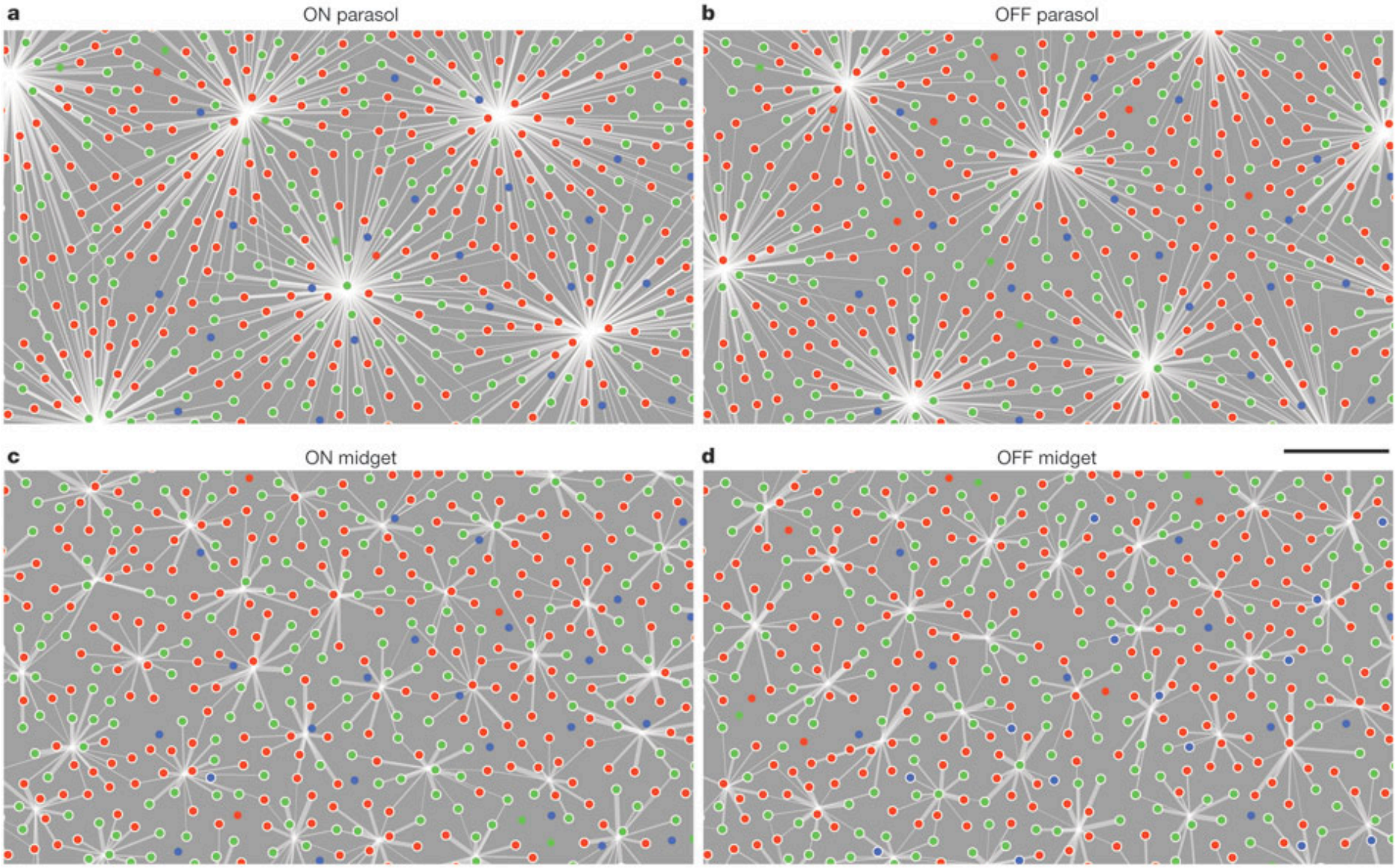

Each panel shows cones identified in a single recording (red, green and blue dots) sampled by receptive-field centres of RGCs of a single type. Cones are identical in all panels. Cones providing input to at least one RGC are highlighted with an annulus. Scale bar, 50 µm.

nature
GD Field *et al. Nature* **467**, 673-677 (2010)
doi:10.1038/nature09424

Cone-type specificity.

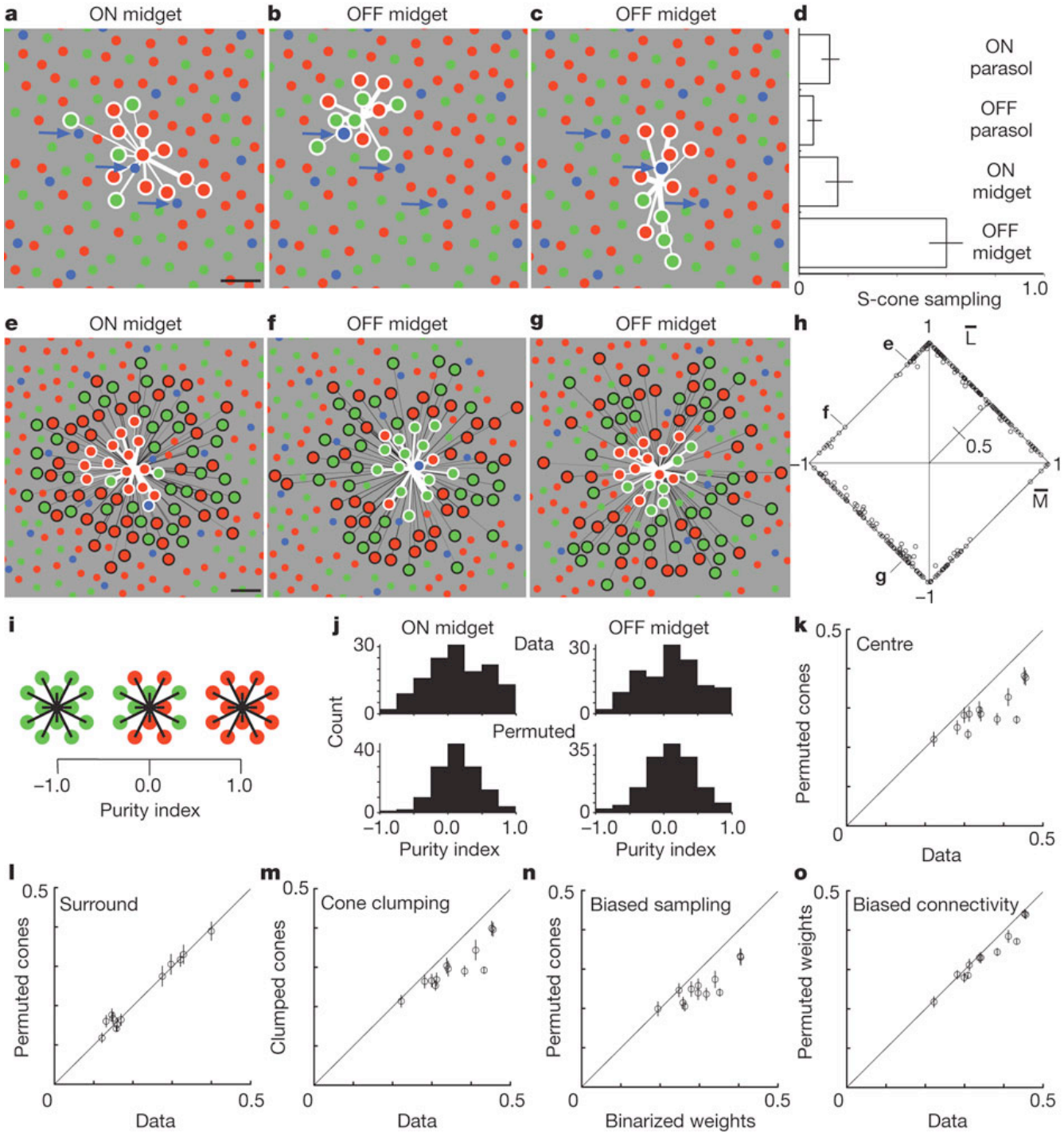

nature
GD Field *et al. Nature* **467**, 673-677 (2010)
doi:10.1038/nature09424

Rabbit Direction-Selective Retinal Ganglion Cells

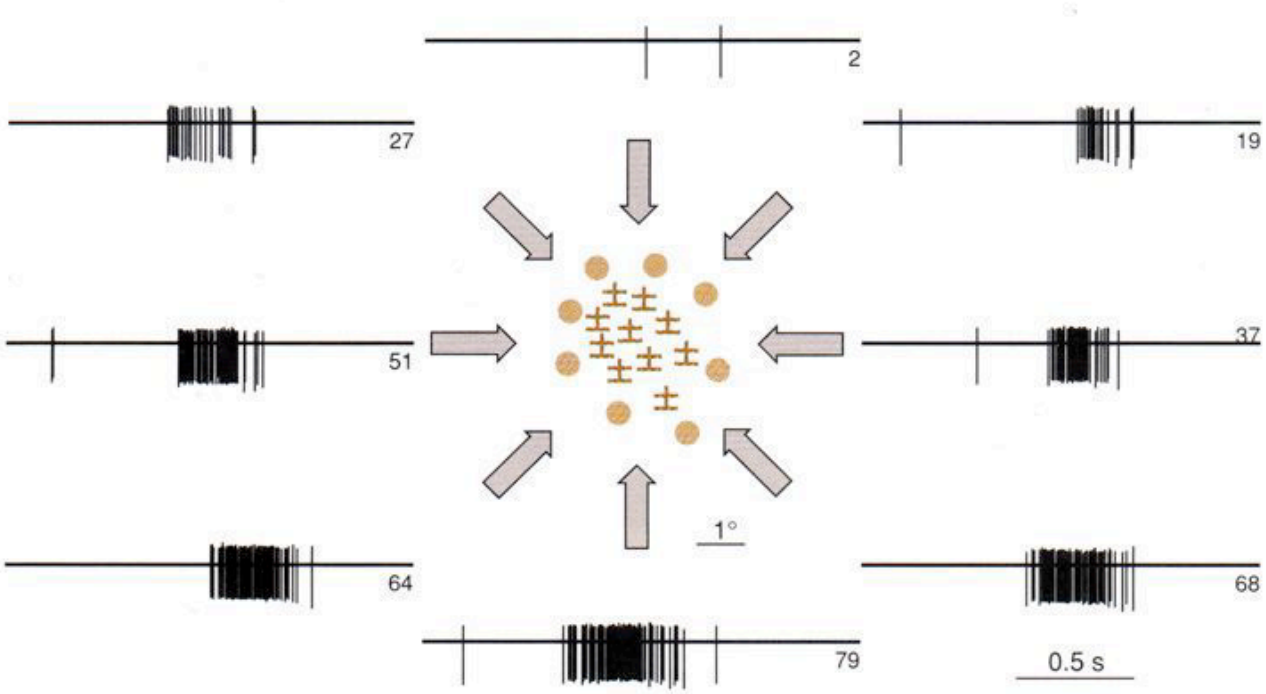

Barlow et al (1964)

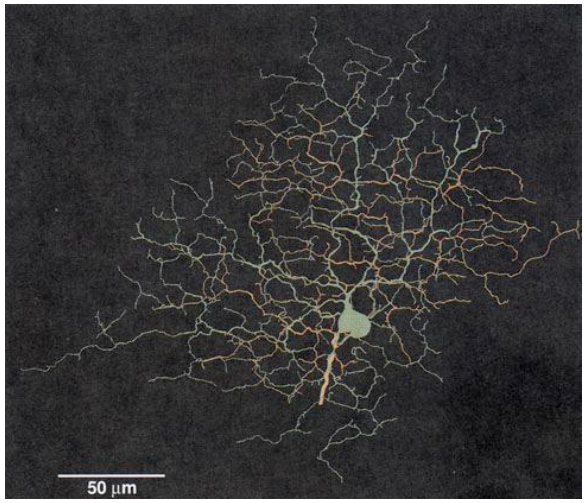

Amthor et al (1989)

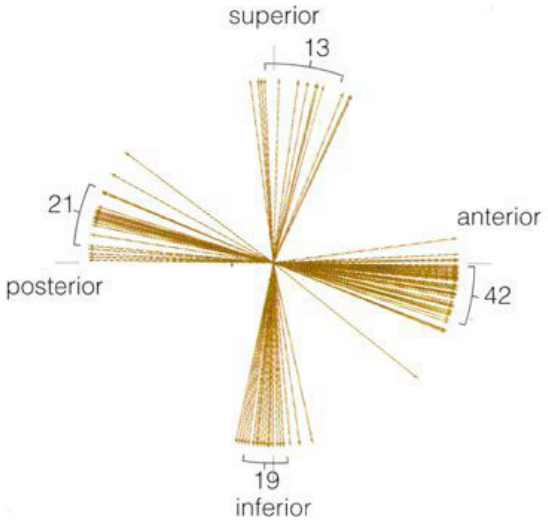

Oyster (1968)

Rabbit Starburst Amacrine Cells

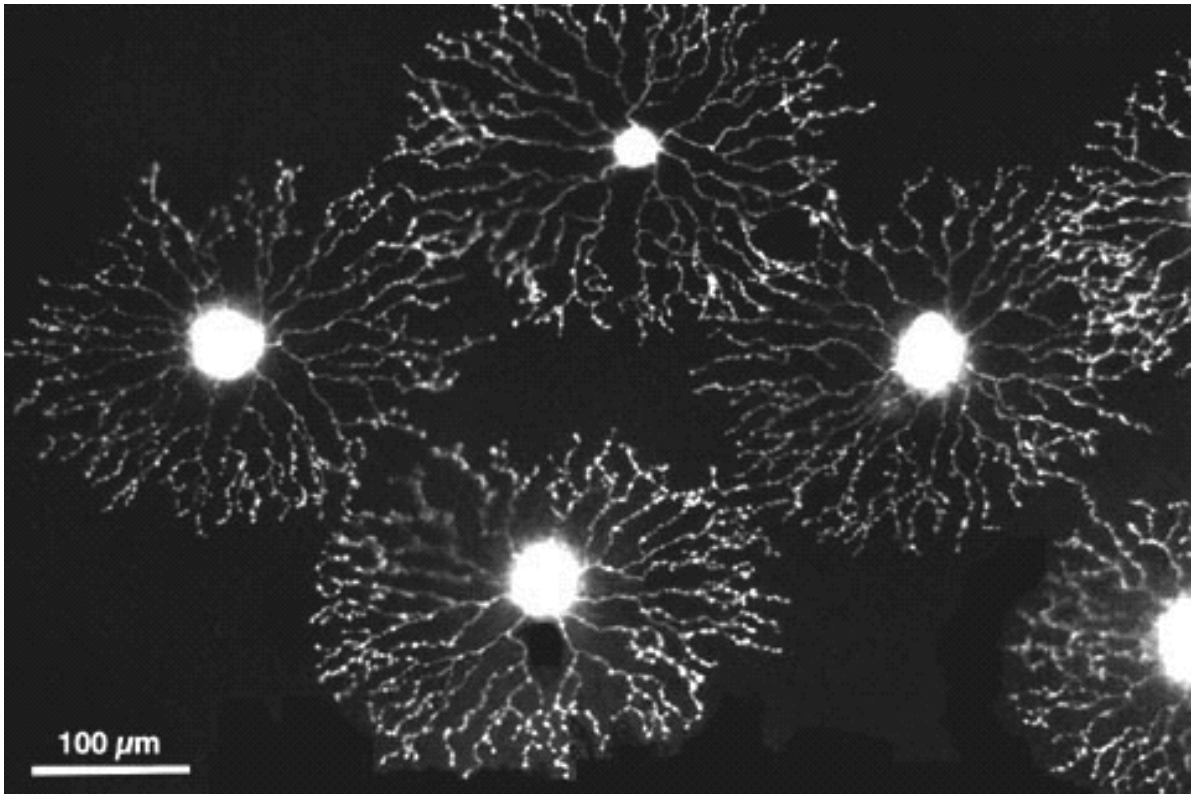

Vaney (1990)

Horace Barlow

Bill Levick

Receptive field properties of on-off directionally selective ganglion cells

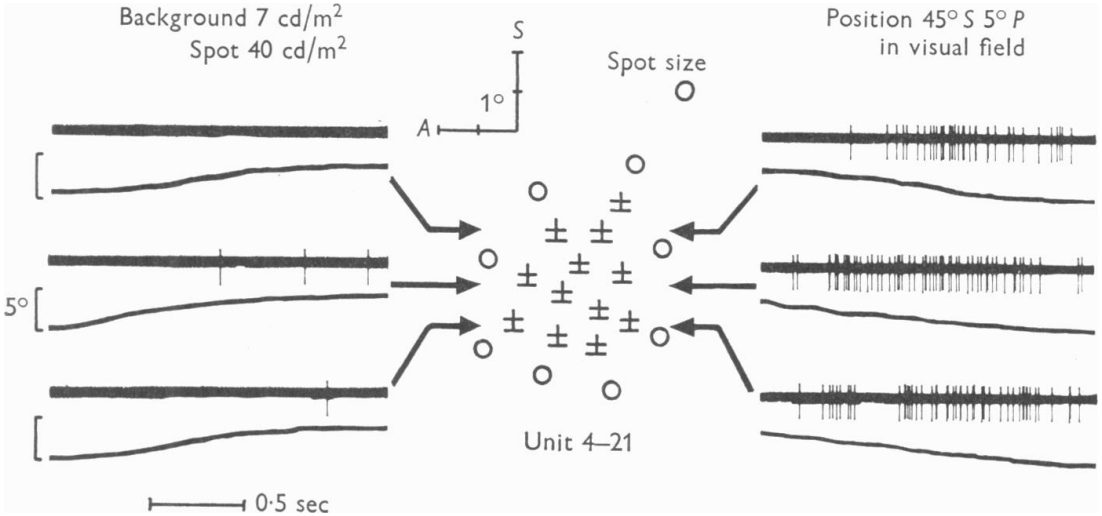

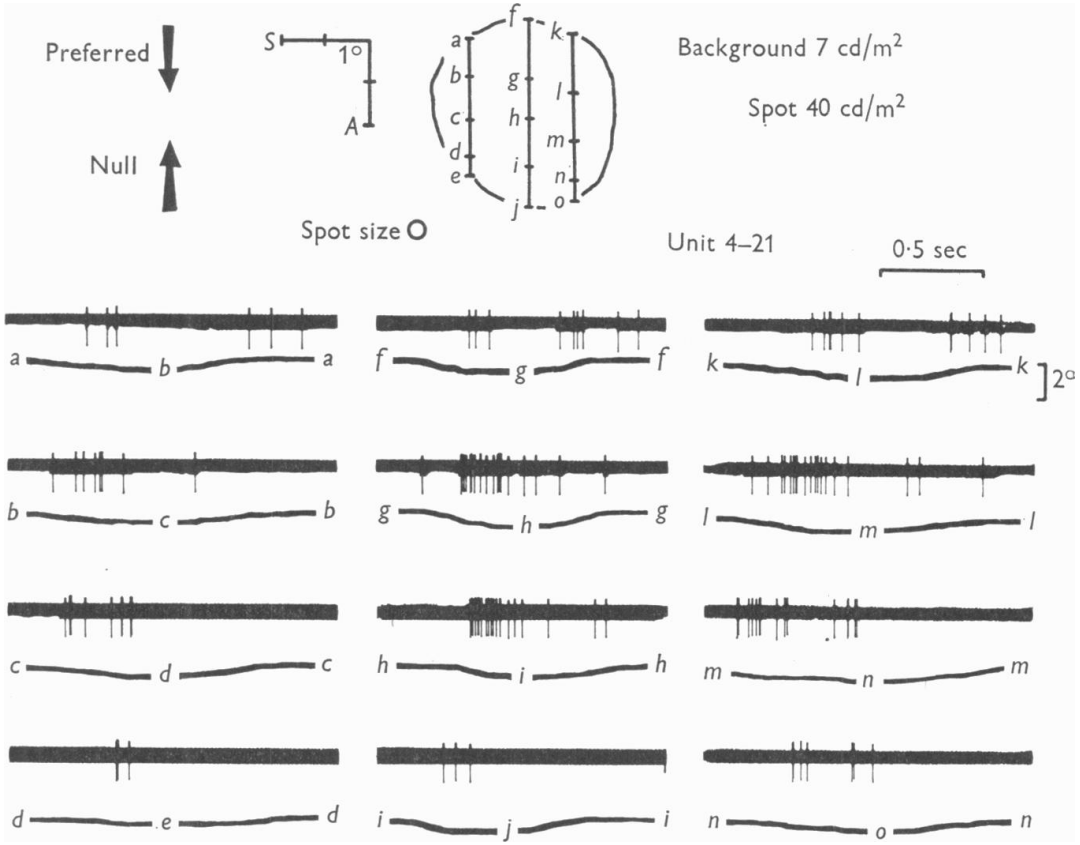

Barlow & Levick, 1965

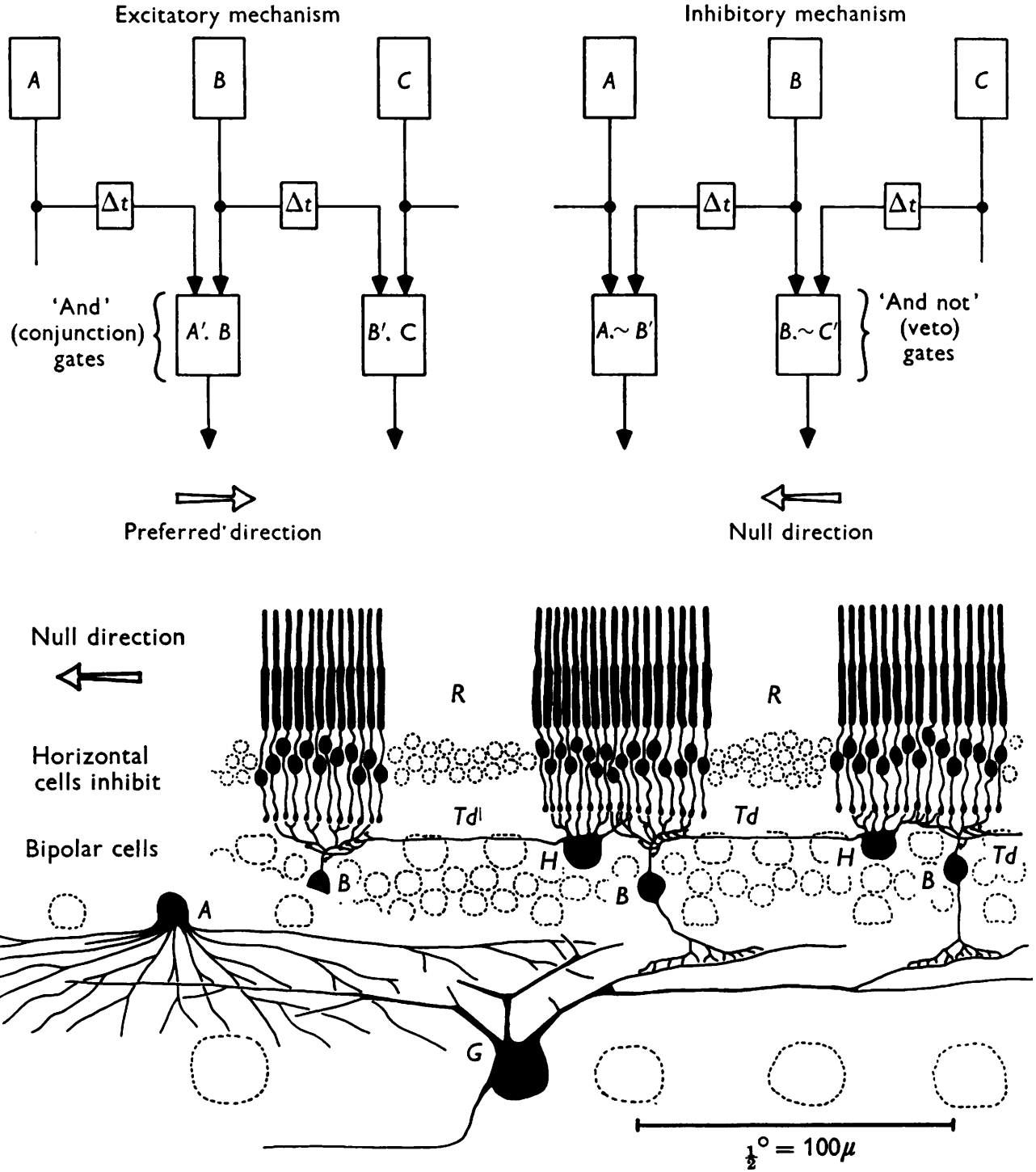

Barlow & Levick, 1965

Receptive field properties of on-off directionally selective ganglion cells

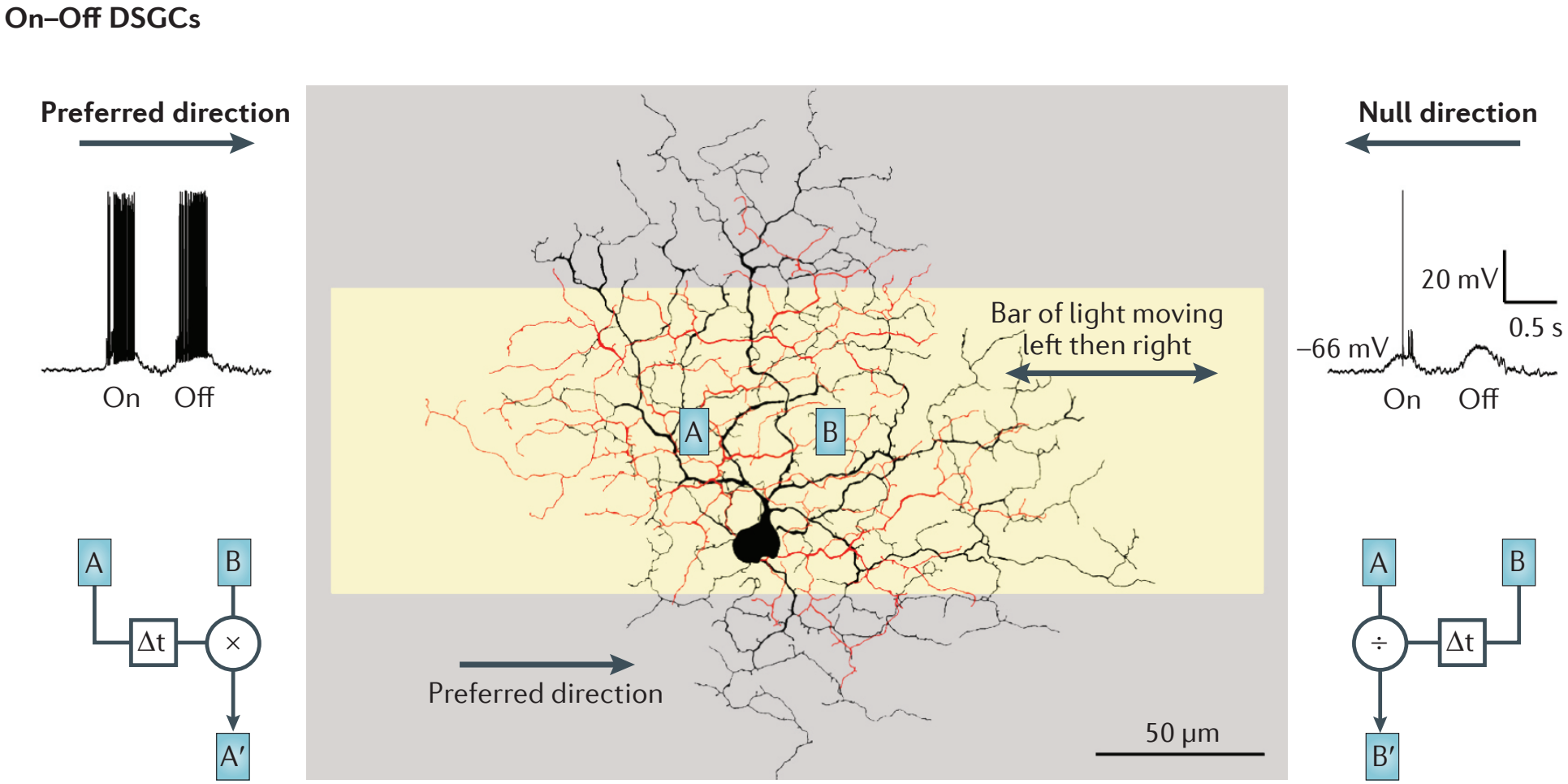

Vaney, et al, 2012

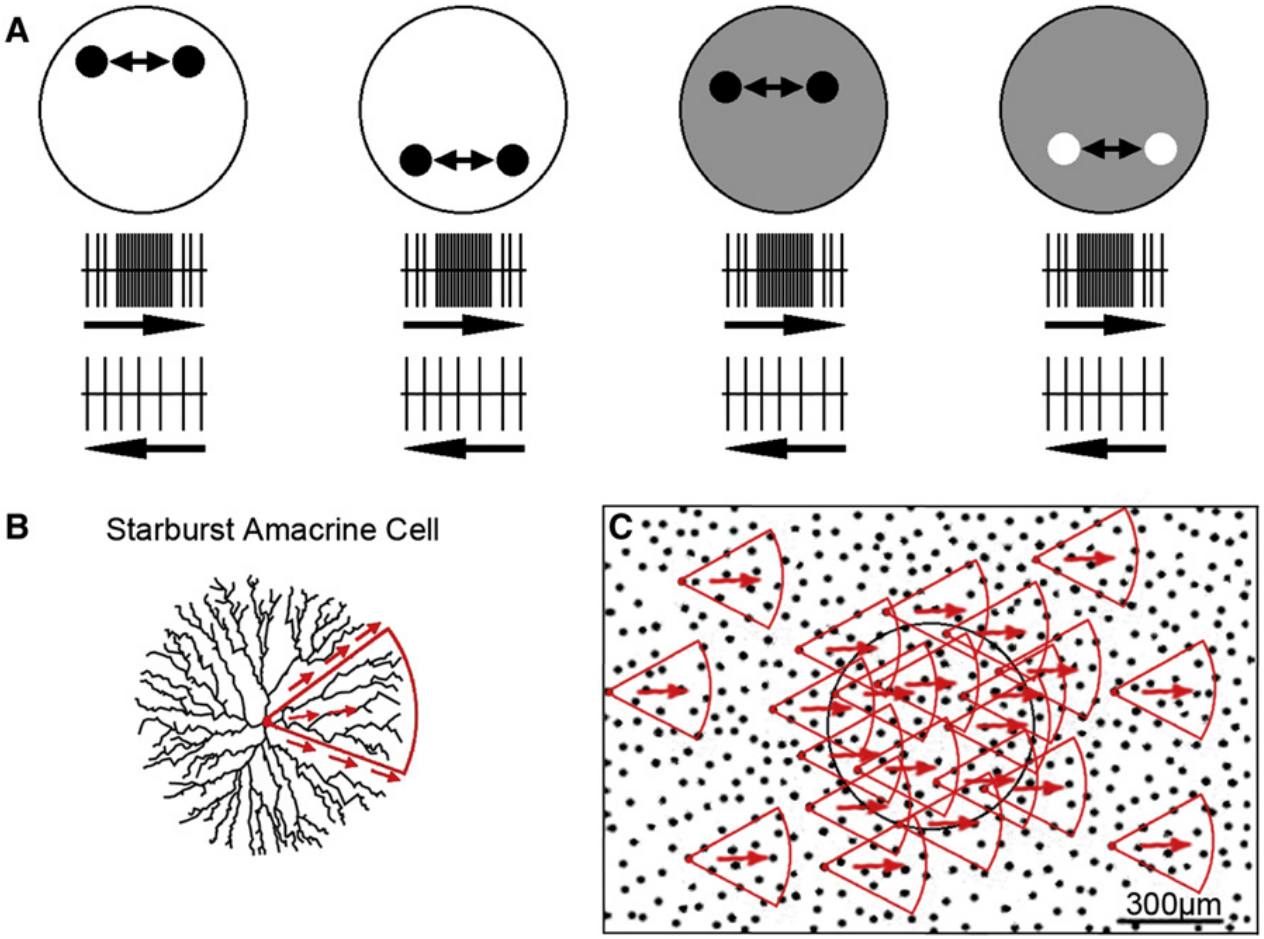

Figure 7. The Cardinal Features of the ON-OFF Direction-Selective Cell, and the Mechanism by Which Direction Selectivity Is Created

(A) The cell can discriminate the direction of motion of small stimuli falling within its receptive field (large circle), and it does not matter where within the field the small stimulus falls—there is a local subunit that is direction selective.

(B and C) The fundamental mechanism of direction selectivity. (B) Shows the dendritic arbor of a starburst amacrine cell. A sector of the arbor (outlined in red) is (1) an independent functional unit, electrically separate from the rest of the cell, and (2) directionally polarized, such that it releases GABA when the stimulus moves in one direction—left to right in this example—and not in others. (C) Starburst sectors pointing in a single direction (red) selectively synapse upon dendrites of an ON-OFF DS ganglion cell (outlined by the black circle). In this example, they would provide inhibition when the stimulus moves from left to right. This cell would thus have a preferred direction for movement right-to-left and a null direction for movement left-to-right. The sectors are smaller than the dendritic field, thus accounting for the ganglion cell's ability to discriminate small movements within the field. Other sectors of the starburst cell, pointing in other directions, would contact other direction selective ganglion cells; those cells would prefer different directions of stimulus movement.

Masland, 2012

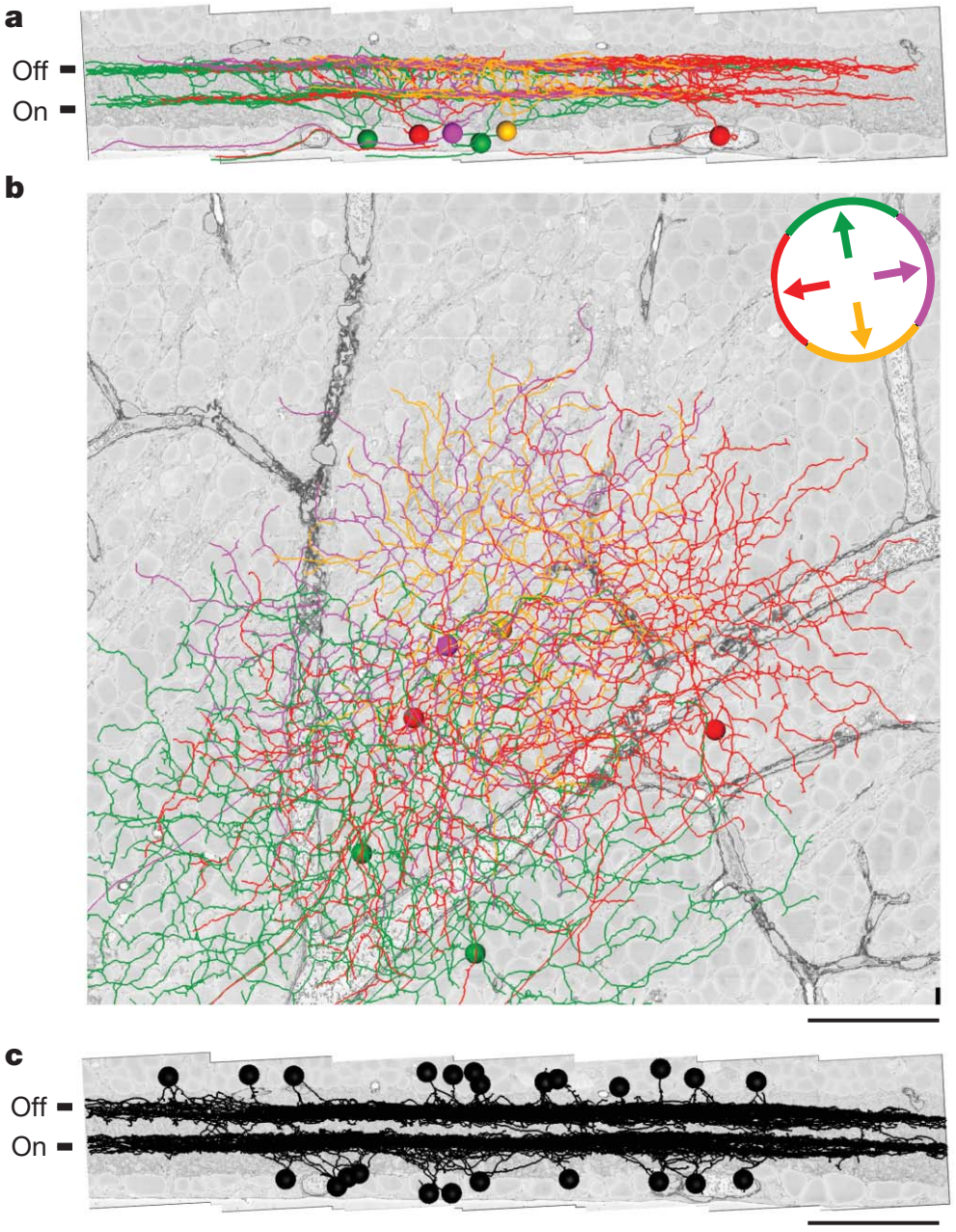

Figure 2 | Skeleton reconstructions of DSGCs and SACs. **a**, **b**, DSGCs, colour-coded by preferred direction (inset), projected parallel to (**a**) and norma to (**b**) the plane of the retina. Note bi-stratification in the inner plexiform layer **c**, Parallel projections of 24 SACs (11 On SACs, 13 Off SACs, black). Scale bar are 50 μm.

Briggman et al, 2011

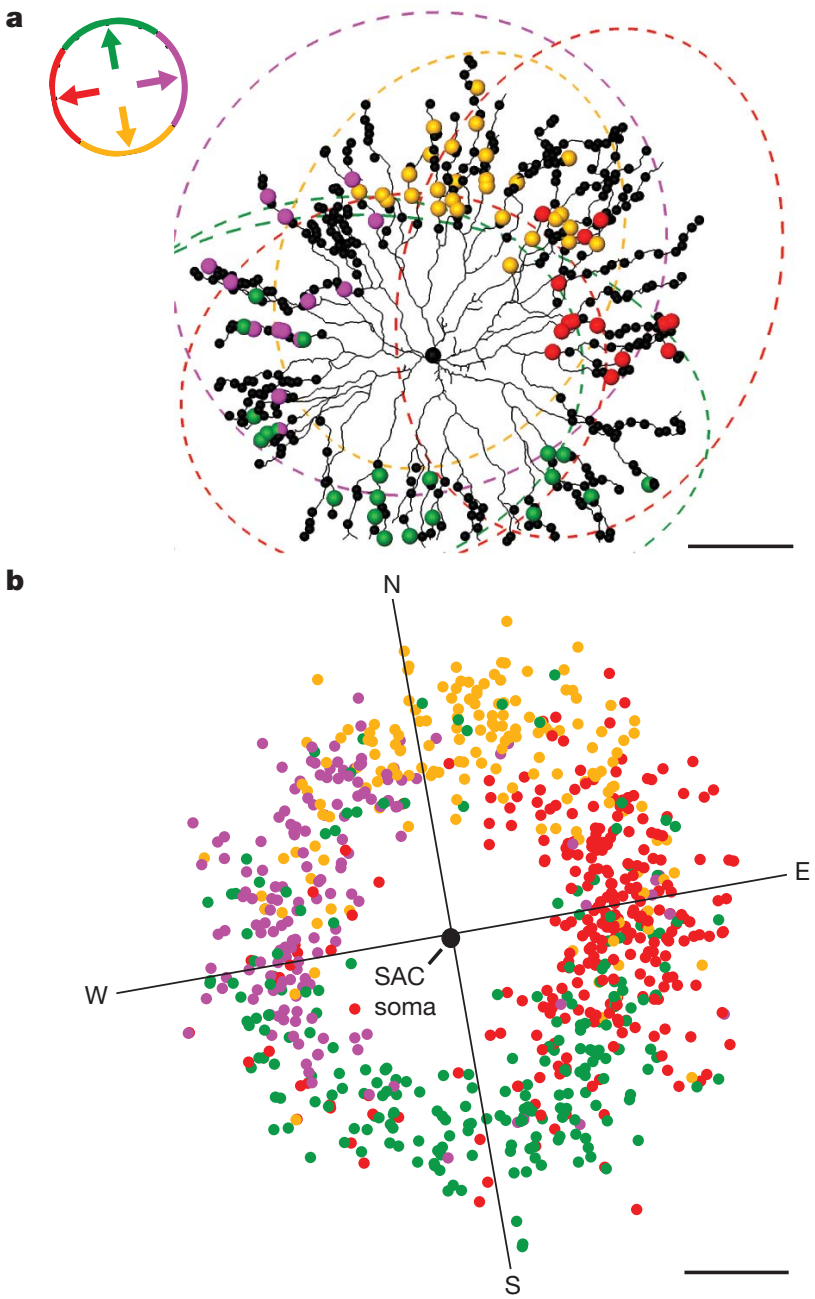

Figure 4 | Specificity of SAC outputs. **a**, An Off SAC (black skeleton), with varicosities indicated by black dots. DSGC dendritic trees are indicated by colour-coded dashed ellipses. Synapses are colour-coded by the preferred direction of the postsynaptic DSGC. **b**, Output synapse locations ($n = 831$ synapses) relative to SAC somata from all 24 SACs. Scale bars are 50 µm.

Briggman et al, 2011

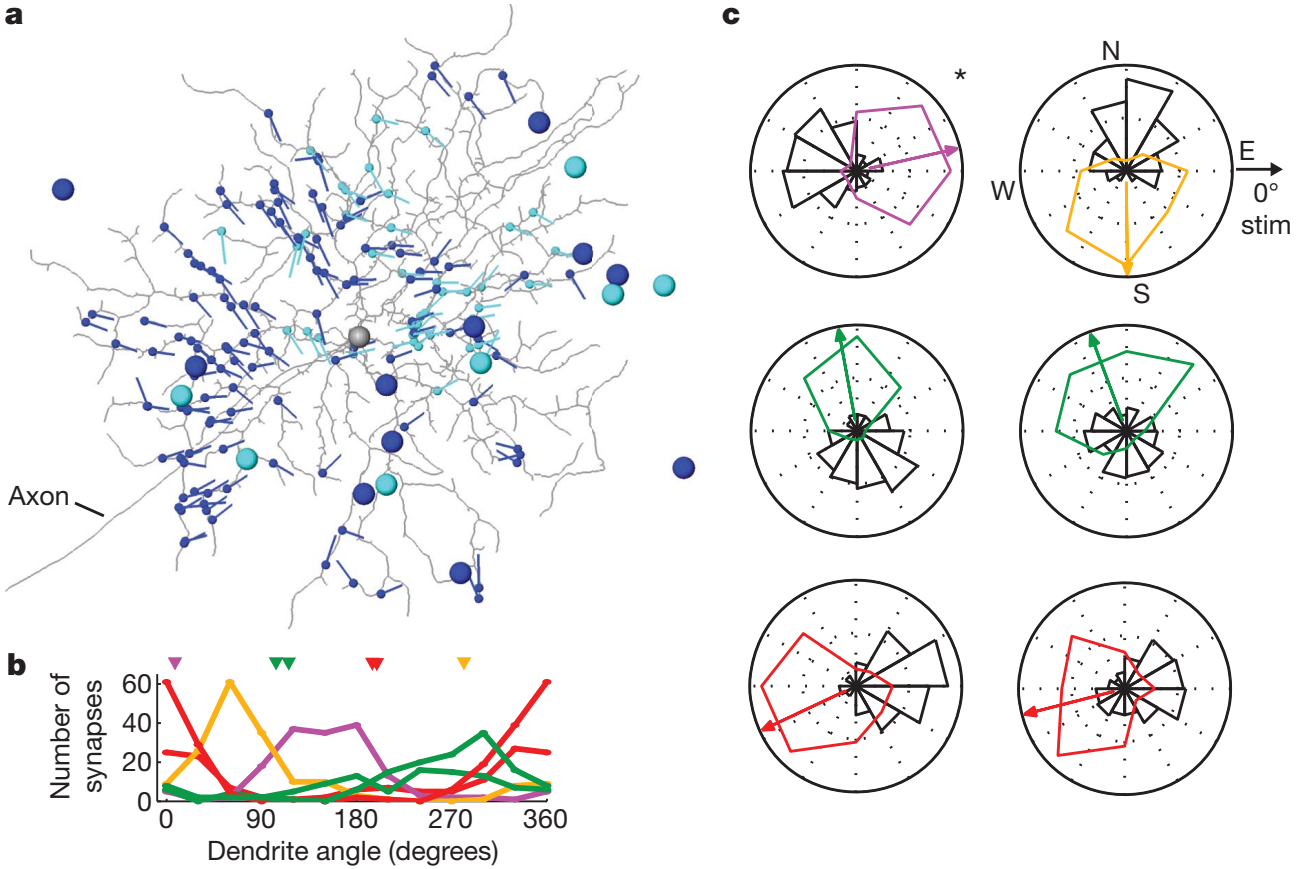

Figure 5 | Specificity of DSGC inputs. **a**, DSGC (grey skeleton) and the connected On and Off SAC somata (large cyan and blue circles, respectively) and associated SAC input synapses (smaller cyan and blue circles) from 18 SACs. **b**, The distribution of all SAC dendrite angles (θ_{dendr}) for each of the six DSGCs; θ_{dendr} is defined by the vectors (cyan and blue lines in **a**) oriented from SAC somata to synapse location. Triangle markers indicate the preferred direction for each DSGC. **c**, Polar histograms of θ_{dendr} (black, plotted as the square root of θ_{dendr} frequencies) together with the DSGC tuning curves (as in Fig. 1). Asterisk denotes the DSGC shown in **a**.